



The role of KAT3 proteins in neural development

PhD Thesis
Rocío González Martínez

Thesis supervisor
Eloísa Herrera González de Molina

Programa de Doctorado en Neurociencias
Instituto de Neurociencias
Universidad Miguel Hernández de Elche
- 2021 -



THE ROLE OF KAT3 PROTEINS IN NEURAL DEVELOPMENT

Tesis Doctoral presentada por

Rocío González Martínez

Directora de Tesis:

Eloísa Herrera González de Molina

Programa de Doctorado en Neurociencias

Instituto de Neurociencias

Universidad Miguel Hernández de Elche

- 2021 -



La presente Tesis Doctoral, titulada “**The role of KAT3 proteins in neural development**” se presenta bajo la modalidad de tesis convencional con el siguiente indicio de calidad del trabajo previamente publicado que no ha sido ni será usado en ninguna otra tesis doctoral:

- **New techniques for studying neurodevelopment.**

Escalante A, **González-Martínez R**, Herrera E.

Faculty Rev. (sección de revisiones de F1000Research) 2020;9:17.

Published 2020 Nov 25. Doi:10.12703/r/9-17.



Sant Joan d'Alacant, 17 de diciembre de 2021

La Dra. Dña. *Eloísa Herrera González de Molina*, Investigadora Científica del Consejo Superior de Investigaciones Científicas (CSIC),

INFORMA:

Que Dña. *Rocío González Martínez (DNI 74521369N)* ha realizado bajo mi inmediata dirección y supervisión el trabajo titulado “**The role of KAT3 proteins in neural development**” conforme a los términos y condiciones definidos en su Plan de Investigación y de acuerdo al Código de Buenas Prácticas de la Universidad Miguel Hernández de Elche, cumpliendo los objetivos previstos de forma satisfactoria para su defensa pública como tesis doctoral.

Lo que firmo para los efectos oportunos, en San't Joan d'Alacant a 17 de diciembre de 2021

Directora de la tesis

Dra. Dña. *Eloísa Herrera González de Molina*



Sant Joan d'Alacant, 17 de diciembre de 2021

Dña. Elvira de la Peña García, Coordinadora del programa de Doctorado en Neurociencias del Instituto de Neurociencias de Alicante, centro mixto de la Universidad Miguel Hernández (UMH) y de la Agencia Estatal Consejo Superior de Investigaciones Científicas (CSIC),

INFORMA:

Que Dña. Rocío González Martínez (DNI 74521369N) ha realizado bajo la supervisión de nuestro Programa de Doctorado el trabajo titulado “**The role of KAT3 proteins in neural development**” conforme a los términos y condiciones definidos en su Plan de Investigación y de acuerdo al Código de Buenas Prácticas de la Universidad Miguel Hernández de Elche, cumpliendo los objetivos previstos de forma satisfactoria para su defensa pública como tesis doctoral.

Lo que firmo para los efectos oportunos, en San't Joan d'Alacant a 17 de diciembre de 2021

Y para que conste, a los efectos oportunos, firmo el presente certificado.

Dra. Elvira de la Peña García
Coordinadora del Programa de Doctorado en Neurociencias

Financiación/subvención/beca



EXCELENCIA
SEVERO
OCHOA

Ayudas para contratos predoctorales
Severo Ochoa para la formación de
doctores 2014

European Research Council Starting
Grants



ERA-NET NEURON grant. Grupo
CHROMISYN

Programa Prometeo de la
Generalitat Valenciana para
grupos de excelencia. Grupo:
NEUROCROM



PROMETEO
PROGRAM



GENERALITAT
VALENCIANA

INDEX

ABSTRACT.....	1
INTRODUCTION.....	7
1. General principles of epigenetics.....	10
2. Regulation of gene expression by lysine acetylation.....	12
3. KAT3 proteins: CBP and P300.....	14
3.1.Molecular structure.....	15
3.2.Functional heterogeneity.....	16
4. Rubinstein-Taybi Syndrome, an intellectual disability disorder caused by defects in the epigenetic regulators CBP and P300.....	18
4.1.The role of KAT3 proteins in neurodevelopment.....	19
4.2.The role of KAT3 proteins in adulthood.....	21
5. The visual system as a model to study the development of neural circuits.....	22
5.1. Basic anatomy of the mammalian visual system.....	22
5.2 Retinal development.....	25
5.3 Development of the visual pathway in mammals.....	29
OBJECTIVES.....	33
MATERIALS AND METHODS.....	37
1. Animals.....	39
2. Lentiviral production.....	42
3. Neurosphere culture.....	43
3.1. Establishment of a primary neural stem cell (NSC) culture.....	43
3.2. Lentiviral infection of NSC cultures.....	44

3.3. The Neurosphere Assay (NSA).....	44
3.4. Clonal differentiation of neurospheres.....	45
4. Primary hippocampal culture.....	46
5. Immunocytochemistry and immunohistochemistry.....	47
5.1. Immunocytochemistry in neurosphere and primary cultures.....	47
5.2. Immunohistochemistry.....	48
6. Cholera toxin injection and whole brain clearing.....	49
7. Image analysis and quantification.....	50
8. Fluorescent-activated cell sorting (FACS).....	51
9. Single-Nuclei RNA Sequencing (snRNA-Seq) and bioinformatical analysis...	52
10. Statistical analyses.....	55
RESULTS.....	59
1. The role of KAT3 proteins in neural stem cells.....	61
1.1 Individual ablation of CBP and P300 do not alter proliferation of neural stem cells.....	63
1.2 CBP and P300 are individually required for proper differentiation of neural progenitor cells.....	68
1.3 Single-nucleus RNA sequencing analysis of differentiated neurospheres revealed alterations in neural populations after removal of CBP or P300	73
2. The role of KAT3 proteins in neural progenitor cells <i>in vivo</i>.....	81
2.1 CBP and P300 are expressed in progenitor and differentiated cells during mouse retinal development and at postnatal stages.....	83

2.2 CBP is expressed in a larger number of retinal progenitor cells than P300.....	85
2.3 Characterization of Rx-Cre mouse line in the retina.....	86
2.4 P300 deficiency in retinal progenitor cells do not affect retinal development.....	88
2.5 The absence of CBP in retinal progenitor cells leads to alteration in retinal development.....	90
2.6 Simultaneous elimination of CBP and P300 in Rx progenitor cells leads to a dramatic phenotype and embryonic lethality.....	94
3. The role of KAT3 proteins in neuronal maturation.....	97
3.1 Newborn neurons lacking P300 do not show alterations in dendritic growth.....	99
4. The role of CBP and P300 in the maintenance of differentiated neurons..	103
4.1 CBP and P300 are not individually required for the maintenance of RGCs identity.....	105
DISCUSSION.....	109
CONCLUSIONS.....	122
BIBLIOGRAPHY.....	129
ANNEX 1. Indications of quality of the thesis.....	149
ACKNOWLEDGEMENTS.....	159

TABLE OF ABBREVIATIONS

ac	Acetylation
ADPRT	ADP-ribosyl transferase
Atoh7	Atonal homolog 7
bFGF	Human recombinant basic fibroblast growth factor
bp	Base pairs
BD	Bromodomain
Brn3b	Brain-Specific Homeobox/POU Domain Protein 3B
CBP	CREB-binding protein
CNS	Central Nervous System
Cre	Cre recombinase
CSPG	Chondroitin sulphate proteoglycan
DIV	Day <i>in vitro</i>
dLGN	Dorsal lateral geniculate nucleus
DNA	Deoxyribonucleic acid
DNMT	DNA methyltransferase
E#	Embryonic day
E3UL	E3 Ubiquitin ligase
EGF	Epidermal growth factor
EP300	E1A-associated protein p300
ESC	Embryonic Stem Cell
f/f	floxed
FACS	Fluorescent-activated cell sorting
GCL	Ganglion cell layer

GFAP	Glial fibrillary acidic protein
GO	Gene Ontology
HAT	Histone acetyltransferase
HDAC	Histone deacetylase
HDM	Histone demethylase
HMT	Histone methyltransferase
IDD	Intellectual Disability Disorder
INL	Inner nuclear layer
IPL	Inner plexiform layer
iPSC	Inducible Pluripont Stem Cell
IQ	Intelligence quotient
Isl1	Islet-1
KAT	Lysine acetyltransferase
KO	Knockout
Lhx2	LIM homeobox 2
LV	Lentiviral particles
MAP2	Microtubule Associated Protein 2
me	Methylation
Ngn2	Neurogenin 2
NPC	Neuronal Progenitor Cell
NR	Neural retina
NRI	Nuclear receptor interaction domain
NSA	Neurosphere assay
NSC	Neural stem cell

O4	Oligodendrocyte marker O4
OD	Optic disc
ON	Optic nerve
ONL	Outer nuclear layer
OPL	Outer plexiform layer
Otx2	Orthodenticle homolog 2
P#	Postnatal day
Pax6	Paired box gene 6
PCA	Principal Component Analysis
RNA	Ribonucleic acid
RNA Pol II	RNA Polymerase II
S100β	S100 calcium binding protein B
Sema	Semaphorin
Shh	Sonic hedgehog
Slit	Slit Guidance Ligand
snRNA-Seq	Single nuclei RNA sequencing
SVZ	Subventricular zone
RGC	Retinal ganglion cell
Robo	Roundabout Guidance Receptor
RPC	Retinal progenitor cell
RPE	Retinal pigmented epithelium
RSTS	Rubinstein-Taybi Syndrome
Rx	Retina and anterior neural fold homeobox
SC	Superior Colliculus

Sox2	Sex-determining region Y-box containing gene 2
Sun1	Sad1 and UNC84 Domain Containing 1
TF	Transcription Factor
Tuj1	Beta III tubulin
wt	Wild type

FIGURE INDEX

Figure 1. Epigenetic regulation of gene expression by chromatin modifications.

Figure 2. Lysine acetylation, chromatin condensation and gene expression.

Figure 3. KAT3 expression levels in different neural cell types.

Figure 4. KAT3 protein structure.

Figure 5. KAT3 proteins regulate transcription through different functions.

Figure 6. Organization of vertebrate retina.

Figure 7. Schematic representation of visual pathway of mice.

Figure 8. Schematic representation of development of the vertebrate eye.

Figure 9. Neurogenesis in the embryonic vertebrate retina.

Figure 10. Temporal fate specification in the retina.

Figure 11. Transcriptional regulation of retinal cell type fates.

Figure 12. Development of the visual pathway and molecular mechanism underlying axon guidance at the optic chiasm.

Figure 13. Analysis of the role of KAT3 proteins in neural stem cells (NSC).

Figure 14. Individual ablation of CBP or P300 does not affect proliferation of NSC.

Figure 15. Individual ablation of CBP or P300 does not affect the expression of proliferative markers of NSC.

Figure 16. CBP lacking neurospheres showed a prominent delay in cell migration.

Figure 17. CBP and P300 lacking neurospheres showed alterations in neural differentiation programs whereas cell death is not altered.

Figure 18. CBP and P300 are individually required for differentiation of NSCs into the three neural lineages.

Figure 19. Single-nucleus RNA sequencing analysis of differentiated neurospheres revealed alterations in neural populations after removal of CBP or P300.

Figure 20. Single-nucleus RNA sequencing analysis of differentiated neurospheres revealed alterations in several populations of CBP lacking cultures.

Figure 21. Single-nucleus RNA sequencing analysis of differentiated neurospheres revealed alterations in several populations of P300 lacking cultures.

Figure 22. Spatio-temporal expression pattern of CBP and P300 in the retina.

Figure 23. CBP is expressed in a large number of retinal progenitors at early embryonic stages.

Figure 24. Characterization of Rx-Cre mouse line in the retina.

Figure 25. P300 ablation in retinal progenitors do not alter retinal formation.

Figure 26. Embryonic ablation of P300 in retinal progenitors do not trigger alterations in retinal cell layers.

Figure 27. CBP ablation in retinal progenitor cells alters retinal formation.

Figure 28. Embryonic ablation of CBP in retinal progenitors generate alterations in retinal cell layers.

Figure 29. CBP ablation in retinal progenitors leads to aberrant retinal structures joined to cell death.

Figure 30. Simultaneous ablation of both KAT3 proteins in retinal progenitors leads to a severe phenotype and embryonic lethality.

Figure 31. Cultured newborn neurons lacking P300 do not show altered maturation.

Figure 32. Individual ablation of CBP or P300 in postmitotic RGCs do not alter RGCs specification.

Figure 33. Simultaneous ablation of both KAT3 proteins in postmitotic RGCs reveal a loss of the RGC marker Brn3a without alteration in the visual pathway.

Table 1. Summary of the results presented in this Thesis work.

ABSTRACT

ABSTRACT

Rubinstein-Taybi syndrome (RSTS) is a genetic neurodevelopmental disorder characterized by mental impairment and a wide spectrum of congenital abnormalities, that is caused by hemizygous mutations in the KAT3 proteins CBP and P300. The precise function of KAT3 proteins during the development of the central nervous system has not been clearly stated. Here, throughout a combination of *in vitro* and *in vivo* approaches we dissect the functions of CBP and P300 in different steps of neural development. We first demonstrate *in vitro* that proliferation of neural progenitors is not affected in the absence of CBP or P300 but is seriously compromised when both proteins are absent simultaneously. In addition, elimination of either CBP or P300 impedes neuronal and glial differentiation although they are not individually required to preserve neuronal identity. Removal of CBP, p300 or both in retinal progenitors or postmitotic retinal ganglion cells confirm these results *in vivo* and demonstrate that CBP plays a more prominent role than P300 during retinal differentiation. These data contribute to a better understanding on the individual roles of KAT3 proteins in neural differentiation and may help on the prevention and treatment of RSTS patients.

RESUMEN

El Síndrome de Rubinstein-Taybi (RSTS) es un trastorno genético del neurodesarrollo caracterizado por retraso mental y un amplio espectro de anomalías congénitas, el cuál es causado por mutaciones en hemizigosis en las proteínas de la familia KAT3 CBP y P300. La función exacta de las proteínas KAT3 durante el desarrollo del sistema nervioso central no está aun clara. Así, mediante la combinación de experimentos *in vitro* e *in vivo* hemos diseccionado las funciones de CBP y P300 en los diferentes pasos del desarrollo neural. Primero, observamos que la proliferación de los progenitores neurales *in vitro* no está afectada en ausencia de CBP o P300, pero si seriamente comprometida cuando ambas proteínas son eliminadas simultáneamente. Además, vimos que la eliminación de CBP o de P300 impide la diferenciación neuronal y glial a pesar de que estas proteínas no son necesarias individualmente para preservar la identidad neuronal. Finalmente, la ausencia de CBP, P300 o ambas tanto en progenitores como en neuronas retinales confirman estos resultados *in vivo* y demuestran que, al menos en retina, CBP ejerce un papel más prominente que P300 durante la diferenciación. Estos datos contribuyen a una mejor comprensión de los papeles individuales de las proteínas KAT3 en la diferenciación neural y podrían ayudar en la prevención y tratamiento de los pacientes con RSTS.

INTRODUCTION

Introduction

With a prevalence of around 2% worldwide, intellectual disability disorders (IDD) are characterized by impaired cognitive abilities, commonly defined by an IQ score of below 70, accompanied by severe deficits in functional, social and adaptive skills. The causes of IDDs are extremely heterogeneous and include environmental factors such as toxic substances, and genetic factors for instance chromosomal aberrations or single gene mutations. Recent human genetics and clinical research have identified multiple genes involved in cognitive and learning disorders, including genes encoding epigenetic factors that control gene expression (Kleefstra *et al.*, 2014). Certain of these ID-linked epigenetic regulators have been identified to regulate chromatin structure at relevant genes involved neurodevelopment and/or neuroplasticity (Kandel, 2001). As a result, during the last decade numerous researches have been focused on figure out the role of epigenetic regulators of the chromatin in developmental and neuronal plasticity processes in the brain (Sweatt, 2013; Zocchi and Sassone-Corsi, 2010).

In particular, the acetylation of lysine in the histone tails, an epigenetic modification of the chromatin associated generally with active transcription, is thought to play a prominent role in the etiology of Rubinstein-Taybi syndrome (RSTS, OMIM #180849, #613684). This rare autosomal dominant disorder, defined by a wide spectrum of congenital abnormalities and intellectual disability (ID), is caused by mutations in the genes encoding the lysine acetyltransferases (KAT3 proteins) CBP and p300, which account for approximately 60% and 5% of the cases, respectively (Negri *et al.*, 2016; Spena *et al.*, 2015). Although the function of these proteins has been extensively studied, the specific events downstream of CBP and p300 deficiencies responsible for neurodevelopmental and cognitive deficits in RSTS patients remain unclear.

The aim of this Thesis work is to determine the precise roles of these KAT3 proteins in the different stages of neural development, using the visual system and neurospheres as a model, to deciphering the involvement and redundancy of KAT3 proteins in processes underlying the etiology of RSTS, which may contribute to improve the diagnostic but also novel therapeutic perspectives.

1.1 General principles of epigenetics

Complex biological processes occurring during development are rigorously regulated by genetic programs refined by epigenetic modifications of the chromatin to establish cell fate, differentiation, cell death or respond to changes in the environment or experience, among others.

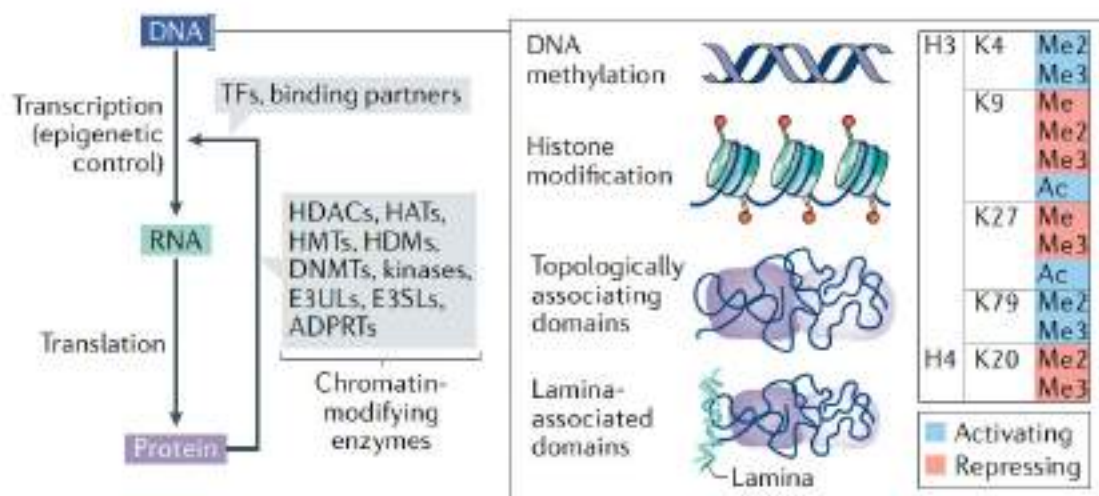


Figure 1. Epigenetic regulation of gene expression by chromatin modifications. Enzymes involved in epigenetic modification include: histone deacetylases (HDACs), histone acetyltransferases (HATs), histone methyltransferases (HMTs), histone demethylases (HDMs), DNA methyltransferases (DNMTs), kinases, E3 ubiquitin ligases (E3ULs), E3 small ubiquitin-like modifier ligases (E3SLs) and ADP- ribosyl transferases (ADPRTs). Typical activating (blue boxes) and repressing (red boxes) histone acetylation (Ac) and methylation (Me) marks in H3 and H4 are represented. Adapted from Nemeč and Kilian 2020.

The dynamic epigenetic regulation of gene expression patterns includes a huge variety of enzymatic activities modifying chromatin (**Fig.1**), for instance, DNA methylation or posttranslational modifications of histone tails such as histone acetylation/deacetylation, methylation/demethylation, phosphorylation, ubiquitination or ADP-ribosylation, activating or repressing gene expression depending on the specific location and environment by adding chemical markers to histone residues ((Alfrey *et al.*, 1964; Opravil *et al.*, 2000; Kouzarides 2007; Guibert *et al.*, 2009; Moore *et al.*, 2012; Rando 2012; Vanzan *et al.*, 2017; Nemeč and Kilian 2021).

1.2 Regulation of gene expression by lysine acetylation

Among the multiple epigenetic mechanisms, acetylation and deacetylation of lysine residues of histone tails by lysine acetyltransferases (KAT) or deacetylases (KDAC) play a key role in modulating chromatin structure and function (Shahbazian and Grunstein, 2007). A switch in the balance of histone acetylation levels change chromatin structure allowing or repressing gene expression (Valor *et al.*, 2013). In that way, the acetylation of lysine residues in histone tails usually counteracts its positive charge and reduces the contacts with the DNA, causing a chromatin relaxation and allowing the recruitment of transcription factors and transcriptional complex to induce gene expression (Roth *et al.*, 2001). In an opposite way, KDACs induce chromatin condensation and silencing of gene expression (Rundlet *et al.*, 1998) (**Fig. 2**). However, genomic studies indicate that both KAT and KDAC proteins are present at the same time (Wang *et al.*, 2009) in active or inactive genes, and the balance between both enzymatic activities

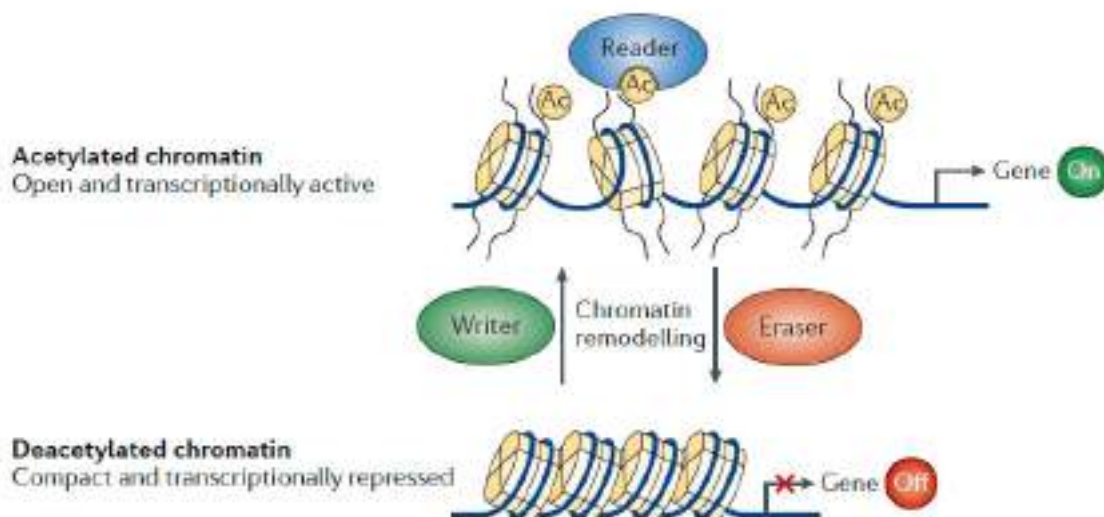


Figure 2. Lysine acetylation, chromatin condensation and gene expression. Acetylation of lysine targets on histone tails results in chromatin decondensation allowing to transcription factors, cofactors and the transcriptional machinery to access, whereas deacetylated chromatin are compact repressing transcription. Adapted from Verdin and Ott 2014.

define gene expression. Therefore, acetylation/deacetylation appear to be necessary but not sufficient to active or repress gene expression.

The balance between acetylation and deacetylation is very plastic and can be modulated according to cell requirements such as neuronal activity (Impey *et al.*, 2002), memory acquisition (Gräff, 2013, Lopez-Atalaya and Barco, 2014), learning (Maddox *et al.*, 2013), plasticity processed (Tapias and Wang, 2017) or in response to stimuli, among others.

In accordance to their cellular location, acetyltransferases are grouped in two general classes: Type B, located in the cytoplasm, which catalyze the acetylation to the new synthesized histones, and Type A, in the nucleus, catalyzing acetylation in transcription-related events. According to their sequence homology, KAT proteins are classified in four families: CBP/P300, GNAT, MYST, Basal transcription factors and Nuclear receptor cofactors (Roth *et al.*, 2001; Tapias and Wang 2017). In this work, I will exclusively focus on the nuclear Type A KATs CBP/P300.

1.3. *KAT3 proteins: CBP and P300*

Due to their low sequence homology with other acetyltransferases, the KAT3 family is integrated only by cAMP Response Element-Binding Protein (CREB)-binding protein (CBP, also known as KAT3A) and E1A binding protein (p300, also called KAT3B). Encoded by *Crebbp* and *Ep300* genes respectively, these genes are highly conserved through evolution and at least one of them is present in multicellular organisms such as flies, worms or plants, but is not present in lower eukaryotes (Arany *et al.*, 1994; Yuang and Giordano 2002; Kalkhoven 2002).

Both CBP and P300 are ubiquitously expressed in vertebrate tissues and, since their discovery, some studies have suggested that they are extensively interchangeable in function. Nevertheless, single-cell RNA sequence studies in mice have recently revealed that although both genes are ubiquitously expressed in the central nervous system (CNS), *Crebbp* gene expression is higher than *Ep300* (**Fig.3**) (Lipinski *et al.*, 2019).

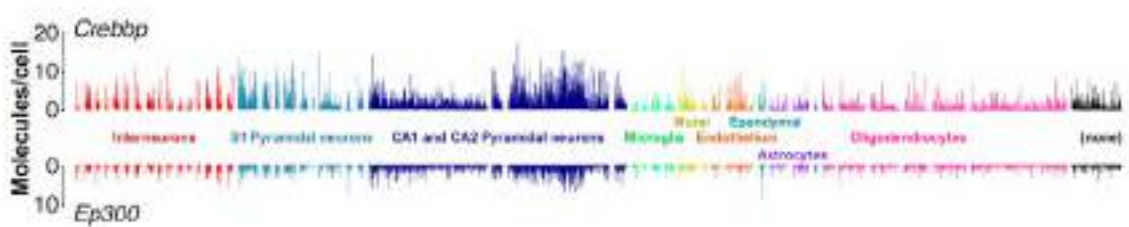


Figure 3. KAT3 expression levels in different neural cell types. Single-cell RNA-Seq data in mice reveals a higher expression of *Crebbp* than *Ep300* in the different neural cell types analyzed. Adapted from Lipinski *et al.*, 2019.

KAT3 proteins have been considered redundant in terms of function but, the differential expression levels and its association with different proteins and substrate specificity (Henry *et al.*, 2015) could be presumably related to their involvement in unique roles as it has been evidenced in myogenesis, in which CBP and P300 regulate different gene sets to control several aspects of myogenic program (Fauquier *et al.*, 2018),

in apoptotic response to DNA damage (Yuang *et al.*, 1999), axonal regeneration (Perrine *et al.*, 2011), tumorigenesis (Wang *et al.*, 2013), or neuronal plasticity and cognition (Roelfsema *et al.*, 2005; Lopez-Atalaya *et al.*, 2012), among others.

1.3.1 Molecular structure

CBP and P300 are large nuclear multidomain proteins with a molecular mass of around 250kDa. Both proteins share a similar structure with differentiated functional domains. From the N-terminal side, a nuclear receptor interaction domain (NRID or RID), that can bind to PXXP motifs, three cysteine-histidine-rich regions (C/H1 to C/H3) involved in protein–protein interactions, which contain zinc finger transcriptional adapters (TAZ1, TAZ2 and ZZ) and C/H2 contains a homeodomain (PHD); the catalytic domain KAT; the KIX domain allows the interaction of phosphorylated CREB and with other transcription factors; and finally, a bromodomain (BD) links acetylated lysines (Abdolmaleky *et al.*, 2005) and specific transcription factors (Polesskaya and Harel-Bellan, 2001). On the C-terminal side of p300/CBP, there is an interferon-binding transactivation domain (IBiD), which contains a nuclear binding coactivator domain (NCBD) (**Fig.4**).

Comparison of amino acid sequence reveals a 58% of sequence identity and the catalytic domain (KAT) and flanking regions have been highly conserved during evolution with 86% of correspondence between CBP and p300 (Breen and Mapp 2018). Other non-catalytic domains also present a high sequence similarity.

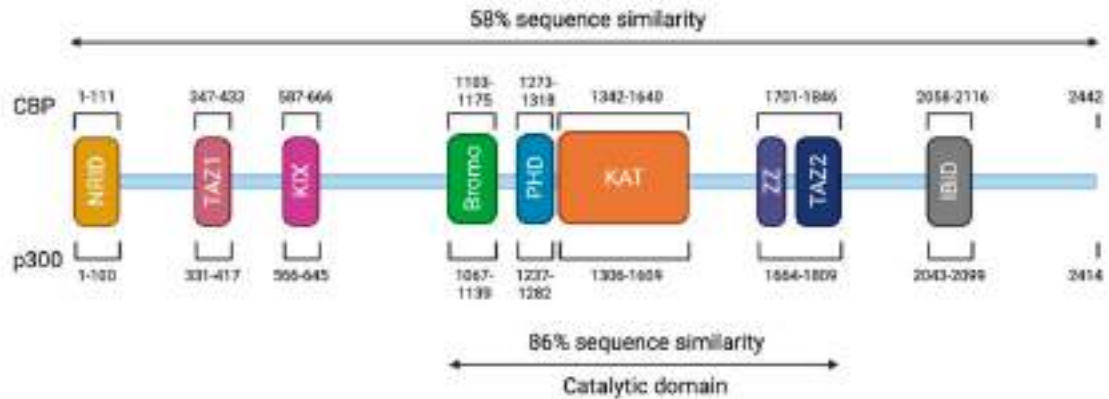


Figure 4. KAT3 protein structure. CBP and P300 proteins share 58% of sequence within their domains. The different domains correspond to nuclear receptor interaction domain (NRID), a kinase-inducible domain for interaction with CREB (KIX), a Bromodomain (Bromo), a Lysine acetyltransferase domain (KAT), an interferon binding transactivation domain (IBiD), and three putative zinc finger domains: transcriptional adapter zinc-binding motifs (TAZ1 and TAZ2), plant homeodomain finger (PHD) and ZZ-type Zinc finger domain (ZZ). Adapted from Van Gils *et al.*, 2021.

1.3.2 Functional heterogeneity

KAT3 proteins have diverse functions related to transcriptional regulation. One of their well-documented functions is to facilitate the formation of the transcription complex, acting as a molecular bridge between DNA-binding transcription factors and the general transcription machinery of RNAPol II. More than 300 transcription factors have been identified as part of this P300/CBP-dependent transcriptional machinery (Chang and La Thangue, 2001; Kasper *et al.*, 2006; Bedford *et al.*, 2010). Thus, CBP and P300 exhibit a widespread occupancy of transcriptional regulatory regions such as enhancers, and they have been proposed to play an important role in transcriptional initiation (Imnof *et al.*, 1997) (**Fig.5**).

CBP and P300 are also able to bind to a large abundance of proteins, more than 410 (Dancy and Cole, 2015), including kinases, chromatin remodelers, acetylated proteins as well as, the cited transcription factors, at the same time (Bedford *et al.*, 2010; Yi *et al.*,

2015) to act as a molecular scaffold that bring a variety of enzymatic activities to the promoter. These interactions are possible because of the domains that flank the catalytic domain (KAT), the bromodomain and the cysteine-histidine rich domains.

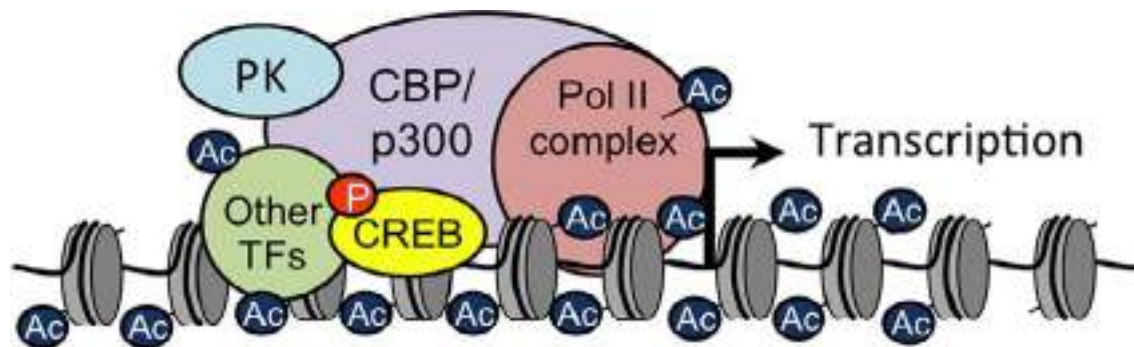


Figure 5. KAT3 protein regulate transcription through different functions. CBP and P300 act as transcriptional coactivators by different mechanisms: 1) acting as a molecular bridge between transcription factors and the RNAPolIII complex; 2) acting as a molecular scaffold that bring numerous enzymatic activities to the promoter; 3) KAT3 catalyze the transfer of acetyl groups on lysine residues in the histone tails and 4) also acetylates non-histone substrates such as transcription factors or subunits of the RNAPol II complex. Adapted from Lopez-Atalaya *et al.*, 2014.

Furthermore, KAT3 proteins have acetyltransferase activity (HAT) (Bannister and Kouzarides, 1996; Ogryzko *et al.*, 1996), transferring an acetyl group to lysine residues of histone and also non-histone substrates which cause the remodeling of the chromatin that has been established to be an essential mechanism of transcriptional regulation (Armstrong and Emerson 1998) (**Fig 5**).

1.4 Rubinstein-Taybi Syndrome, an intellectual disability disorder caused by defects in the epigenetic regulators CBP and P300

Rubinstein-Taybi Syndrome (RSTS) is a rare neurodevelopmental genetic disorder, described in 1963 (Rubinstein and Taybi 1963) caused by CBP (RSTS1; OMIM #180849) or P300 (RSTS2; OMIM #613684) haploinsufficiency (Stevens 2002; López-Atalaya et al., 2014) that affects 1 in 100.000 to 1 in 125.000 newborns (Hennekam 2006). The transmission is autosomal dominant and, in general, RSTS occurs as the result of *de novo* mutations (99% of the cases) although a few familiar cases have been reported (Hennekam *et al.*, 1989; Bartsch *et al.*, 2010; López *et al.*, 2016).

RSTS patients present skeletal abnormalities such as broad thumbs and big toes which are used in diagnosis and alternatively refer the disease as “broad thumb-hallux syndrome (Tapias and Wang, 2017). This syndrome is characterized by a broad spectrum of alterations such as delayed cognitive development, mild to severe intellectual disability or postnatal growth deficiency (Hennekam 2006). Their facial features are also distinctive, with arched eyebrows, highly arched palate, microcephaly, down-slanting palpebral (eyelid) fissures, broad nasal bridge, beaked nose, eye anomalies and mild micrognathia (Roelfesma and Peters 2007). Numerous malformations have been reported, including visual (Brei *et al.*, 1995; Van Genderen et al., 2000), cardiac, digestive, skin anomalies and patients also present a high risk of developing tumors (Milani *et al.*, 2015; Boot *et al.*, 2018).

Related to the neurological symptoms, RSTS patients exhibit anatomical defects in the brain such as agenesis of the corpus callosum, cortical clefts, cerebellar and cranial malformations; and poor motor coordination, short attention, seizures and autistic

features (Milani *et al.*, 2015). Intellectual disability in patients with RSTS is constant and present from birth and increasing with the age ranging from 25 to 79 (Wiley *et al.*, 2003). The analysis of cells from RSTS patients have shown that this syndrome could be caused by aberrant chromatin regulation (López-Atalaya *et al.* 2014) and defects in neuronal function (Alari *et al.*, 2018).

The frequency of mutations in *Crebbp*, located on chromosome 16 p13.3, is approximately 55-75% of the RSTS cases (Roefselma *et al.*, 2005; Perez-Grijalba *et al.*, 2019) and mutations in *Ep300*, on chromosome 22q13.2, 8-11% of RSTS cases (Fergelot *et al.*, 2016; López *et al.*, 2018; Cross *et al.*, 2020), with milder symptomatology and IDD than *Crebbp* mutations (Tapias and Wnag 2017; López *et al.*, 2018). The mutational spectrum includes deletions, insertions, truncating mutations, splicing mutations, missense mutations and large rearrangements (Van Gils *et al.*, 2021).

1.4.1 Role of KAT3 proteins in neurodevelopment

The use of animal models, in particular of genetically modified mice, has greatly clarified the important role of KAT3 proteins in neural development.

In mammals, both proteins are required for early development. Homozygous mice lacking a functional *Crebbp* or *Ep300* gene die early during development, between embryonic day (E) 9 and E12.5 (Yao *et al.* 1998, Tanaka *et al.* 2000) due to a failure in neural tube closure and extensive brain hemorrhage. Death may also occur by exencephaly, abnormal blood vessel development and heart malformations (Yao *et al.*, 1998; Oike *et al.*, 1999; Tanaka *et al.*, 2000). The inability of one protein to compensate for the loss of the other suggests important divergence in function between CBP and p300 at these early steps.

Double heterozygous mice *Crebbp*^{+/-} and *Ep300*^{+/-} are also lethal (Yao *et al.*, 1998) whereas simple heterozygous mice for CBP or P300 are viable and fertile but exhibits skeletal abnormalities as RSTS patients (Tanaka *et al.*, 1997) indicating that specific levels of each of these proteins are essential for proper development.

Although early embryonic death of the conventional knockout mutant mice has not allowed to dissect the specific cellular and molecular function of CBP and p300 during development, the generation of a large number of conditional knockout mice make now possible their study through the different stages of development and analyses of CBP and P300 deficient mice have revealed specific processes in which only one of these proteins are required. For instance, mice with alteration in the KAT domain of P300 have defects in skeletal muscle, heart, lung of intestine whereas these defects are not observed in CBP mutants (Shikama *et al.*, 2003; Roth *et al.*, 2003).

Also several studies have been performed to analyze the role of CBP in differentiation and maturation of neurons. CBP has been involved in differentiation in glial cells and neurons of cortical precursors at later stages and *Cbp* haploinsufficiency causes early cognitive dysfunction in mice as it does in humans (Wang *et al.*, 2010); CBP is also involved in differentiation of spinal motor neurons (Lee *et al.*, 2009), interneurons (Tsui *et al.*, 2014; Medrano-Fernandez *et al.*, 2018), in differentiation of the fly retina (Kumar *et al.*, 2004), in synaptic maturation of hippocampal neurons (Del Blanco *et al.*, 2019) or in excitability of neurons derived from iPSCs of RSTS patients, which exhibit an impaired morphology and hipoexcitability (Alari *et al.*, 2018). Transcriptomic analyses of these neurons derived from iPSCs of RSTS patients reveals also a dysregulation during differentiation by deregulation of specific synaptic genes (Calzari *et al.*, 2020).

However, distinguishing the functions and redundancy of CBP and P300 during neuronal specification has not been clearly stated which is an important step to understand and in order to find treatments to RSTS.

1.4.2 Role of KAT3 proteins in adulthood

In adulthood, animal models have shown that some cognitive deficits are not due to defects originated during development but result from the continued requirement of CBP/p300 activities throughout life (Korzus et al., 2004; Viosca et al., 2010; Valor *et al.*, 2013; Lopez-Atalaya *et al.*, 2014). For instance, CBP deficiency causes severe histone deacetylation in neurons (Alarcon *et al.*, 2004; Wang *et al.*, 2010; Valor *et al.*, 2011), which may play an essential role in the etiology of cognitive deficits, because a number of studies have shown that histone acetylation correlates with memory formation in diverse paradigms (Graff and Tsai, 2013). Importantly, similar histone deacetylation defects have been also reported in cell lines derived from patients (Lopez-Atalaya *et al.*, 2012). A recent study have shown that the absence of both KAT3 proteins in adult forebrain excitatory neurons results in loss of neuronal identity (Lipinski *et al.*, 2020).

Overall, despite the consequences in the adult are milder compared to the dramatic phenotypes observed during development, these studies highlighted the significant role of KAT3 proteins in processes related to neural plasticity including memory formation and consolidation, or learning.

1.5 Visual system as a model to study the development of neural circuits

The vertebrate visual system is a well-characterized and widely used model to unravel the different processes occurring in CNS development. The separated location of neuronal cell bodies in different layers of the retina as well as the long projecting axons of the retinal ganglion cells to the visual nuclei of the brain facilitate the dissection of different processes such as proliferation and differentiation; or axon guidance and assembly at the visual targets.

1.5.1 Basic anatomy of the mammalian visual system

The adult vertebrate retina is integrated by three layers of nerve cells bodies separated by two plexiform layers containing the synapses between these cells. These layers are composed by six neuronal cell types: the photoreceptors (rods and cones), located in the outer nuclear layer (ONL). These cells are specialized in detecting and responding to light and transmit the electrical signals to the three types of retinal interneurons (amacrine, bipolar and horizontal cells). Retinal interneurons are located in the inner nuclear layer (INL), which filter, shape and transmit this visual information to retinal ganglion cells (RGCs). RGCs are in the inner surface of the retina or ganglion cell layer (GCL) (Huberman *et al.*, 2011) (**Fig 6**). One glial cell type is present in the retina, the Müller glial cells, which are located in the INL.

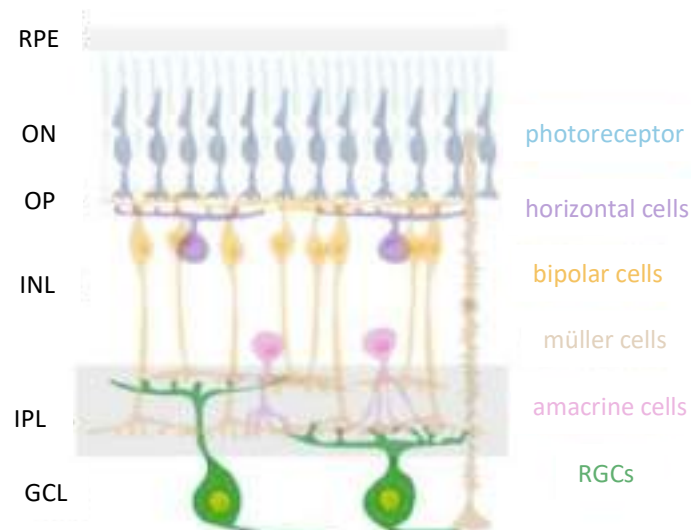


Figure 6. Organization of vertebrate retina. From the inner surface of the retina, the ganglion cell layer (GCL) containing RGCs and few displaced amacrine cells; the inner plexiform layer (IPL) where bipolar cell axons synapse with RGCs and amacrine cells; the inner nuclear layer (INL) containing bipolar, horizontal, amacrine and Müller glial cells; the outer plexiform layer (OPL) with axonal projections of photoreceptors which synapse with dendrites of bipolar and horizontal cells; and the outer nuclear layer (ONL) where cell bodies of rods and cones are located. In the outer part of the retina is located the retinal pigmented epithelium (RPE). Adapted from Belmonte and Erksine 2019.

Among 46 transcriptional subtypes of RGCs have been described, that are the only retinal cell type that send axons to the visual targets at the brain (Sanes and Masland 2015; Baden *et al.*, 2016; Rheaume *et al.*, 2018; Laboissoniere *et al.*, 2019; Tran *et al.*, 2019). They are specialized in specific aspects of visual modalities. RGCs axons pass across the internal surface of the retina to exit the eye at the optic disc and form the optic nerve travelling along the ventral midline of the diencephalon to reach the optic chiasm. At this point, the majority of axons cross the midline at the chiasm and project contralaterally to their visual targets but, depending of the degree of binocular overlap in the visual field of each mammal species, a variable number of axons do not cross and project ipsilaterally. Through evolution, the development of binocular vision has been correlated with the frontalization of eyes and, as a result, a higher number of ipsilateral projecting axons (Jeffery and Erksine, 2005). From the chiasm, axons navigate through the ipsilateral or contralateral optic tracts to their visual targets. Although RGCs connect to numerous nuclei at the brain (Morin *et al.*, 2014), the dorsal lateral geniculate nucleus (dLGN) and the superior colliculus (SC) are their main targets. In these visual targets, axons arborize creating a topographic map. Thus, the spatial distribution among RGCs in the retina is maintained in the visual target cells in a nonoverlapping territories called eye-specific domains (Godement *et al.*, 1984). Ipsilateral and contralateral projections form different

patterns at the visual nuclei. Thalamocortical neurons then synapse at the cortex where visual information is integrated with other sensory modalities (**Fig. 7**).

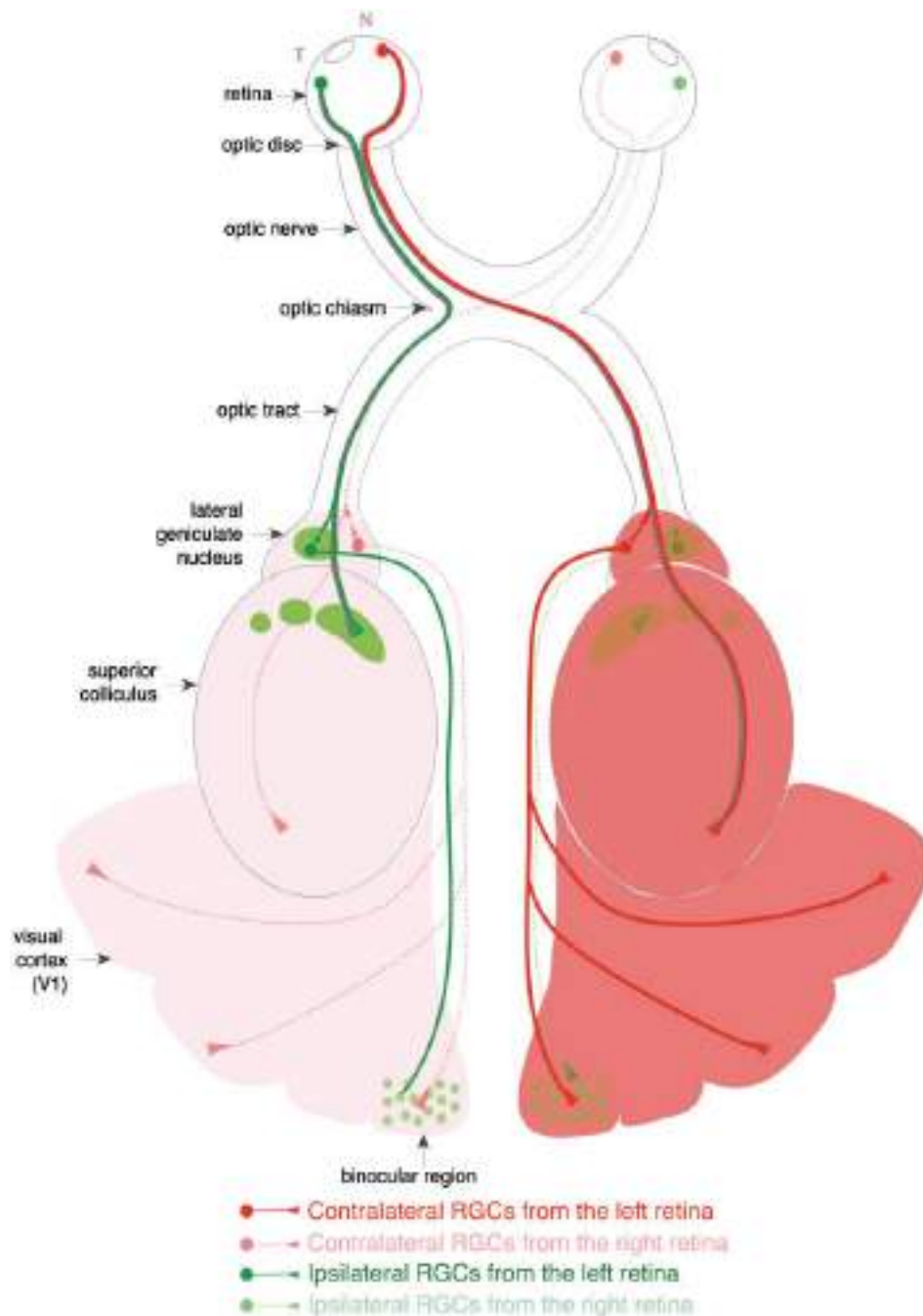


Figure 7. Schematic representation of visual pathway of mice. RGCs extend their axons to leave the retina through the optic disc, forming the optic nerve. Optic nerves reach the chiasm where they cross or avoid the midline and project contralaterally or ipsilaterally in the optic tracts to the main visual targets: dLGN and the SC. Ipsilateral and contralateral axons form different topological patterns at the visual nuclei. Visual information from dLGN is transmitted to the visual cortex. Adapted from Erksine and Herrera 2014.

1.5.2 Retinal development

The optic vesicles emerge very early during embryonic development from a single field located centrally in the developing forebrain. The vertebrate retina is derived from the lateral neuroepithelium of the anterior neural plate that begins to evaginate after neural tube closure generating the bilateral optic vesicles (in the mouse at embryonic day 8.5 (E8.5)). Each optic vesicle contains the retinal stem cells that give rise to all the retinal cell types. In mice, around E8.5 of mouse development, optic vesicles come into contact with the epithelium where lens placode will form, and this contact induces the coordinated invagination of the lens placode and the optic vesicles leading to the formation of a double-layered structure known as the optic cup while lens placode forms the lens pit. The inner layer of the optic cup develops into the neural retina (NR) whereas the outer layer will give rise to the retinal pigmented epithelium (RPE). An additional invagination takes place in the ventral optic cup to generate the optic stalk which subsequently diminishes and leads to the optic nerve, along which retinal axons traveling to the brain and arteries entering the eye (**Fig. 8**) (Heavner and Pevny 2012).

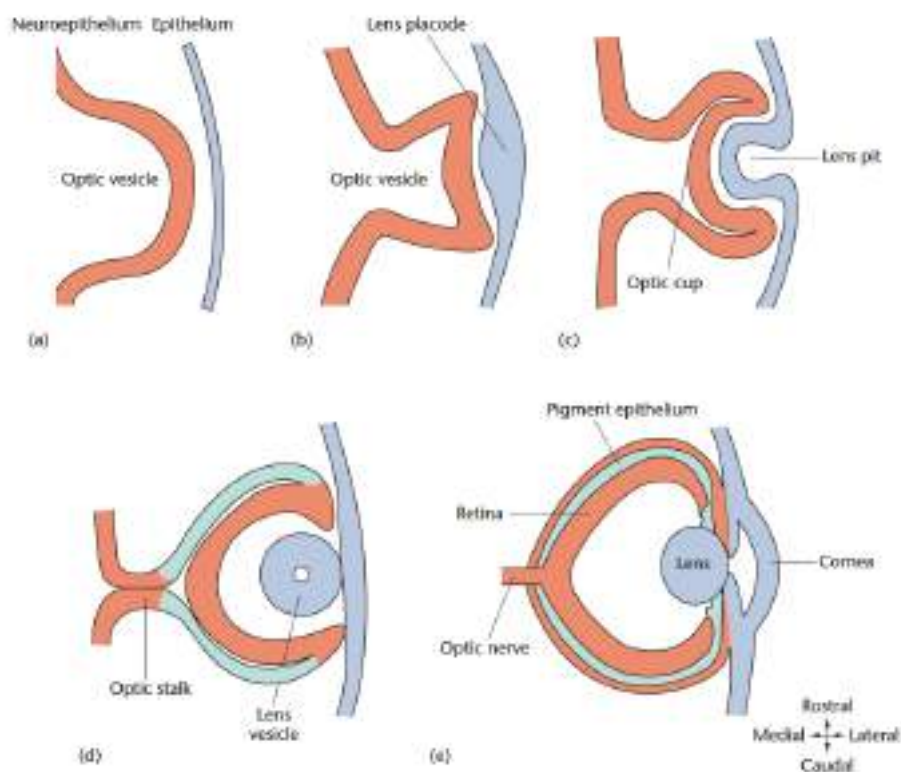


Figure 8. Schematic representation of development of the vertebrate eye.(a) Lateral neuroepithelium invaginates to form the optic vesicles which contact with epithelium (b) to form the bilayered optic cup whereas lens placode forms the lens pit (c). (d) Lens tissue gives rise the lens vesicle and the constriction of neuroepithelium forms the optic stalk. (e) The outer part of the optic cup established the RPE and the inner part forms the retina, whose retinal axons exit the eye to the brain forming the optic nerve. Adapted from Herrera and Erksine 2005.

Throughout neurogenesis, retinal progenitor cells (RPCs) suffer symmetric and asymmetric divisions, giving rise to both RPCs as well as postmitotic neurons. By embryonic day 10.5 (E10.5), RPCs are translocated to the apical-basal membrane while their cell fate is determined. When these cells divide, their nuclei migrate from the outer surface (apical membrane) of the NR to the inner part (basal membrane) and back again during cell cycle, producing a pseudostratified epithelium in a process called interkinetic nuclear migration (Baye and Link, 2007). After several divisions, a combination of intrinsic and extrinsic factor determines whether RPCs remain in cell cycle or activate an appropriate differentiation program and migrate to their correct final location in the retina to terminal differentiation (Buenaventura *et al.*, 2018) (**Fig. 9**).

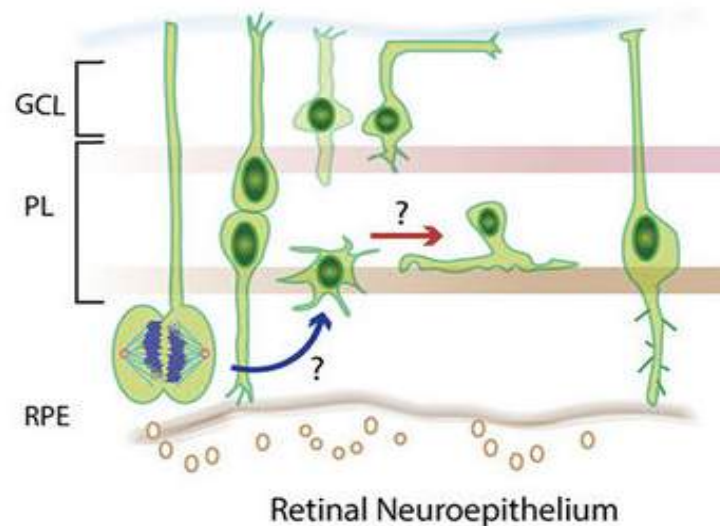


Figure 9. Neurogenesis in the embryonic vertebrate retina. RPCs at the apical membrane divide repeatedly. The establishment of the retinal layers requires postmitotic detachment of retinal progenitors from the apical surface, reorganization of polarity and migration to the appropriate layers. Daughter cells migrate from the RPE to its final spatial location depending on the acquired fate. Adapted from Sigh and Solecki 2015.

Cell lineage analyses have shown that RPCs remain multipotent and give rise in their progenies to several different cell fates (Turner and Cepko, 1987; Wetts and Fraser, 1988). Differentiation begins in the center of the neural retina to the periphery and occurs in a stereotyped birth order, that is well conserved in vertebrate species. The different retinal cell types are generated in overlapping but sequential waves with RGCs differentiating first, from embryonic day 11 (E11) to postnatal day 0 (P0), and migrating to the inner surface and extending a single axon (Drager 1985; Turner *et al.*, 1990; Hugnagel *et al.*, 2010). The next neurons to be produced are cone photoreceptors, amacrine interneurons and horizontal interneurons which are born mainly during embryonic development (first wave of retinogenesis E11-E18). A temporal switch in differentiation of RPC produce, postnatally, late-born bipolar interneurons and rod photoreceptors (second wave of retinogenesis P0-P7). Müller glia cells are the last to differentiate from the multipotent RPC (**Fig.10**). Despite to this general order, it is important to highlight that there is an overlap in the production of retinal cell types through the time.

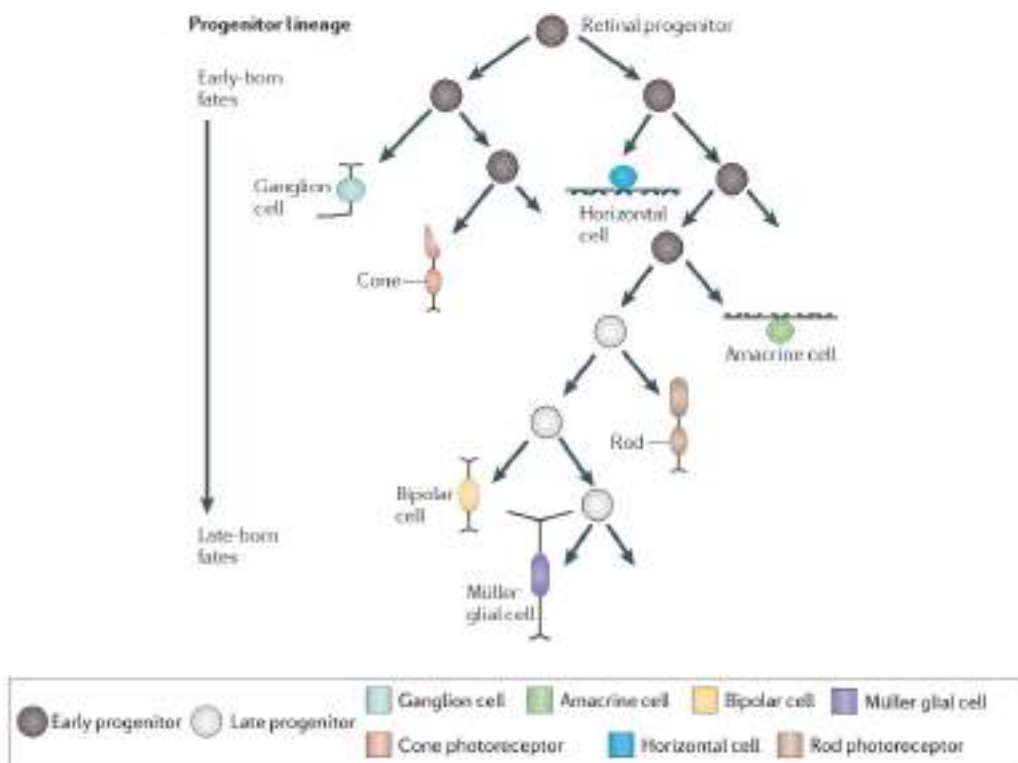


Figure 10. Temporal fate specification in the retina. RPCs give rise all the retinal cell types in an overlapping but sequential order. Early retinal differentiation is characterized by the production of early-born neurons: RGCs, cone photoreceptors, amacrine cells, horizontal interneurons. Late progenitors generate bipolar interneurons, rod photoreceptors and Müller glial cells. Adapted from Kohwi *et al.*, 2013

Transcriptome analysis of single retinal progenitor cells from different developmental stages revealed the sequential expression of transcription factors that includes paired box gene 6 (*Pax6*), sex-determining region Y-box containing gene 2 (*Sox2*), retina and anterior neural fold homeobox (*Rax* or *Rx*), or orthodenticle homolog 2 (*Otx2*) (Graw 2010), LIM homeobox 2 (*Lhx2*) and SIX homeobox 3 (*Six3*), among others. Several of these factors act as a key regulators of RPC development at later stages. For instance, *Pax6* is essential for maintenance of RPC multipotency (Marquardt *et al.*, 2001). Conditional inactivation of *Pax6* leads to generate only two retinal cell types: photoreceptor lineage and amacrine lineage (Oron-Karni *et al.*, 2008) since in the absence of *Pax6*, the key cell fate determination genes for differentiation of RGCs, neurogenin 2 (*Ngn2*) and atonal homolog 7 (*Atoh7/Math5*) are not expressed. *Sox2* regulates also multipotency of RPCs and it is required for neurogenesis in the retina (Taranova *et al.*, 2006; Pevny and Nicolis 2009). In these *Sox2*-deficient mice, *Pax6* expression is increased and RPCs fail to differentiate in neurons, adopting a non-neuronal fate that is characteristic of the peripheral retina. Moreover, in the central retina when neurons differentiate, the expression of *Sox2* is higher and *Pax6* lower. These findings suggest that a precise different balance between *Sox2* and *Pax6* expression is required for the maintenance of multipotency or differentiation in the retina (Matsushima *et al.*, 2011).

The different retinal cell types similarly require specific transcriptional programs that determine their fate (**Fig. 11**). More than 40 transcription factors involved in RPC differentiation through different activation and repression regulatory networks have been

described as well as their interaction with intrinsic and extrinsic mechanisms (Basset and Wallace 2012) (**Fig. 11**). Regarding the RGCs, the only retinal neurons that extend axons to the brain, the commitment of RPC to RGCs fate requires the expression of the transcription factor *Atoh7* (*Math5*), although this expression is necessary but not sufficient for RGC fate. RGCs specification requires key *Atoh7*-downstream targets such as the transcription factor *Brn3b* (*Pouf42*) or *Islet-1* (*Isl1*) to regulate their morphological differentiation and survival.

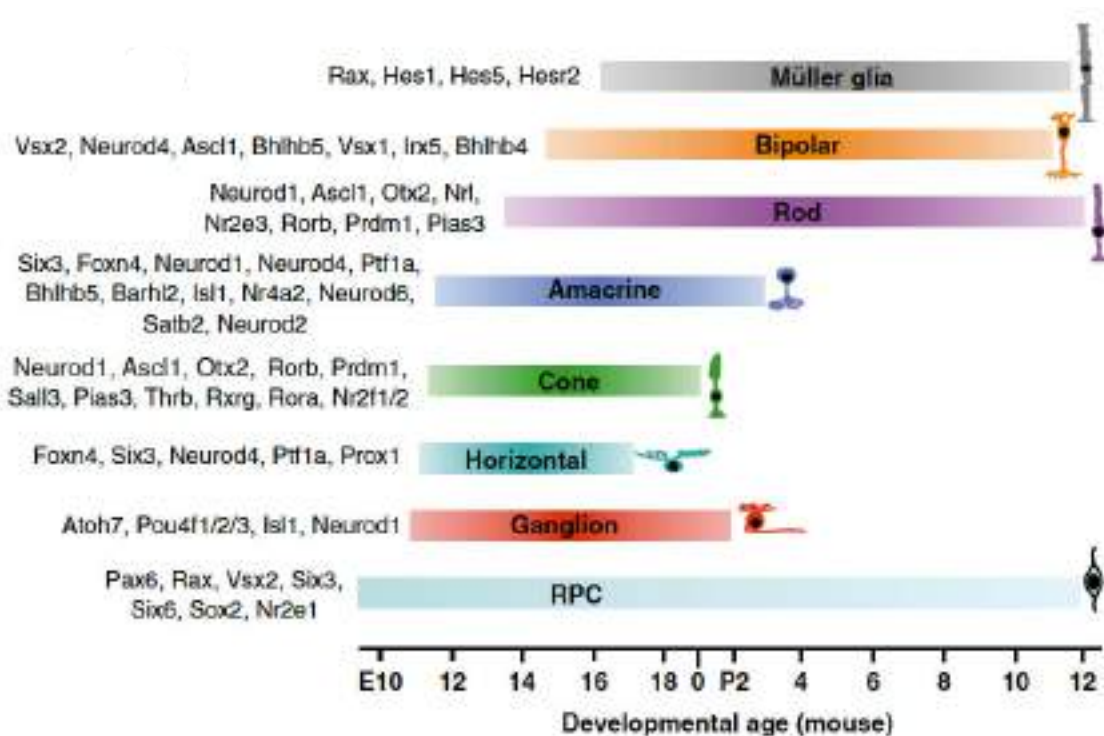


Figure 11. Transcriptional regulation of retinal cell type fates. Chronological expression of transcription factors expressed through RPCs proliferation and differentiation in the different retinal cell types. Adapted from Basset and Wallace 2012.

1.5.3 Development of the visual pathway in mammals

The development of the visual pathway begins at E10.5 just after differentiation of RGCs, when visual axons grow to exit the eye through the optic disc because of the repulsive environment created by chondroitin sulphate proteoglycan (CSPG) (Brittish *et*

al., 1997) and other inhibitory signaling molecules in the periphery of the retina, such as Slit proteins, whose receptor Robo is expressed by RGCs (Thompson *et al.*, 2006); as well as the higher expression of attractive signaling molecules in the central retina, such as Sonic hedgehog (Shh) (Kolpak *et al.*, 2005). Axon guidance cues force RGC axons to grow towards the optic disc, where the presence of a chemoattractive gradient of the axon guidance molecule Netrin-1 causes axons turn into the optic nerve (Deiner *et al.*, 1997). From E13 to E17, axons navigate throughout at the optic nerve due to the repulsive-free corridor delineated by Sema5A and Slit2 expression (Plump *et al.*, 2002; Oster *et al.*, 2003), reaching the optic chiasm (**Fig 12a**).

At the chiasm, many guidance molecules are essential to avoid or permit midline crossing (**Fig. 12b**). Axons from the ventrotemporal RGCs project to the ipsilateral side of the brain thanks to the expression of midline avoidance guidance cues including ephrin-B, whose receptor, EphB is expressed in ipsilateral RGCs controlled by Zic2 transcription factor (Herrera *et al.*, 2003; Garcia-Frigola *et al.*, 2008). Coupled to Eph-ephrin signaling, the Wnt signaling is also essential for axon midline decisions at the chiasm, being essential for both ipsilateral and contralaterally projecting axons (Morenilla-Palao *et al.*, 2020). Contralateral axons cross the midline and project into the contralateral tract mediated by the expression of the combination of NrCAM, Sema6D and Plexin-A1 (Kuwajima *et al.*, 2012) or neuropilin-1 (NRP1) and VEGF-A (Erksine *et al.*, 2011).

At postnatal stages, axons reach their visual targets (mainly dLGN and SC) and arborize extensively forming a fuzzy map, in which ipsilateral and contralateral axons overlap. During the first postnatal week, axons segregate by a refinement process to arbor specific domains and creating the final topographic map regulated by ephrin/Eph gradients (Herrera *et al.*, 2019) (**Fig. 12c**).

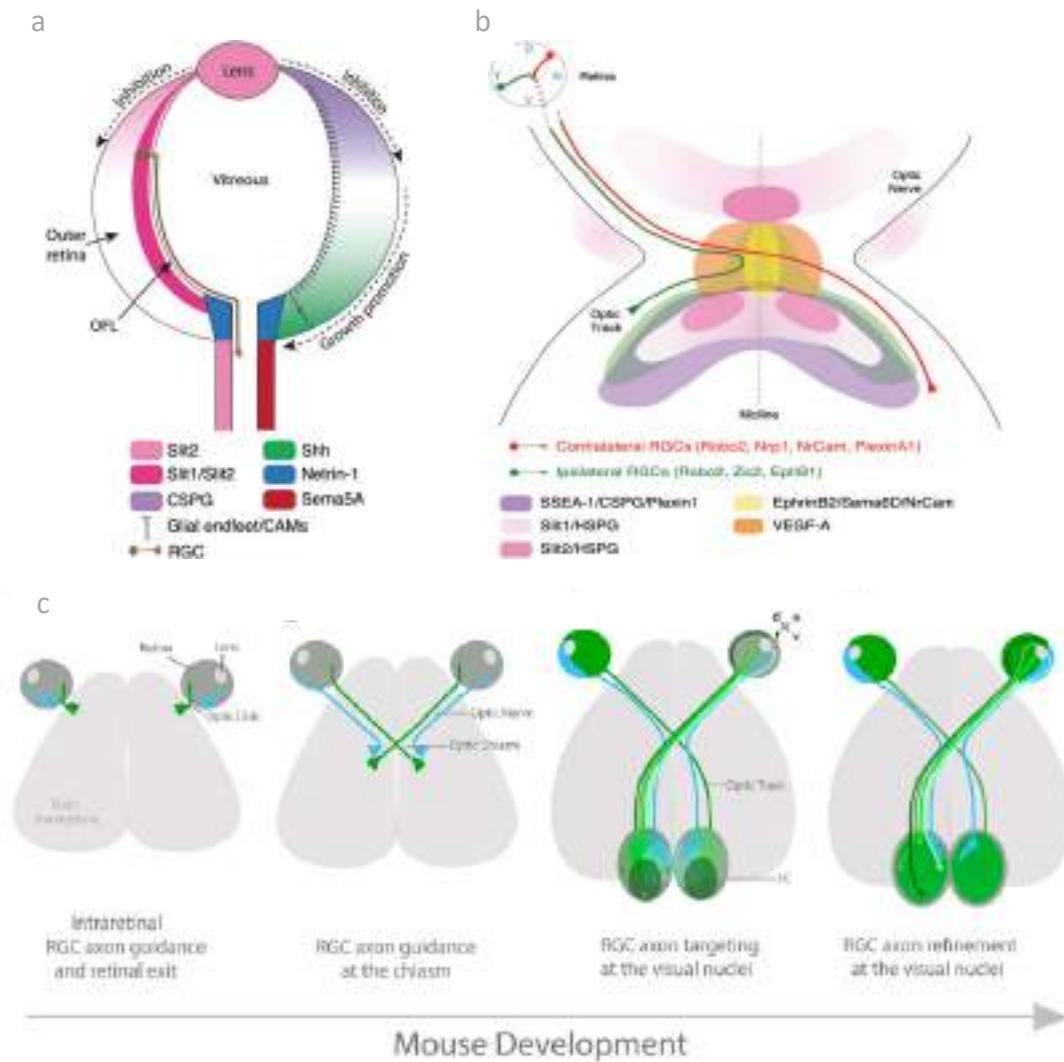


Figure 12. Development of the visual pathway and molecular mechanism underlying axon guidance at the optic chiasm. (a) Expression pattern of key axon guidance molecules that regulate RGC axon navigation at the retina. (b) axon guidance molecules expressing at the optic chiasm controlling axon midline avoidance or crossing. (c) At E10.5, RGCs begin to differentiate and extend their axons to the optic disc. From E13-E17, RGCs axons reach the optic chiasm, where axons from RGCs located in the ventrotemporal retina (blue) reach the midline and project into the ipsilateral optic tract. In contrast, axons from RGCs, located in the rest of the retina, cross the midline to project contralaterally. At postnatal stages, RGCs axons reach their different visual targets, mainly dLGN and SC. At these visual nuclei, axons arborize extensively, overlapping their projections following a topographic map. After a refinement process, RGCs establish their final topographic projection pattern. Adapted from Erksine and Herrera 2014 (a,b) and Herrera *et al.*, 2019 (c).

OBJECTIVES

Objectives

The main aim of this thesis work was to determine the role of KAT3 proteins in neural development. To address this issue, we defined the following objectives:

1. To answer whether CBP and P300 are required for proliferation and/or differentiation of neural progenitor cells.
2. To determine whether KAT3 proteins are necessary for maintenance of postmitotic retinal neurons.
3. To establish the extent of redundancy of these proteins in different cell types.

MATERIAL AND METHODS

1. Animals

We have used several transgenic mouse lines in this study. The generation of *Crebbpf/f* (CBP^{f/f}) (Zhang *et al.*, 2004), *Ep300f/f* (P300^{f/f}) (Kasper *et al.*, 2005), *CMVfxSTOPfx-tdTomato* (tdTomato^{f/f}) (Madisen, Zwingman *et al.* 2010), *CAG-Sun1/sfGFP-Myc* (Sun1-GFP^{f/f}) (Mo *et al.*, 2015), *Rx-Cre* (Swindell *et al.*, 2006), *Nestin-Cre* (Tronche *et al.*, 1999) and *Pou4f2-Cre* (*Brn3b-Cre*) (Simmons *et al.*, 2016) mice has been previously described. CBP^{f/f}, P300^{f/f} and *Nestin-Cre* mice were kindly provided by Angel Barco's lab (Institute de Neurociencias, Alicante, Spain). *Rx-Cre* and *Brn3b-Cre* mice were generously provided by Victor Borrell's lab (Instituto de Neurociencias, Alicante, Spain) and George Vann Bennett's lab (Duke University School of Medicine, Durham, United States) respectively. tdTomato^{f/f} and Sun1-GFP^{f/f} strains are available at the Jackson Laboratory with the stock number #7914 and #021039 respectively. The genetic background of all mice was C57BL/6. For developmental studies, embryonic day 0.5 (E0.5) was defined by the day of vaginal plug detection and day of birth as postnatal day 0 (P0). Mice were crossed in order to obtain double or triple transgenic mice.

To obtain CBP conditional knock-out mice, we crossed *Crebbp* flox/flox mice with mice carrying one allele of Cre recombinase under the control *Rx* promoter or *Brn3b* promoter. *Rx-Cre::CBP^{f/f}* or *Brn3b-Cre::CBP^{f/f}* were crossed with CBP^{f/f} to obtain homozygous mice for CBP^{f/f} and Cre recombinase.

To produce P300 conditional knock-out mice, we crossed P300^{f/f} mice with mice carrying one allele of Cre recombinase under the control *Rx* promoter, *Nestin* promoter or *Brn3b* promoter. *Rx-Cre::P300^{f/f}*, *Nestin-Cre::P300^{f/f}* or *Brn3b-Cre::P300^{f/f}* were crossed with P300^{f/f} to obtain homozygous mice for P300^{f/f} and Cre recombinase.

In order to generate double knock-out mice for *Crebbp* and *Ep300*, we crossed *CBP^{f/+}* and *P300^{f/+}* with mice carrying one allele of Cre recombinase under the control *Rx* promoter because homozygous mice for the two KAT3 proteins and Cre recombinase positive were lethal during development. *Rx-Cre::CBP^{f/f}::P300^{f/f}* were crossed with *CBP^{f/f}::P300^{f/f}* to obtain homozygous mice for *CBP^{f/f}::P300^{f/f}* and Cre recombinase.

NestinCre::P300^{f/f}, *Rx-Cre::CBP^{f/f}::P300^{f/f}*, *Brn3bCre::CBP^{f/f}*, *Brn3bCre::P300^{f/f}* and *Brn3bCre::CBP^{f/f}::P300^{f/f}* were compared with their control littermates, with no Cre recombinase expression. *Rx-Cre::CBP^{f/f}::tdTomato^{f/f}* mice were compared with *Rx-Cre::tdTomato^{f/f}* controls.

CBP, P300, TdTomato, Sun1 and Cre genotypes of mice were determined by PCR on DNA extracted from tail tissue using the following primers:

- CBP floxed allele (wild-type band 230 bp; mutant band 300 bp).
 - o fw: 5'-CCTCTGAAGGAGAAACAAGCA-3'
 - o rv: 5'-ACCATCATTCATCAGTGGACT-3'

- P300 floxed allele (wild type band 247bp; mutant band 400bp).
 - o fw: 5'-GTGAGTTGATGTCCCTGTCG-3'
 - o rv: 5'-CAGACACCC TCTTGCACTCA-3'

- TdTomato floxed allele (wild type band 297 bp; mutant band 196 bp).
 - o Wt fw: 5'-AAGGGAGCTGCAGTCGAGTA-3'
 - o Wt rv: 5'-CCGAAAATCTGTGGGAAGTC-3'
 - o Mut fw: 5'-CTGTTCCCTGTACGGCATGG-3'
 - o Mut rv: 5'-GGCATTAAAGCAGCGTATCC-3'

- Sun1 floxed allele (wild type band 557 bp; mutant band 300bp).
 - fw: 5'-GCACTTGCTCTCCCAAAGTC-3'
 - Wt rv: 5'-CATAGTCTAACTCGCGACACTG-3'
 - Mut rv: 5'-GTTATGTAACGCGGAACTCC-3'

- Nestin Cre recombinase transgene (wild type band 246bp; Cre band 150bp).
 - Fw: 5'-CCGCTTCCGCTGGGTCACACTGT-3'
 - Wt rv: 5'-CTGAGCAGCTGGTTCTGCTCCT-3'
 - Cre rv: 5'-GACCGGCAAACGGACAGAAGCA-3'

- Rx Cre recombinase transgene (Cre band 362bp).
 - fw: 5'-GTTGGGAGAATGCTCCGTAA-3'
 - rv: 5'-GTATCCCACAATTCCTTGCG-3'

- Brn3b Cre recombinase transgene (wild type band 500bp; Cre band 800bp).
 - fw: 5'-CGGAGCAGGGCACCTCTCG-3'
 - Wt rv: 5'-GGGTTGGAAGACAAGCTCTCCG-3'
 - Cre rv: 5'CGACCGGTAATGCAGGCAAAT-3'.

For all PCR reactions performed, thermocycling conditions were as follow: 95°C for 4 min followed by 35 cycles of 1 min at 95 °C, 1 min at 54 °C, and 1 min at 72 °C and a final extension at 72 °C for 10 min. All genotyping reactions contained

approximately 200 ng of DNA template, 0.5 μ M of each primer, 1.25 mM MgCl₂, 5 U/ μ L KAPA Taq DNA Polymerase and 1x KAPA Taq buffer in a 20 μ l final volume.

Mice were maintained at the Instituto de Neurociencias (IN) in a specific pathogen-free facility with 12 hr light/dark cycle, controlled temperature (22 ± 1 °C) and relative humidity ($55 \pm 5\%$) with food and water *ad libitum*. All animal experiments were approved by and performed in accordance with the protocols of the IN Animal Care and Use Committee and met Spanish (RD 53/2013 and European (2013/63/UE) regulations.

2. Lentiviral production

Lentiviral constructs of interest were *LV-CRE-mCherry* (Addgene #27546) to express Cre recombinase and ablate CBP, P300 or both proteins; and *LV-RFP* (Addgene #17619) as a control. Lentiviral particles (LV) were produced as previously described (Lois *et al.*, 2002). HEK293T cells were seeded in 25cm dishes at a density of 10^7 cells/dish, incubated overnight at 37°C with 5% CO₂ and transfected using calcium phosphate (CaPO₄) method with 20 μ g of lentiviral expression vector (*LV-CRE-mCherry* or *LV-RFP*), 15 μ g of *pCMV- δ 8.9* plasmid that expressing the gag and pol viral genes, and 10 μ g of *pCAG-VSVg*, a plasmid encoding VSV-G envelope gene. At 48h after transfection, supernatants were collected, centrifuged at 2000rpm for 5min and filtered to eliminate cell debris. Viral particles were concentrated with ultracentrifugation at 25.000rpm for 90min and aliquoted for immediate use or long-term storage at 80°C. Viral titers were determined by serial dilution on HEK293T cells and FACS analysis (BD FACSAria™ III Flow Cytometer), using non-infected cells as negative control. Usually with this protocol, viral titers were in the order of 10^8 - 10^9 viral particles/ml. Neural stem

cell (NSC) cultures were transduced at DIV1 with concentrated lentivirus at a multiplicity of infection (m.o.i) of 1-10.

3. Neurosphere culture

3.1 Establishment of a primary neural stem cell (NSC) culture

To establish primary neurosphere cultures, protocol was adapted from previous studies (Tropepe *et al.*, 1999; Belenguer *et al.*, 2016; Ferron *et al.*, 2007; Vernerey *et al.*, 2013; Xiong *et al.*, 2011). $CBP^{f/f}$, $P300^{f/f}$ or $CBP^{f/f}::P300^{f/f}$ mice pups (P0-P3) were sacrificed by decapitation and brains were extracted on iced cold Hank's balanced salt solution (HBSS, Gibco) removing meninges and blood vessels microscopically. Slices of 2-3mm containing the lateral ventricles were dissected under microscope, removing olfactory bulbs and the rest of the brain caudal to the slices. The subventricular zone (SVZ) were immediately dissected, incubated with 12.5 mg/ml trypsin (Sigma) at 37°C for 5 min followed by resuspension in HBSS with 10% fetal bovine serum (FBS, Gibco) to block enzymatic activity. SVZs were mechanically dissociated into a cell suspension with a fire-polished Pasteur pipette, centrifuged and resuspended in NSC complete serum-free media containing DMEM/F12 with L-Glutamine 1X (Gibco) supplemented with 0.6% D-glucose (Panreac), 0.1% $NaHCO_3$ (Sigma), 5mM HEPES (Gibco) 2mM L-Glutamine (Gibco), 1% penicilin/streptomycin (Gibco), 0.7 U/ml heparin sodium salt (Sigma), 4mg/ml bovine serum albumin (BSA) (Sigma), 0.8 mg/ml apo-transferrin (Sigma), 500nM bovine insulin (Sigma), 0.1mg/ml putrescine (Sigma), 0.2nM progesterone (Sigma), 0.3 μ M sodium selenite (Sigma), with growth factors (10ng/ml human recombinant basic fibroblast growth factor (bFGF) (Sigma) and 20ng/ml epidermal growth factor (EGF) (Gibco)) as mitogens. Cells were counted in a Neubauer

chamber and seeded at a density of 5×10^4 cells/ml in 24-well (0.5ml/well) uncoated ultra-low attachment plates (Corning®) and placed at 37°C with 5% CO₂ for 14 days. The day of plating was considered day *in vitro* 1 (DIV1).

3.2 Lentiviral infection of NSC cultures

To ablate CBP, P300 or both proteins, we infected NSC cultures with lentivirus that drive the expression of Cre recombinase with mCherry reporter (*LV-CRE-mCherry*) or with lentivirus with RFP reporter (*LV-RFP*) in control cultures at ODIV.

After 3-4d in culture, NSC had proliferated to form neurospheres and lentivirus began to be expressed. Fresh NSC complete medium with growth factors was added every 2-3 days.

3.3 The Neurosphere Assay (NSA)

In order to assess self-renewal and proliferation of NSC, we performed the clonal neurosphere assay (NSA) (Belenguer *et al.*, 2016). Free-floating neurospheres were pooled for enzymatic dissociation with Accutase® (Sigma), a reproducible method to obtain a single cell suspension with high viability. Approximately neurospheres from 20-24 wells were pooled in a 15ml tube per experimental condition and incubated with 200µL of Accutase for 10 min and mechanically dissociated to a single-cell suspension. After homogenization and dilution with complete medium, cell suspension was sorted by BD FACSAria™ III flow cytometer, isolating red fluorescent positive cells (lentiviral infected cells). Red fluorescent positive cells were seeded at a density of 2.5 cells/µL in 96-well ultra-low attachment plate (PrimeSurface® 3D culture S-Bio) to obtain a single pure isolated clone per well (Seaberg *et al.*, 2014). Cells were incubated at 37°C with 5%

CO₂ for 7days in complete medium with growth factors. Growth factors were added every 3 days.

After 7DIV, wells were photographed using a camera system coupled to an inverted microscope and primary sphere diameter of the single clonal neurospheres was estimated using Fiji analysis software and GraphPad Prism7™. To estimate average size of neurosphere population, 120 neurospheres from a minimum of 3 independent cultures were measured, taking the mean of the population diameter as a measure of culture proliferation (Xiong *et al.*, 2011).

3.4 Clonal differentiation of neurospheres

NSCs are able to proliferate and expand in the presence of mitogens (bFGF and EGF). Nevertheless, if mitogens are removed and we provide an adherent surface, NSCs stop proliferating and begin a differentiation program in the three main neural lineages: neurons, astrocytes and oligodendrocytes (Reynolds and Weiss, 1992).

To asses differentiation potential and multipotency, DIV7 clonal neurospheres were plated onto 12mm glass coverslips (VWR) coated with Matrigel® (Corning®) in differentiation medium I (NSC complete medium supplemented with 10ng/ml of bFGF) at 37°C with 5% CO₂ for 48h to allow neurospheres to attach to the coated surface and produce neuronal and oligodendroglial progenitor cells. After 2d differentiation medium I was replaced with differentiation medium II (NSC complete medium supplemented with 2% FBS in the absence of mitogenic factors) at 37°C with 5% CO₂ for 13d leading to the generation of a dense layer of astrocytes with neurons and oligodendrocytes. Media was not change for the rest of the culture. Differentiated cultures at 15DIV were used for single-nuclei RNA Sequencing (snRNA-Seq) or were fixed for immunocytochemistry.

In order to visualize migration of neurosphere cells across the surface in real-time, clonal neurospheres were plated on 24-well plate (Falcon) coated with Matrigel® (Corning®) in differentiation medium I. 24-well plates were inserted into IncuCyte FLR (Essen Biosciences) for real-time imaging, with whole well imaged under 4× magnification every 30 min for a total of 48 h. Data were analyzed using the IncuCyte Confluence version 1.5 software. All IncuCyte experiments were performed in triplicate.

4. Primary hippocampal culture

Primary hippocampal neurons were obtained from E17.5 embryos of NestinCre-P300^{fl/fl} where each embryo was used separately. Hippocampi were dissected as described previously (Benito *et al.*, 2011). Embryos were sacrificed by decapitation and brains were extracted on iced cold Hank's balanced salt solution (HBSS, Gibco) removing meninges and blood vessels microscopically. Hippocampi were dissected in cold HBSS (Gibco) and dissociated with 2.5% trypsin (Invitrogen) and 1% (wt/vol) DNase (Sigma) at 37°C for 5 min. After incubation, trypsin was carefully washed 3 times with plating medium (DMEM supplemented with 10% FBS (Sigma), 0.45% glucose (Panreac), 2 mm glutamine (Gibco), and 1% penicillin/streptomycin (Gibco)) and then mechanically dissociated. After tissue homogenization, cells were counted in Neubauer chamber and seeded in plating medium at a density of 130.000 cells/well in 24-well plates (Corning) on 12 mm glass coverslips (VWR) coated with poly-D-lysine (Sigma). After 2-3h plating medium was replaced with maintenance medium (Neurobasal medium (Gibco) supplemented with 2% B27 (Gibco), 2 mm glutamine, and 1% penicillin/streptomycin). Neurons were placed at 37°C with 5% CO₂ for 10 days. The day of plating was considered day *in vitro* 1 (DIV1).

For morphometric assays, hippocampal cultures at DIV9 were transfected with a plasmid driving the expression of GFP under synapsin promoter (pSyn-GFP) using Lipofectamine 2000 (Invitrogen) and cultures were fixed 24h after transfection.

5. Immunocytochemistry and immunohistochemistry

5.1 Immunocytochemistry in neurosphere and primary cultures.

To analyze the expression of neural progenitor markers, pure clonal neurospheres at DIV7 in 96-well plate were fixed with prewarmed 4% paraformaldehyde (PFA) prepared in phosphate buffered saline (PBS, 0.01M) for 15min at room temperature followed by 3 washes with PBS (5min each). Then neurospheres were permeabilized with 0.25% Triton™ X-100 (Sigma) in PBS for 10 minutes and incubated with blocking solution (1% BSA and 0.1% Triton™ X-100 in PBS) for 1h at room temperature. After blocking, they were incubated overnight at 4°C with the following primary antibodies: rabbit anti-Ki67, rabbit anti-. Neurospheres were then rinsed 3 times with PBS (5min each) and subsequently the Alexa Fluor™ secondary antibody incubation was performed at room temperature for 1h. After washing 3 times with PBS (5min each), all neurospheres were incubated in 2mM 4',6-diamidino-2-phenylindole (DAPI, Sigma) nuclear stain for 10min at room temperature. Neurospheres were transferred with Pasteur pipette to coverslips to be mounted in Mowiol®.

To evaluate the multipotency of NSC cultures, coverslips with differentiated neurospheres at DIV15 were fixed. The procedure was identical to above described except that the primary antibodies used were to detect different neural cell types: anti-glial fibrillary acidic protein (anti-GFAP) and anti-S100 calcium binding protein B (anti-

S100 β) to detect astrocytes and mature astrocytes, respectively; anti-beta III tubulin (Tuj1) to detect neurons and oligodendrocyte marker O4 (anti-O4) for oligodendrocytes.

To analyze NestinCre-P300^{f/f} hippocampal cultures, the immunocytochemistry procedure was identical to above described and the primary antibodies used were chicken anti-Green florescent protein (GFP), rabbit anti-GFAP, mouse anti-Microtubule Associated Protein 2 (MAP2) and mouse anti-P300.

Primary and secondary antibodies are detailed in Table 1 at the end of this section.

5.2 Immunohistochemistry

For immunohistochemistry of embryonic tissue, mouse embryos were extracted from pregnant mice and fixed with 4% PFA in PBS (0.01M) by immersion overnight. Embryonic tissue was cryoprotected with 30% sucrose, embedded in optimal cutting temperature compound (OCT) and frozen at -80°C. Coronal sections of 20 μ m were cut with cryostat.

For immunohistochemistry at postnatal stages, mice were anesthetized with isoflurane and intracardially perfused with 4% paraformaldehyde (PFA) in PBS (0.01M) and post-fixed overnight by immersion in the same fixative. Brains and retinas were dissected, embedded in 5% agarose and cut on Leica vibratome into 50 μ m sections.

Cryostat and vibratome sections were incubated in blocking solution (1% BSA and 0.3% Triton™ X-100 in 0.01M PBS) for 1h at room temperature. Subsequently, sections were incubated overnight at 4°C with the primary antibodies diluted in blocking solution: rabbit anti-CBP, mouse anti-P300, mouse anti-Brn3a, rabbit anti-Calbindin, rabbit anti-Caspase, goat anti- Sox2, mouse anti-Chx10. After primary antibody

incubation, sections were rinsed 3 times in PBS (5min each) and incubated for 1h at room temperature with Alexa Fluor™ secondary antibodies.

Finally, nuclei were counterstained with 2nM DAPI (Sigma), rinsed 3 times with PBS (5min each) and mounted with Mowiol®.

For some antibodies, antigen retrieval was performed at 96°C in sodium citrate buffer (10mM Sodium Citrate pH 6.0) for 20min, before blocking and incubation with primary antibodies.

Primary and secondary antibodies are detailed in Table 1 at the end of this section.

6. Cholera toxin injection and whole brain clearing

For axonal tracing studies at postnatal stages, animals were anesthetized with isoflurane and injected with 1µL of 2mg/ml Cholera toxin B conjugated with Alexa Fluor™ 594 (Thermo Fisher) into the eye. After 2 days, animals were intracardially perfused with 4% paraformaldehyde in PBS 0.01M, and their brains were post-fixed in the same fixative.

For brain clearing, iDISCO+ protocol (Renier *et al.*, 2016) was performed without immunolabeling. Samples were dehydrated in methanol/H₂O series: 20%, 40%, 60%, 80%, 100%, 100% (1hr each) followed by 66% DiChloroMethane (DCM, Sigma)/33% Methanol incubation at RT for 3h with shaking. After that, brains were incubated with 100% DCM twice for 15min and incubated with DiBenzylEther (DBE, Sigma) until samples were cleared. DBE was changed by clean DBE after clearing brains.

7. Image analysis and quantification

Images were acquired with inverted confocal microscope Olympus FV1200, Super-resolution inverted confocal microscope Zeiss LSM 880-Airyscan Elyra PS.1, Leica DM4000 microscope and Light-sheet UltramicroscopeII LaVision BioTec, for 3D images of cleared samples.

Stained neurospheres and differentiated cultures were examined and photographed by Super Resolution fluorescent microscopy (Zeiss). For quantitative analysis in differentiated neurospheres, images were acquired with 25X objective and cell quantification was performed in 4 regions of interest (ROIs) per differentiated neurosphere (a minimum of 5 coverslips per condition in 3 independent experiments) with image-analysis software Fiji.

Primary hippocampal cultures transfected with GFP were visualized under Leica DM4000 fluorescence/transmitted light microscope with a motorized stage. Dendritic trees of GFP transfected neurons were traced and reconstructed with NeuroLucida tracing software (MBF Bioscience). Sholl analysis was performed in neuron reconstructions, where the number of intersections was calculated every 2 μm starting at 5 μm from the center of neuronal soma. 4-5 neurons from three independent cultures were analyzed and quantified.

Stained retinas were photographed by inverted confocal microscope Olympus FV1200 with 10X, 20X or 40X objective. The thickness of retinas was measured with DAPI-stained using image-analysis software Fiji. For quantitative analysis of retinal cell populations, single plane images were acquired with 40X objective and cell quantification was performed in 9 regions of interest (ROIs) per retinal section, in a minimum of 3 retinal sections per animal and 9 animals per genotype, with image-analysis software Fiji.

3D imaging of brain samples was performed with a bidirectional light-sheet microscope (Ultramicroscope II, LaVision BioTec), controlled by the InspectorPro Software (LaVision BioTec), with a stereomicroscope (MVX10, Olympus, Japan) equipped with a 2x objective (MVPLAPO, Olympus). Images were acquired using a Neo sCMOS camera (Andor, Oxford Instruments, UK) at a magnification of 0.8X, 1.6X and 6.3X, with the tissue submerged in Ethyl Cinnamate. Alexa 561 was excited with laser line 561 nm and collected with a BP 620/60 filter; Alexa 647 was excited with laser line 639 nm and collected with a BP 680/30 filter. To avoid saturated pixels, laser intensities were set at 4-6%. The numerical aperture (NA) of the light sheet was set at 0.078 and the step size was fixed at 2 μm . Imaris software (Bitplane, <http://www.bitplane.com/imaris/imaris>) was used to generate three-dimensional volume and movie files, using the volume rendering function and the snapshot and animation tools.

8. Fluorescent-activated cell sorting (FACS)

Experimental mice were sacrificed by isoflurane and cervical dislocation, and eyes were extracted from the head to obtain the retinas. Isolated retinas were enzymatically dissociated in a mixture of 1ml of Collagenase type IV (Sigma), 1ml Trypsin-EDTA 0.25%, 40 μl 10% BSA (Sigma) and 5 units/ml DNase I (Sigma) for 20 minutes at 37°C followed by mechanical dissociation. Single cell suspension was filtered on 35 μm nylon mesh (Falcon) and resuspended in cold HBSS (Gibco) medium supplemented with 20% FBS (Sigma). Cell suspension was centrifugated at 500 rcf for 5min at 4°C. Supernatant was removed and cell pellet was resuspended in 4% PFA in PBS (0.01M) and incubated at room temperature for 10min to fix cells. Cell suspension

was centrifugated and washed three times with HBSS (5 min each). Three independent samples with the same genotype were pooled together (6 retinas per replicate). The resulting cell suspension was incubated with blocking solution (1% BSA and 0.1% Triton™ X-100 in PBS) for 30min at room temperature and after that, was stained for 2h in rotation with the following primary antibodies: mouse anti-Brn3a, rabbit anti-DsRed or rabbit anti-Calbindin. Primary antibodies were washed three times with PBS (5min each) and secondary antibodies were incubated for 30min in rotation. Nuclei were counterstained with 2nM DAPI (Sigma), rinsed 3 times with PBS (5min each) and resuspended in 1X PBS with 1.0% BSA. Cell suspension was sorted on FACS Aria III (BD Biosciences) selecting by size (FSC), complexity (SSC), DAPI staining, singlet nuclei, Brn3a positive cells, Calbindin positive cells and RFP positive cells. Flow cytometry data was analyzed using FACs Diva Software (BD biosciences). A pool of the retinas from 3 animals per sample and condition, of 3 independent experiments were analyzed.

9. Single-Nuclei RNA Sequencing (snRNA-Seq) and bioinformatic analysis

For the single nucleus RNA-Seq experiment, a pool of ~15 differentiated neurosphere cultures from control, CBP^{f/f}+Cre and P300^{f/f}+Cre at 15DIV were used. Differentiation medium II was removed and wells were washed with cold HBSS. Cold Lysis Buffer (10 mM Tris-HCl, 10 mM NaCl, 3 mM MgCl₂, and 0.1% Nonidet™ P40 Substitute in Nuclease-Free Water) was added (500μl) immediately to every well, gently pipetted until cells were completely suspended and kept on ice for 5 min to lyse cells. The nuclei suspension from the different samples (control, CBP^{f/f}+Cre and P300^{f/f}+Cre) was transferred to a 15ml tube and centrifuged at 500 rcf for 5min at 4°C. Supernatant were

removed and nuclei pellet was resuspended in 1 ml of Nuclei Wash and Resuspension Buffer (1X PBS with 1.0% BSA and 0.2U/ μ l RNase Inhibitor). Centrifugation and nuclei wash steps were repeated twice. Nuclei suspension was sorted on FACS Aria III (BD Biosciences) at 4°C and immediately proceed to 10x Genomics single cell protocol. 16.000 nuclei per sample (pool of~15 differentiated neurosphere cultures) were loaded into single cell Chromium Chip B and Chromium Controller was run to generate partitioning thousands of nuclei into nanoliter-scale Gel Beads-in-emulsion (GEMs) and immediately reversed transcribed, where all generated full-length cDNA (from polyadenylated mRNA) share a common 10x Barcode. Post-GEM-RT cleanup, cDNA amplification and 3' Gene Expression Library Construction were performed with Chromium Single Cell 3' Library & Gel Bead Kit v3. Quality control of cDNA and libraries were performed with Agilent Bioanalyzer in a High Sensitivity chip.

Libraries were sequenced on Illumina HiSeq2500 to obtain 75 bp paired-end reads following manufacturer instructions sequencer, with a sequencing depth of an average of 290 Million reads per sample. Quality control was performed using FastQC v0.11.9. Sequenced samples were processed using the Cell Ranger v3.1 pipeline (10X Genomics) and aligned to the CRGm38 (mm10) mouse reference genome (gene annotation version 94).

Bioinformatic analysis were performed as described previously in Lipinski *et al.*, 2020 and Cid *et al.*, 2021. Single-nucleus RNA-seq data were pre-processed and further analyzed in R using Seurat v2.3.4 (Butler *et al.*, 2018; Stuart *et al.*, 2019) using the following filter parameters: genes, nCell < 5; cells, nGene < 200. Barcodes with total unique molecular identifier (UMI) count > 10% of the 99th percentile of the expected recovered cells were selected for further analysis. We retrieved 4.884 (control), 3.017

(CBPf/f+Cre) and 4.648 (P300f/f+Cre) high nuclei per sample. Mean reads per nucleus were 62.810 (control), 99.066 (CBPf/f+Cre) and 65.928 (P300f/f+Cre). Data were then normalized using global-scaling normalization (method: LogNormalize, scale.factor = 10,000).

To identify major cell populations in the differentiated cultures, datasets were analyzed separately. Highly variable genes (HVGs) were detected using FindVariableGenes function with default parameters. Principal component analysis (PCA) was performed over the first ranked 1000 HVGs.

Plots of the two principal components of the PCA, where cells were colored by dataset, excluded the presence of batch effects. Cluster detection was carried out with Louvain algorithm using 20 first PCA dimensions at resolution = 0.6 (the default and the optimal according to cell number, data dispersion, and co-expression of previously reported cell markers).

Visualization and embedding were performed using tSNE (van der Maaten and Hinton, 2009) and uniform manifold approximation and projection (UMAP) (McInnes et al., 2018) over PCA using the 20 first PCA dimensions. UMAP plots of gene expression show normalized count (UMIs) per nucleus. Clustering was performed on merged dataset from control, CBP ablated and P300 ablated conditions and populations were identified combining these results with clustering information obtained in the datasets separately, together with co-expression of population markers. FindAllMarkers function with default parameters was used to identify gene markers for each cluster and to assign cell-type identity to clusters based on scRNA-seq dataset of the Allen Brain Map portal (Mouse Whole Cortex and Hippocampus SMART-seq (2019) with 10x-SMART-seq taxonomy (2020)).

Differential expression analysis (DEA) was used to identify population gene markers. For DEA, the nuclei of each population were compared against all the other nuclei in the merged dataset using Wilcoxon Rank Sum test on normalized counts with the following parameters (logFC.threshold = 0.1; min.pct = 0). Gene Ontology (GO) functional enrichment analyses for Biological Process (BP) were performed using clusterProfiler (v3.15.2). All enriched terms were considered significant at adjusted P values by BH cutoff < 0.05. The reference gene set used to perform the analysis was C5 (GO Biological Process) collection from the Molecular Signatures Database (MSigDB) (v6.2).

10. Statistical analyses

Statistical analyses were carried out in GraphPad Prism8 Software. Sample size was based on previous experience and literature. Data were presented as mean \pm standard error of mean (SEM). Statistical comparison between two groups was first tested for normality using Kolmogorov-Smirnov or Shapiro-Wilk tests and for variance with F-test. Data with normal distribution were compared using unpaired two-tailed Student's t test. When normality test failed Mann-Whitney U-Test was performed. Statistical significance (*) were considered with P values below 0.05; **p-value <0.01 and ***p-value <0.001.

Antibody	Host	Dilution	Provider (#Cat. no)
Primary antibody			
Ki67	Rabbit	1:200	Abcam (ab16667)
Phospho-Histone H3	Mouse	1:800	Cell Signalling Technology (9706)
Cleaved-Caspase 3	Rabbit	1:500	Cell signalling Technology (9661)
GFAP	Mouse	1:1000	Sigma (G3893)
GFAP	Rabbit	1:1000	Sigma (G9269)
S100β	Rabbit	1:100	Abcam (ab52642)
Tuj1	Rabbit	1:1000	Abcam (ab18207)
Tuj1	Mouse	1:300	Covance (MMS-435P)
GFP	Chicken	1:2000	Aves Labs (GFP 1020)
MAP2	Mouse	1:500	Sigma (M9942)
O4	Mouse	1:300	R&D Systems (MAB1326)
CBP	Rabbit	1:300	Santa Cruz Biotechnologies (sc-583)
P300	Mouse	1:300	Abcam (ab14984)
P300	Rabbit	1:300	Santa Cruz Biotechnologies (sc-585)
Brn3a	Mouse	1:300	Millipore (MAB1585)
Calbindin	Rabbit	1:2000	Swant (CB-38a)
Sox2	Goat	1:200	R&D Systems (AF2018)
Chx10	Mouse	1:200	Santa Cruz Biotechnologies (sc-365519)
Rhodopsin	Mouse	1:100	Santa Cruz Biotechnologies (sc-57432)
DsRed	Goat	1:500	Santa Cruz Biotechnologies (sc-33354)

Antibody	Host	Dilution	Provider (#Cat. no)
Secondary antibody			
Alexa 546 anti-rabbit	Donkey	1:1000	Invitrogen (A10040)
Ig-G			
Alexa 647 anti-rabbit	Donkey	1:1000	Invitrogen (A31573)
Ig-G			
Alexa 488 anti-mouse	Donkey	1:1000	Invitrogen (A21202)
Ig-G			
Alexa 546 anti-mouse	Donkey	1:1000	Invitrogen (A10036)
Ig-G			
Alexa 647 anti-mouse	Donkey	1:1000	Invitrogen (A31571)
Ig-G			
Alexa 647 anti-rat Ig-G	Donkey	1:1000	Jackson ImmunoResearch (712-605-150)

Table 1. Primary and secondary antibodies for immunocytochemistry and immunohistochemistry.

RESULTS

I. The role of KAT3 proteins in neural stem cells

1. Individual ablation of CBP or P300 does not alter neural stem cell proliferation

The early embryonic death of individual CBP or P300 null embryos between E9.5-E11 (Yao *et al.*, 1998; Tanaka *et al.*, 2000) demonstrated that KAT3 proteins are essential in neural tube development but did not clarify in which steps of neural development these proteins are involved.

In order to precisely elucidate the specific requirement of KAT3 proteins in proliferation of neural stem or progenitor cells, in differentiation, maturation and/or in the maintenance of differentiated neurons, we took advantage of the existence of conditional mutant mice for these KAT3 proteins to ablate them in the different steps of neural development. To investigate CBP functioning during development we used a CBP floxed mouse line (CBP^{f/f}) in which exon 7 (encoding KAT domain) of *Crebbp* is flanked by loxP sites (**Fig. 13a, left panel**) and a STOP codon. The result of this genetic manipulation is a truncated C-terminal *Crebbp* with 260bp comparing with 750bp from wild type, demonstrated by PCR; lacking 24 of 31 exons, including KAT domain (aa 1300-1700) and other critical domains (KIX, CH3) encoding by exons downstream of the recombination (Zhang *et al.*, 2004) and unable to interact with a number of transcription factors.

To study the role of P300, we used a P300 floxed mouse line, in which exon 9 (encoding KIX domain) of *Ep300* is flanked by loxP sites (**Fig. 13a, middle panel**). This genetic manipulation results in the absence of transcription and translation products, confirmed by qRT-PCR, immunohistochemistry and Western blot (Kasper *et al.*, 2006), indicating that P300^{f/f} is a null allele.

The removal of both KAT3 proteins simultaneously have been carried out using mice carrying homozygous floxed allele for CBP and P300 (**Fig. 13a, right panel**).

To address the function of KAT3 in proliferation and differentiation of neural stem cell (NSC) we performed neurosphere cultures from the subventricular zone (SVZ), a neurogenic niche of stem cells both in embryonic stages and in postnatal stages.

Under appropriate conditions, neural stem cells from SVZ are able to proliferate and display most of the criteria that characterize stem cells from other tissues, forming multipotent clonal aggregates called neurospheres (Reynolds and Weiss, 1992). The neurosphere assay is a powerful tool that enables to study the main features of NSC: self-renewal and proliferation as well as differentiation of the three neural lineages, neurons, astrocytes and oligodendrocytes.

To generate neurospheres, we isolated neural stem cells from the SVZ of P0-P3 $CBP^{f/f}$, $P300^{f/f}$ or $CBP^{f/f}::P300^{f/f}$ newborn mice. The same day of the dissection, cultures were infected with a lentiviral vector encoding red fluorescent protein (RFP), as a control, or Cre recombinase fused to mCherry in order to remove CBP, P300 or both proteins at the same time from these neural stem cells. Cells were seeded in growth medium supplemented with EGF (epidermal growth factor) and FGF (fibroblast growth factor) as mitogens and in the absence of adherent substrate to promote proliferation (**Fig. 13b**).

Neurosphere cultures were maintained for 14 days in order to be sure of complete removal of KAT3 proteins. After 14 days in vitro (14DIV) primary neurospheres from $CBP^{f/f}$, $P300^{f/f}$ and $CBP^{f/f}::P300^{f/f}$ were formed, but a reduction in the size of primary neurospheres was observed in those generated from the double KAT3 mice (**Fig. 13c**).

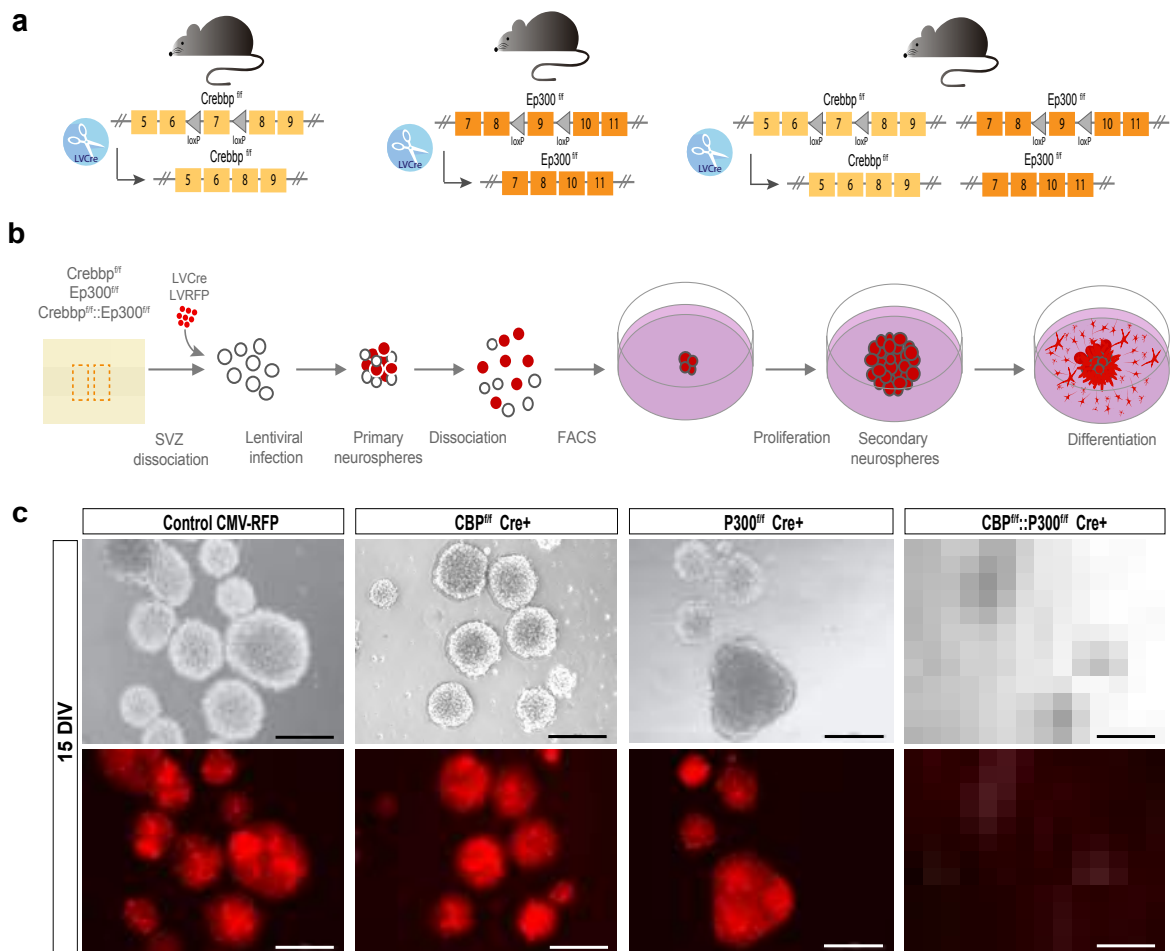


Figure 13. Analysis of the role of KAT3 proteins in neural stem cells (NSC). (a) Scheme representing the genetic strategy to precisely study the ablation of KAT3 proteins in the different steps of neural development. (b) Experimental design of the approach used to generate neurosphere cultures to investigate the particular role of KAT3 proteins in neural stem cells (NSCs). (c) Representative primary neurospheres at 15DIV from CBP^{fl/fl}, P300^{fl/fl} or CBP^{fl/fl}::P300^{fl/fl} NSC infected with lentivirus carrying Cre recombinase (Cre-mCherry) or RFP as a control at 1DIV. Scale bars 200µm.

We noticed that in these primary neurospheres, only a percentage of cells were infected with the lentivirus and therefore recombined. For that reason, we dissociated primary neurospheres and isolated the infected cells using fluorescent-activated cell sorting. Infected red positive cells were seeded at low density (2,5 cell/µl) to generate clonal secondary neurospheres lacking CBP, P300 or both proteins.

It has been previously described a correlation between larger diameter and a higher proliferation capacity (Ohtsuka et al., 2001). Therefore, we analyzed the proliferation of clonal secondary neurospheres by measuring neurosphere diameter. CBP-lacking neurospheres showed similar proliferation rate than control neurospheres (**Fig. 14a,b**), indicating that CBP is not essential for proliferation. In contrast, we observed an increase in the diameter of P300-lacking clonal secondary neurospheres (**Fig. 14c,d**). We wonder whether the increase in the diameter of P300 ablated neurospheres could be explained by a larger cell size or by a higher proliferation rate. To test these possibilities, we quantified the number and size of P300 ablated NSC by fluorescent-activated cell sorting. Flow cytometry results revealed that P300 ablated NSC presented a higher cell size (mean 124.96) and higher nuclei size (mean 74.82) compared to control NSC (cell: mean 84.74; nuclei mean 69.84), in accordance with forward scatter (FSC) that measures the volume/diameter of particles (**Fig. 14g,h**). This result indicates that P300 elimination impacts cell size but does not affect proliferation of NSC. The expression of proliferative markers of NSCs for instance Ki67 or Phospho-histone H3 (PH3) in CBP or P300-lacking neurospheres was similar to control cultures (**Fig.15**).

Importantly, clonal secondary neurospheres where CBP and P300 were concurrently depleted showed a great reduction in diameter compared to control neurospheres (**Fig. 14e,f**).

Overall, these results demonstrate that whereas proliferation of NSC is not affected in the absence of CBP or P300, simultaneous removal of both KAT3 proteins seriously compromised proliferation, indicating that at least one of the KAT3 proteins is required for NSC proliferation.

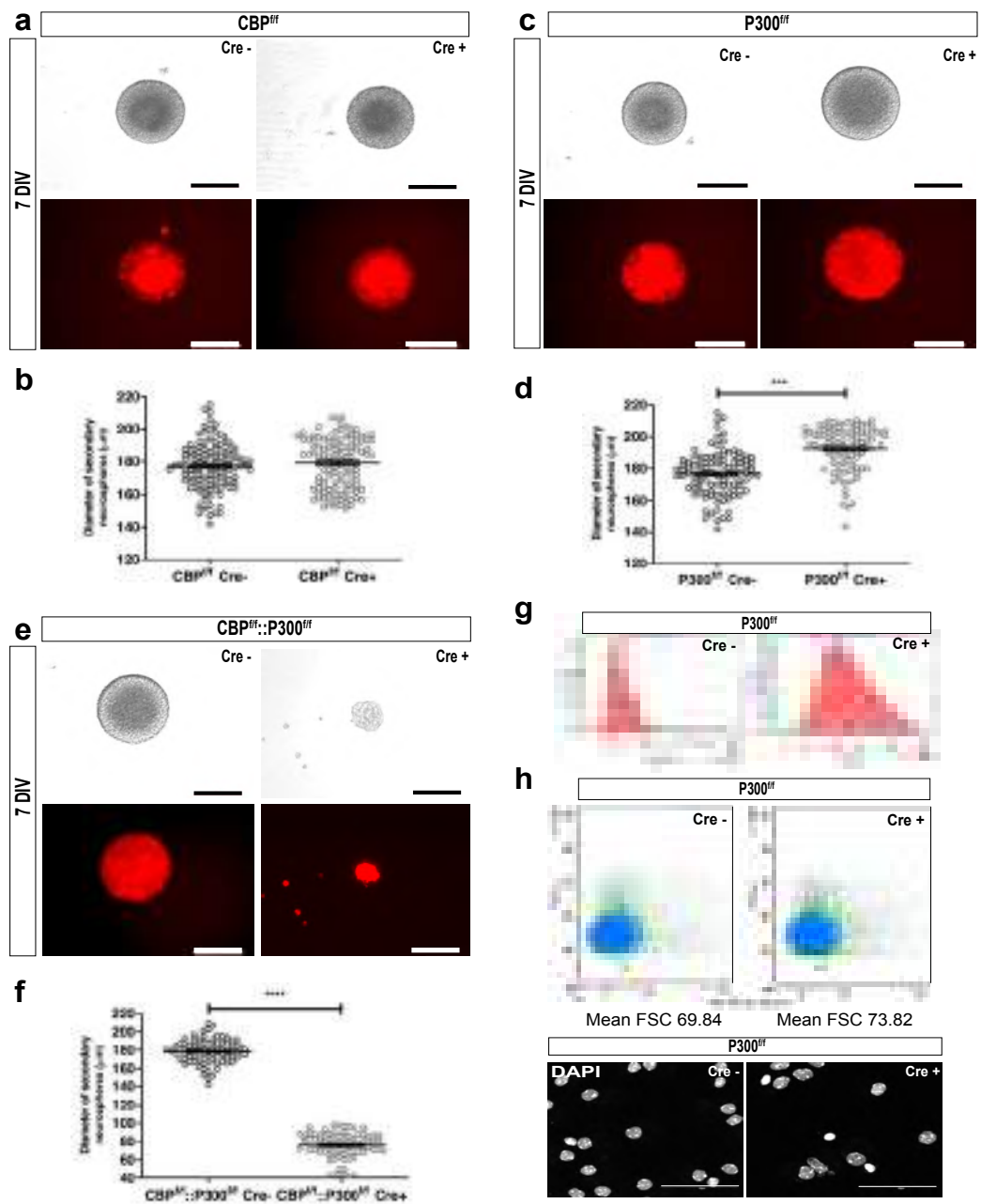


Figure 14. Individual ablation of CBP or P300 does not affect proliferation of NSC. (a,c,e) Representative infected clonal secondary neurospheres lacking CBP (a), P300 (c) and both KAT3 proteins (e) at 7DIV. (b,d,f) Quantitative analysis of the diameter of clonal secondary neurospheres in the absence of CBP (b), P300 (d) or both proteins (f) at 7DIV. *** $p < 0.001$; **** $p < 0.0001$ ($n \approx 120$ neurospheres from 3 independent experiments). Statistic: t-test (b,f), Mann-Whitney (d). (g) Flow cytometry sorting plots for infected cells from controls and P300 ablated NSCs showing counts against forward scatter (FSC) (h) (top) Fluorescent-activated sorting analysis plots showing forward scatter (FSC) against red fluorescence of nuclei from controls and P300 ablated NSC ($n = 3$; each sample contains a pool of 15 neurospheres). (bottom) High magnification of nuclei counterstained against DAPI of control and P300 ablated NSC. Error bars denote SEM. Scale bar 200µm (a,c,e) and 50µm (g).

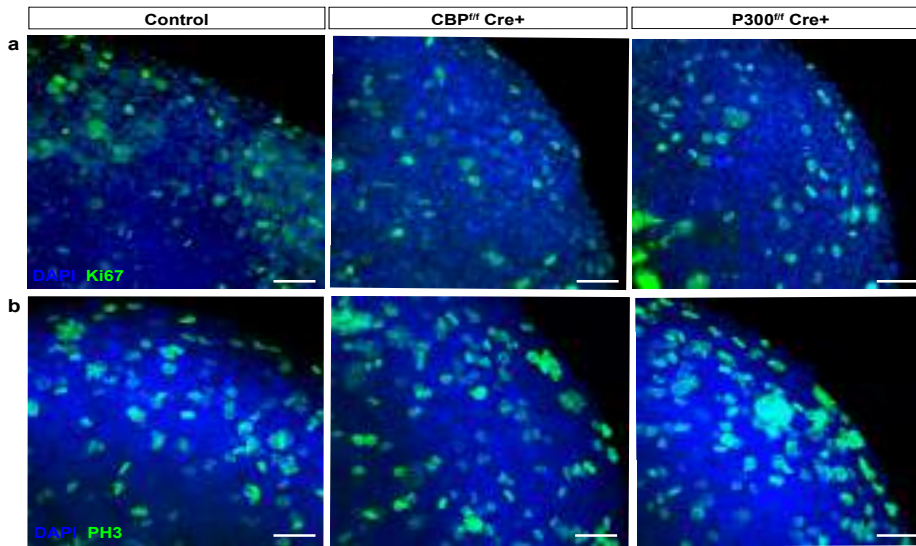


Figure 15. Individual ablation of CBP or P300 does not affect the expression of proliferative markers of NSC. Representative clonal secondary neurospheres immunolabeled for the proliferative markers Ki67 (**a**, green) and Phospho-Histone H3 (PH3) (**b**, green) and counterstained with DAPI (blue) showed no differences in clonal secondary neurospheres lacking CBP or P300 compared to control neurospheres at 7DIV. Scale bar 50 μ m.

2. CBP and P300 are individually required for proper differentiation of neural progenitor cells.

Differentiation and multipotency are main features of NSC that may be studied in neurosphere cultures because they can be induced to differentiate onto an adherent substrate in the presence of serum. In these culture conditions neurosphere cells are able to generate the three main neural lineages (Reynolds and Weiss, 1992) in a typical profile: 80% astrocytes, 17% neurons and 1-3% oligodendrocytes (Singec *et al.*, 2006; Chaddah *et al.*, 2012).

To examine the capacity of neurospheres lacking CBP or P300 to produce the different neural lineages, clonal secondary neurospheres of 7DIV were plated onto coverslips coated with Matrigel, in the absence of the mitogen EGF to allow neurospheres to attach to the coated substrate and produce neuronal and oligodendroglial progenitor

cells. After 2 days, medium was supplemented with serum leading to the generation of a dense layer of astrocytes with neurons and oligodendrocytes.

To visualize migration of neurosphere cells across the surface in real-time, plates were inserted into IncuCyte imaging system, which were tracked every 30 min. Live-cell imaging assays revealed that after 48h of plating, cells from CBP lacking cultures exhibited a strong delay in cell migration compared to control cultures whereas P300 ablated cells showed slightly slower migration than control cells (**Fig. 16**).

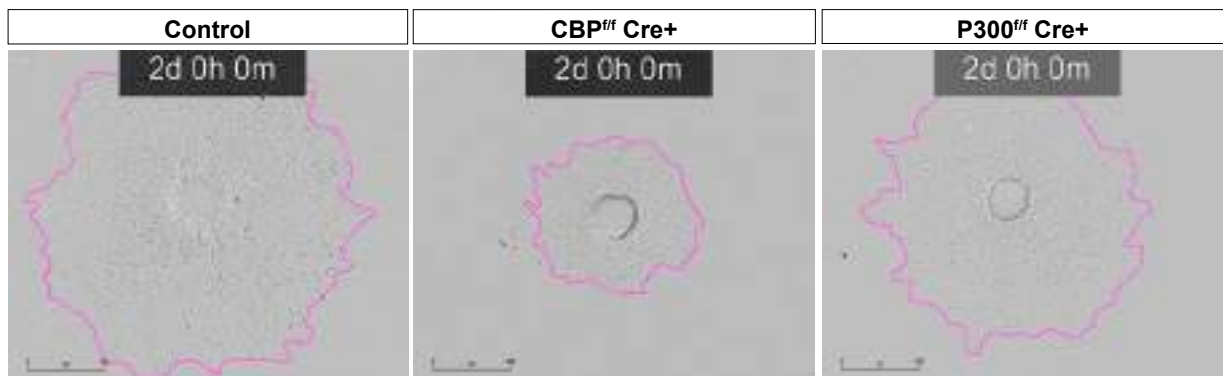


Figure 16. CBP lacking neurospheres showed a prominent delay in cell migration. Overlaid brightfield depicting cell migration obtained by real-time IncuCyte imaging system for 48h. CBP lacking neurospheres showed a prominent delay in cell migration whereas P300 lacking neurospheres exhibited a slightly reduction compared to control neurospheres (n=3/genotype). Scale bar 800 μ m.

After 15DIV, cultures did not show enhanced cell death after the elimination of CBP and p300 compared to control cultures (**Fig. 17c**). Control cells showed a complete differentiation into neurons and glia while neurospheres lacking CBP or P300 showed altered neuronal (**Fig. 17a**) and glial differentiation, showing differences in glial morphology (**Fig. 17b**). Astrocytes from control cultures exhibited typical stellate and large filamentous astrocyte morphology while a ramified morphology and low level of GFAP immunoreactivity was present in neurospheres lacking CBP or P300.

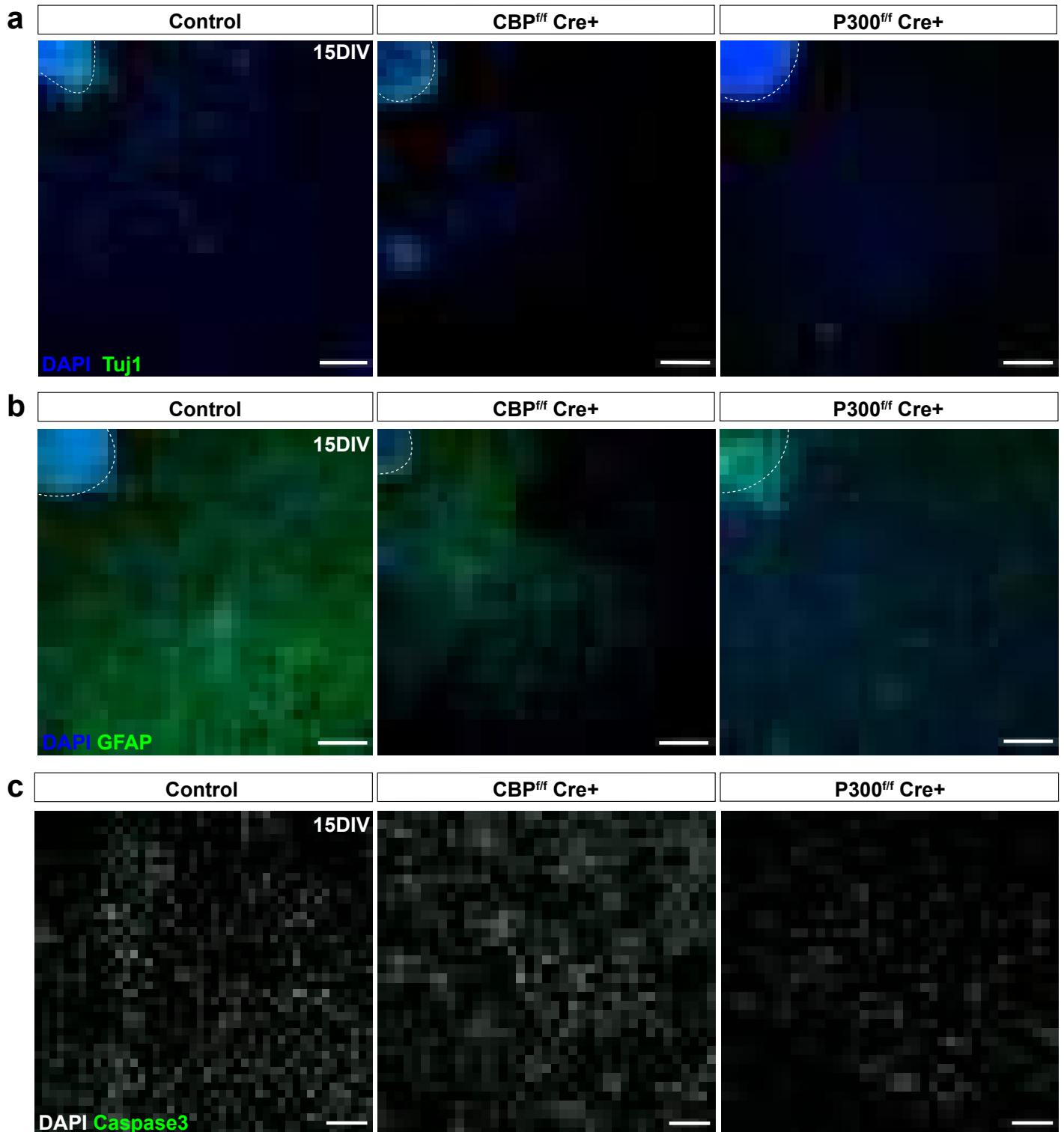


Figure 17. CBP and P300 lacking neurospheres showed alterations in neural differentiation programs whereas cell death is not altered. (a,b) Representative images of low magnification of differentiated neurospheres lacking CBP or P300 at 15DIV exhibit alterations in neuronal differentiation (TuJ1 positive cells) (a) and glial differentiation (GFAP positive cells) (b) compared to differentiated control neurospheres. (c) Immunostaining against Caspase 3 showed no differences in cell death after differentiation of NSCs lacking CBP or P300 compared to control NSCs. Scale bars 200 μ m (a,b) and 100 μ m (c).

Fifteen days after inducing differentiation, we determined the proportion of cells positive for the neuronal marker β III tubulin (Tuj1), s100b, a marker for mature astrocytes and O4, an oligodendrocyte marker. We observed a dramatic loss of Tuj1 positive cells in CBP and in P300 lacking cultures compared to the controls (**Fig. 18a,b**).

There was also a significant decrease in the proportion of terminally differentiated astrocytes in both CBP and P300 mutant cultures compared to the controls (**Fig. 18c,d**). Regarding oligodendrocytes, NSCs lacking CBP or P300 appear not to be altered expression of the immature oligodendrocyte marker O4 compared to the controls although this was difficult to determine due to the low number of O4 positive cells in the cultures (**Fig. 18e**).

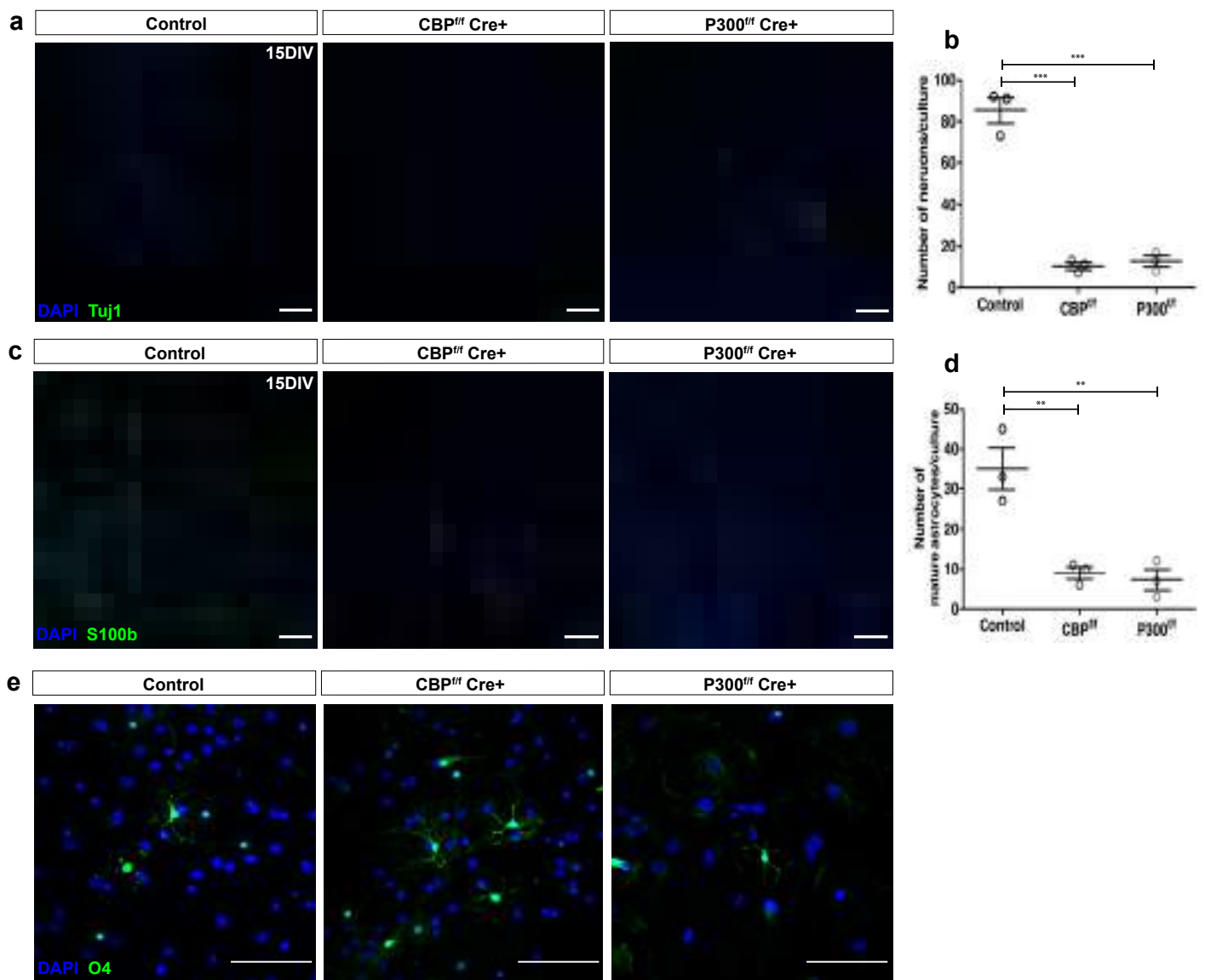


Figure 18. CBP and P300 are individually required for differentiation of NSCs into the three neural lineages. (a,c,e) Representative images of immunofluorescent staining for neurons (TuJ1, a), mature astrocytes (S100β, c) and immature oligodendrocytes (O4, e) in differentiated CBP or P300 ablated neurospheres at 15DIV. (b,d) Quantification of neurons (b) and mature astrocytes (d) in neurospheres lacking CBP or P300 after 15DIV of differentiation. **P<0.01; ***p < 0.001 (n=5 coverslips per condition from 3 independent cultures). Statistic: One-way ANOVA. Error bars denote SEM. Scale bars 100μm.

3. Single-nucleus RNA sequencing analysis of differentiated neurospheres revealed alterations in neural populations after removal of CBP or P300.

To determine the molecular basis of this dramatic reduction of neurons and mature astrocytes in CBP and P300 deficient cultures, we conducted a single nuclei RNA sequencing (snRNA-Seq) in the differentiated cultures (15DIV).

To identify major cell populations in the differentiated cultures, datasets were analyzed separately. After quality control, nuclei filtering and integration process of the 3 conditions (**Fig.19a**), we first performed unsupervised consensus clustering to identify major cell types and canonical marker genes. The integrated bioinformatical analysis identified 12 clusters (**Fig19b**) based on the top 20 bona fide marker genes per cluster from scRNA-seq dataset of the Allen Brain Map portal (Mouse Whole Cortex and Hippocampus SMART-seq (2019) with 10x-SMART-seq taxonomy (2020)) (**Fig. 19e**). Enrichment analysis for genes in relation with Gene Ontology (GO) biological process (BP) was also performed to characterize cell populations based on the top 100 bona fide marker genes per cluster (**Fig. 19f**). The gene expression patterns of these clusters identified them as astrocytes (*Slc1a3*, *Gpc5*, *Atp1a2*, cluster 3), oligodendrocytes (*Mog*, *Mbp*, *Mag*, cluster 6), immature (*Kcnj6*, *Nel2*, *Cacng4*, cluster 5) and mature neurons (*Ascl2*, *Cpn4*, *Adarb2*, cluster 9), glial progenitor cells (GPC) (*GFAP*, *Mgat5*, *Aqp4*, cluster 2), oligodendrocytes progenitor cells (OPC) (*Bcas1*, *Sirt2*, *Enpp6*, cluster 4), microglia (*Inpp5d*, *Fyb*, *Fli1*, cluster 10), and proliferating cells (*Mki67*, *Klf4*, *Rbfox1*, cluster 8). The other four clusters were not characterized by a single cell type, suggesting a spectrum of cells in transition between different states (Neuron/OPC (cluster 0) and radial glial cells/pluripotent stem cells 1-3 (RGC/PSC 1-3, clusters 1,7,11)).

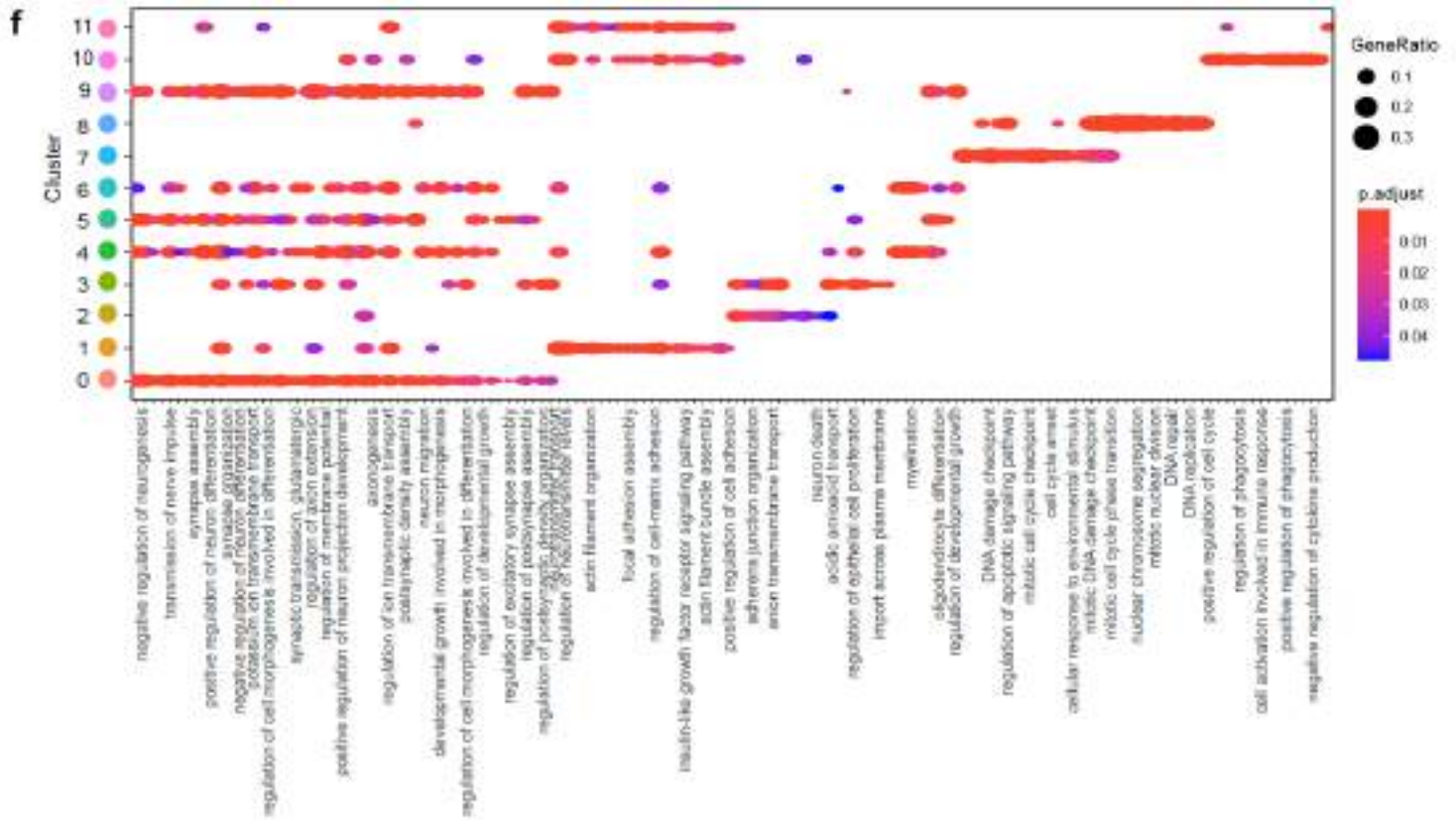


Figure 19. Single-nucleus RNA sequencing analysis of differentiated neurospheres revealed alterations in neural populations after removal of CBP or P300. (a) Uniform manifold approximation and projection (UMAP) plots showing the integration of single-nucleus RNA-seq datasets from differentiated neurospheres at 15DIV segregated by experimental condition: Control (green, 4884 nuclei), CBP ablated culture (red, 3017 nuclei) and P300 ablated culture (blue, 4648 nuclei). Each dot represents a single nucleus. (b) UMAP plots displaying differential clustering on differentiated neurospheres of control, CBP or P300 ablated nuclei. Nuclei are colored by their classification label as shown in panel. (c) UMAP embedding of single nucleus profile for CBP or P300 lacking cultures and control cultures. (d) Bar plot showing the proportion of nuclei in each cluster of the three different cultures. (e) Heatmap of z score of single nuclei expression levels of the 20 top-ranked bona fide marker genes, with select genes displayed on y axis and cells on x axis. Each row represents a gene, the columns are nuclei and the color-code represents the normalized expression for upregulated genes (yellow) or downregulated genes (purple). (f) Dot plot showing GO biological process (BP) enrichment analysis for each major nucleus population based on the top 100 bona fide marker genes. The size of the dot represents the ratio of enriched genes in a given major population and the color of the dot represents adj. P value. RGC: radial glia cells, PSC: pluripotent stem cells, OPC: oligodendrocytes progenitor cells, GPC: glial progenitor cells.

Uniform Manifold Approximation and Projection (UMAP) plots displaying differential clustering showed the clear absence of astrocytic population in CBP and P300 lacking cultures (**Fig. 19c**). This cluster includes bona fide markers such as *Scl1a3* (GLAST), *Scl7a11*, *Gpc5*, *ApoE*, *Rorb* or *Ntm*, among others. We next wondered whether this absence of astrocytes may be compensated by alterations in other cell populations. Analysis of cluster proportion revealed that several populations such as Neuron/OPC, OPC, oligodendrocytes or RGC/PSC clusters displayed altered nuclei proportion in CBP or P300 lacking cultures compared to the controls (**Fig. 19d**). Moreover, the immature neuronal population, enriched in canonical neuronal markers such as *Kcnj6* and *Nel2* showed no alteration in terms of proportions although this cluster exhibited a strong deviation in CBP deficient cultures compared to the control or the P300 ablated condition showing that CBP lacking cultures contained a specific cell population in the cluster of immature neurons that is not present in control or P300 ablated condition (**Fig.19c,d**).

Next, we investigated more in detail the transcriptional changes associated with CBP or P300 removal. Enrichment analysis identified differentially expressed genes (DEGs) in several populations, including Neuron/OPC, OPC, immature neuron, or GPC population in CBP or P300 ablated condition compared to controls (**Fig. 20a, Fig21a**). This prompted us to perform Gene Ontology (GO) overrepresentation of the DEGs between control and CBP or P300 lacking cultures to analyze biological processes affected by these transcriptional changes.

Downregulated DEGs in CBP lacking cultures showed robust association with many Gene Ontology (GO) biological process terms (adj. $p < 0.05$) linked to immature neuronal processes (**Fig. 20b-f**), such as synapse organization and assembly, glutamatergic synaptic transmission or neuron projection development, including many

well-known modulators of these processes such as *Nrxn1*, *Grik2*, *Sema3d*, *Nlgn1* or *Ntm*. However, enrichment analysis showed that mature neuronal population (cluster 9) had no differences in DEGs and there were no GO terms significantly enriched between CBP lacking cultures and control cultures (**Fig. 20a**).

Hence, regarding upregulated genes, CBP ablation induced cell-type-specific upregulation of oligodendrocytes genes, such as *Mbp*, *Plp1*, *Tcf7l2*, *Bcas1*, *Sox6* or *Sox10* among others, with key roles in oligodendrocyte development, differentiation or myelination (**Fig. 20b,c,f**).

Among the downregulated DEGs in P300 ablated condition, we identified several genes, including transcription factors, that are known to be highly expressed in neuron synapse or dendritic spine maintenance, such as *ErbB4*, *Nrxn1*, *Sema5a*, *Grik2*, *Grin2b* or *Snca*, while we also found other enriched DEGs related to other neuronal processes such as transmission of nerve impulse, axon regeneration or developmental maturation (*Xylt1*, *Ntrk3*, *Cacng4*, *Ncam1* or *Sox10*, among others) (**Fig.21b-e**).

Thus, our differential gene expression analysis from snRNA-Seq confirmed profound transcriptional changes related to the astrocytic population and suggested that neuronal differentiation is also altered in the absence of CBP or P300 proteins. Hence, in the absence of CBP oligodendrocyte markers are upregulated.

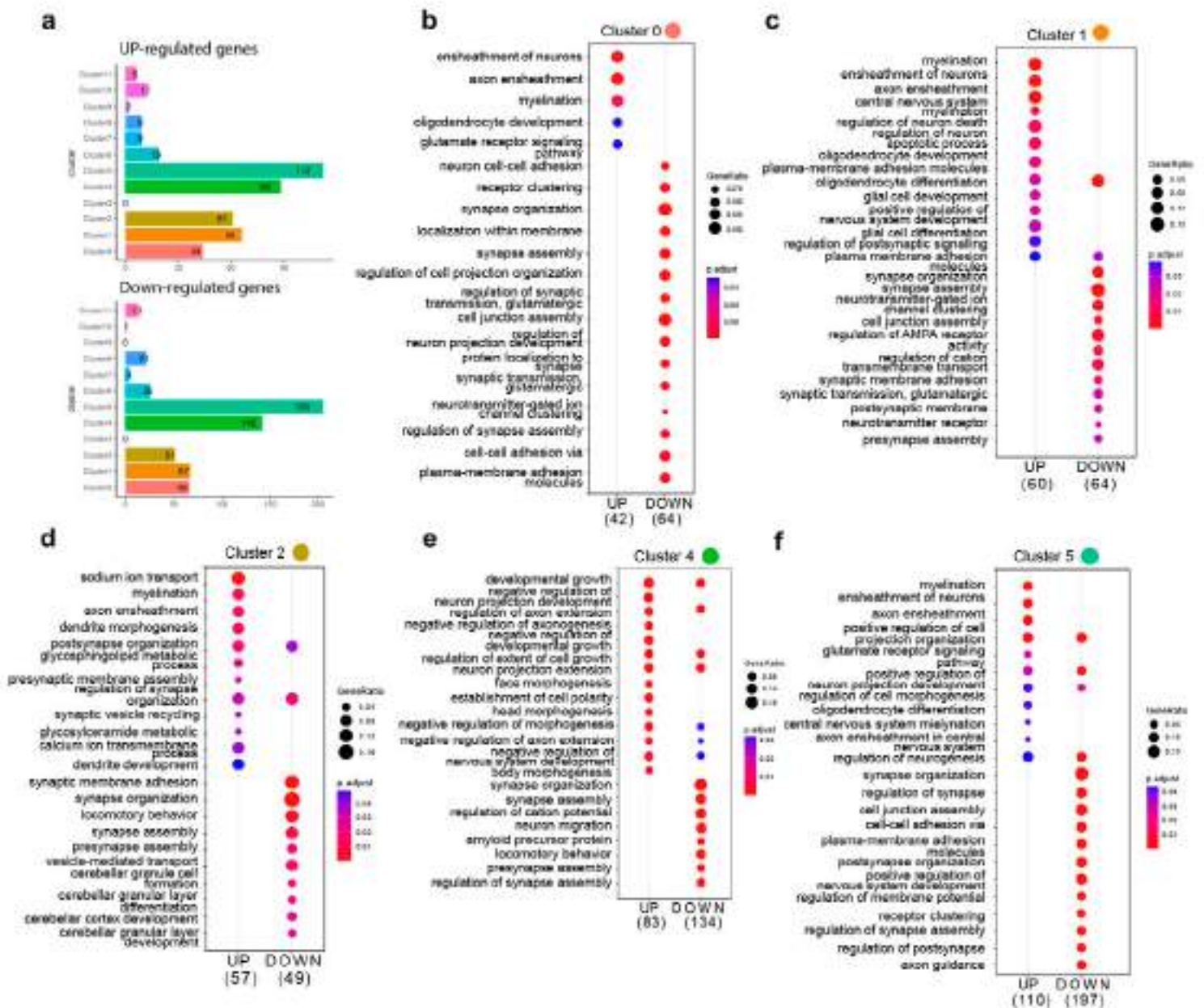


Figure 20. Single-nucleus RNA sequencing analysis of differentiated neurospheres revealed alterations in several populations of CBP lacking cultures. (a) Bar plot comparing upregulated and downregulated differentially expressed genes (DEGs) per cluster in CBP lacking cultures compared to control cultures. (b-f) Visualization of Gene Ontology (GO) analysis for differentially expressed genes (DEGs) in Neuron/OPC population (cluster 0) (b), RGC/PSC1 population (cluster 1) (c), GPC population (cluster 2) (d), OPC population (cluster 4) (e) and immature population (cluster 5) (f). Numbers indicate upregulated or downregulated genes in the different clusters of CBP lacking cultures.

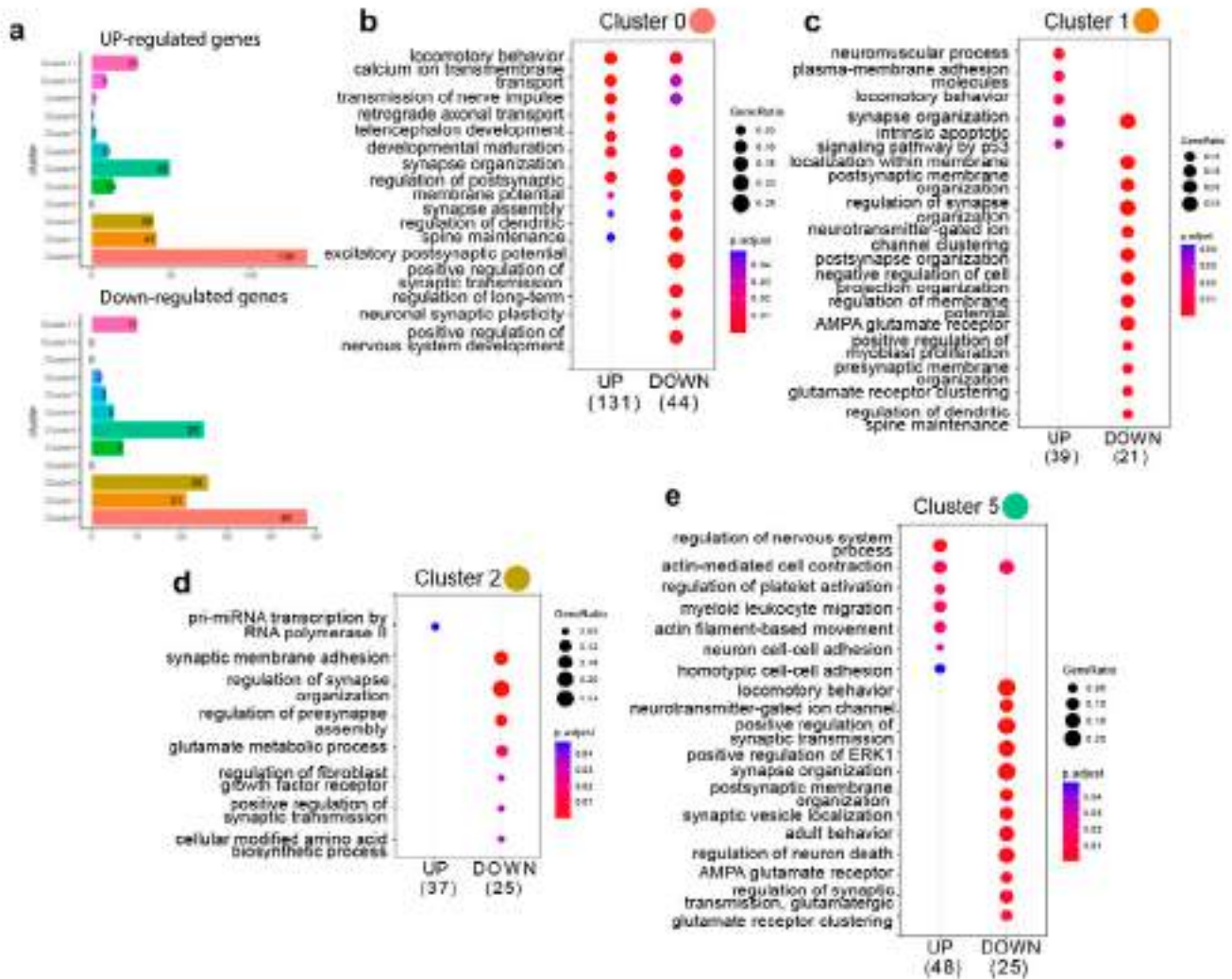


Figure 21. Single-nucleus RNA sequencing analysis of differentiated neurospheres revealed alterations in several populations of P300 lacking cultures. (a) Bar plot comparing upregulated and downregulated differentially expressed genes (DEGs) per cluster in CBP lacking cultures compared to control cultures. **(b-f)** Visualization of Gene Ontology (GO) analysis for differentially expressed genes (DEGs) in Neuron/OPC population (cluster 0) **(b)**, RGC/PSC1 population (cluster 1) **(c)**, GPC population (cluster 2) **(d)** and immature population (cluster 5) **(e)**. Numbers indicate upregulated or downregulated genes in the different clusters of P300 lacking cultures.

II. The role of KAT3 proteins in neural progenitor cells *in vivo*

1. CBP and P300 are expressed in progenitor and differentiated cells during mouse retinal development and at postnatal stages

To dissect whether CBP and p300 play a role in progenitors and/or differentiated neurons *in vivo*, we use the developing visual system of mice as a model.

We first studied the spatio-temporal expression pattern of CBP and P300 in the developing retina. For that purpose, we performed immunostaining against CBP and P300 at different time points through embryonic development, perinatal stages and late postnatal stages. We observed that KAT3 proteins are both highly expressed at early embryonic day 13.5 in retinal progenitor cells (RPC) colocalizing with Sox2 (**Fig. 22a,b**). Later, when these retinal progenitor cells begin to differentiate, CBP and P300 are expressed in differentiated cell layers along the retina, colocalizing for instance with Brn3a, a marker for differentiated RGCs (**Fig. 22c, d**).

At perinatal stages, the expression of both KAT3 proteins is detected in all the retinal layers (**Fig. 22e,f**). However, at late postnatal stages when all retinal cell types are mature and cells have reached their proper layer, we noticed that CBP and P300 are still expressed in the amacrine and RGC layer, and the horizontal and bipolar layers (Inner nuclear layer, INL) but not in the photoreceptor layer (**Fig. 22g,h**).

This spatiotemporal characterization of KAT3 proteins in the developing retina allowed us to start performing different functional experiments in order to unravel the role of these proteins *in vivo*.

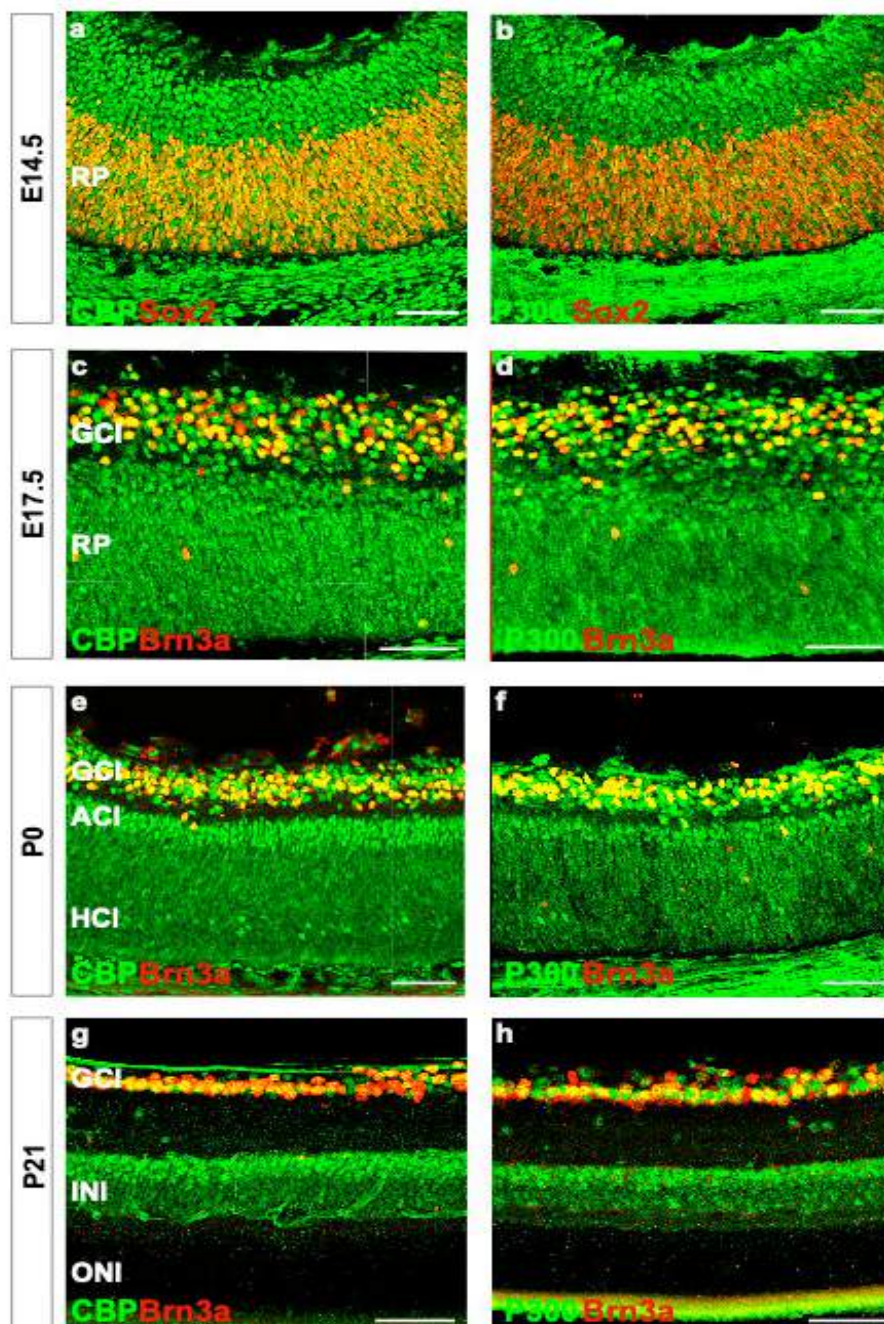


Figure 22. Spatio-temporal expression pattern of CBP and P300 in the retina. Immunohistochemistry in coronal retinal sections from wild-type mice showing the expression pattern of CBP and P300 at embryonic stages (E13.5 and E17.5), perinatal (P0) and late postnatal stages (P21), colocalizing with markers of retinal progenitor cells (**a, b**) and differentiated retinal ganglion cells (RGCs) (**c-h**). Scale bars 50 μ m.

2. *CBP is expressed in a larger number of retinal progenitor cells than P300*

Interestingly, when we analyzed the expression pattern of KAT3 proteins in the developing retina, we noticed that although both proteins are expressed in retinal progenitor cells and differentiated cells, CBP levels appeared to be higher in the proliferative zone of the retina than P300.

To evaluate this observation, we performed immunohistochemistry for CBP and P300. We confirmed that at E14.5, CBP is expressed in a larger number of Sox2-retinal progenitor cells than P300. At this stage, mitotic RPCs are located in the outer surface of the retina and begin to generate the different retinal populations (**Fig. 23**).

This finding suggests that CBP plays a more relevant role than P300 in retinal progenitor cells.

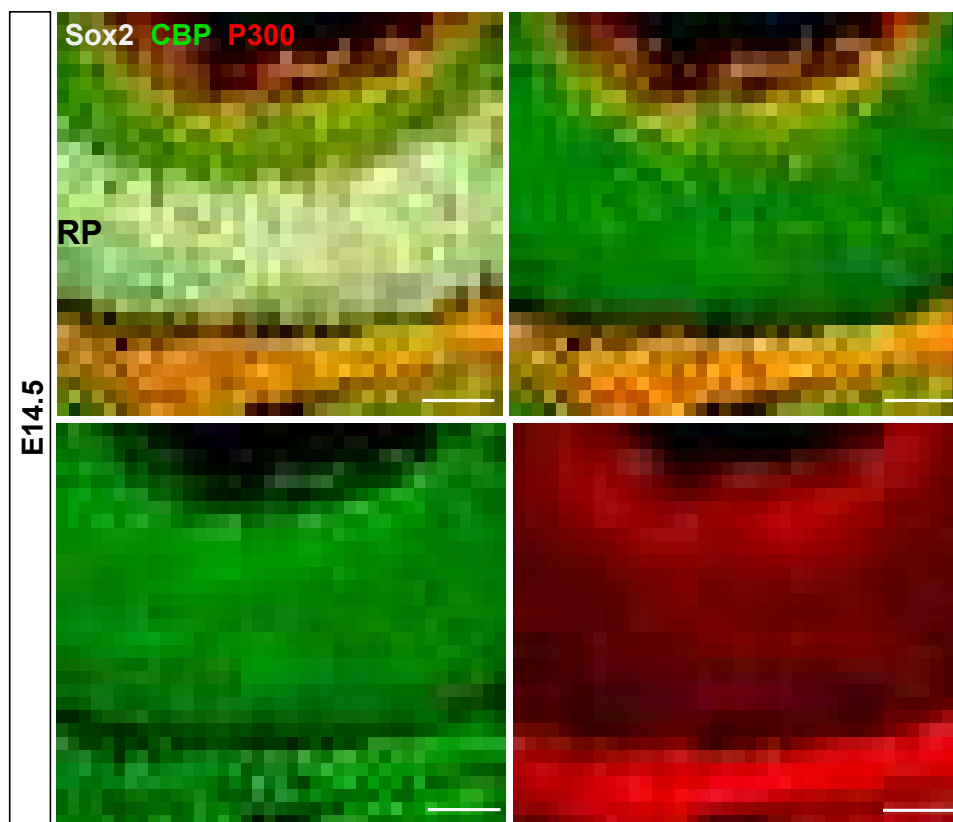


Figure 23. CBP is expressed in a large number of retinal progenitor cells at early embryonic stages. Immunofluorescent staining showing CBP colocalization with a large number of progenitor cells, expressing Sox2, than P300 at E14.5. Scale bars 50 μ m.

3. *Characterization of Rx-Cre mouse line in the retina*

In order to determine the role of KAT3 proteins in neural progenitor cells *in vivo*, we aimed to remove KAT3 proteins from retinal progenitor cells at E9, when early optic vesicles begin to evaginate. To achieve such an early ablation, we employed the *Rx-Cre* driver line in which Cre recombinase is expressed under the Retina and anterior neural fold homeobox (*Rx*) promoter. *Rx* is expressed since embryonic day E7.5-E8 in the anterior neural plate and later on, at E9, begins to be expressed in the ventral forebrain and in the retinal pigmented epithelium of the optic cups, the niche of retinal progenitor cells (Mathers *et al.*, 1997; Furukawa *et al.*, 1997).

This *Rx-Cre* line has been used in different studies as a driver of neural progenitor cells. However, the specific pattern of the Cre recombinase activity driven by *Rx-Cre* in the retina was not been precisely reported. To determine the retinal cell populations arising from *Rx*-progenitor cells, we crossed *Rx-Cre* mice with *Sad1* And *UNC84* Domain Containing 1-GFP (*Sun1-GFP*) reporter line in which GFP is expressed in the nuclear envelope after deletion of stop cassette flanked by loxP sites (**Fig. 24a**). We confirmed that after cre recombination, *Rx* progenitor cells generate all the main retinal cell populations. The nuclear envelope GFP expression colocalized with the RGCs marker *Brn3a*, with the amacrine and horizontal cells marker *Calbindin*; with *Chx10*, a transcription factor specific for bipolar cells and with the photoreceptor cell marker *rhodopsin* (**Fig. 24b,c**). GFP expression pattern revealed a broad area of recombination in the retina but a variable ratio of cells escaped from *RxCre*-mediated ablation generating some areas of recombination-free columns (**Fig. 24b,c dotted lines**).

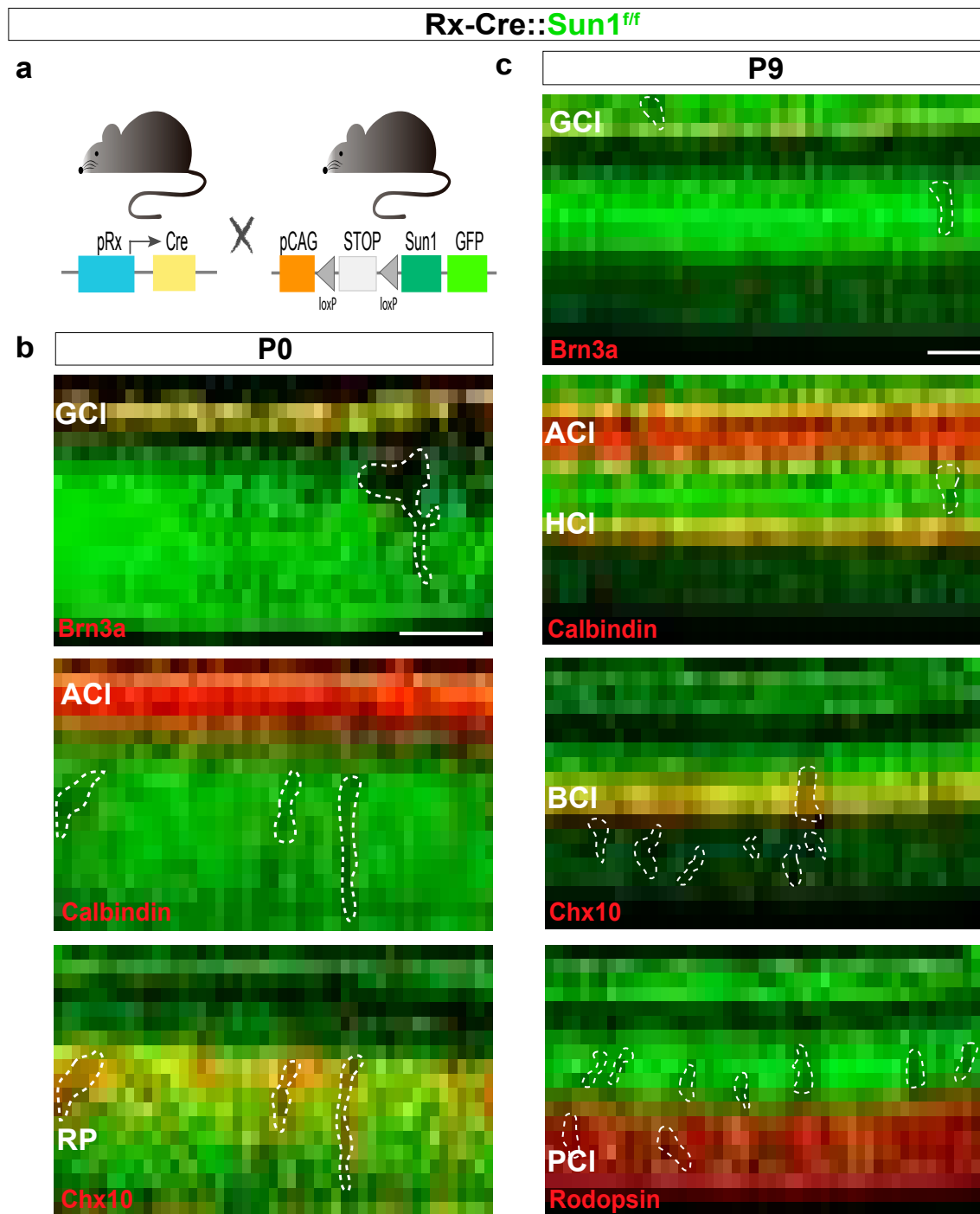


Figure 24. Characterization of Rx-Cre mouse line in the retina. (a) Genetic strategy for the production of Rx-Cre::Sun1-GFP^{ff} mice in which GFP is expressed in nuclear envelope after recombination of loxP sites flanked stop cassette. (b, c) Immunostaining in retinal sections of P0 (b) and P9 (c) Rx-Cre::Sun1GFP^{ff} mice for GFP and Brn3a, marker of retinal ganglion cell (RGC) population; Calbindin, marker of amacrine and horizontal cell population; Chx10, marker of bipolar cell population and rhodopsin, marker of photoreceptor population. Dotted layers correspond to non-recombined columns of retinal cells. Scale bars 50µm.

4. P300 deficiency in retinal progenitor cells do not affect retinal development

To investigate the role of P300 in retinal progenitor cells we crossed the RxCre mouse line with the P300 floxed mouse line (previously described in the part I in the results section) (**Fig. 25a**). To ensure that Cre-mediated recombination removed P300 in the retina, we performed immunostaining against P300 at different stages. Analysis of P300 expression in RxCre::P300^{f/f} at E17.5 and P21 retinas revealed a reduction of this acetyltransferase throughout the retina, affecting all retinal cell types and, although in agreement with Sun1-expression, some retinal cells escaped from RxCre-mediated recombination and maintained P300 expression (**Fig. 25b**).

To explore whether P300 is essential in retinal progenitor cells, we analyzed the retinas of 21-day postnatal RxCre::P300^{f/f} mice, because at this stage all retinal layers are already mature. We did not observe alterations in cell distribution or in the layering of cells, and plexiform layers were neither altered in the mutant mice. In addition, retinal thickness of mutant mice was similar to control mice and did not show any obvious sign of alteration (**Fig. 25c**).

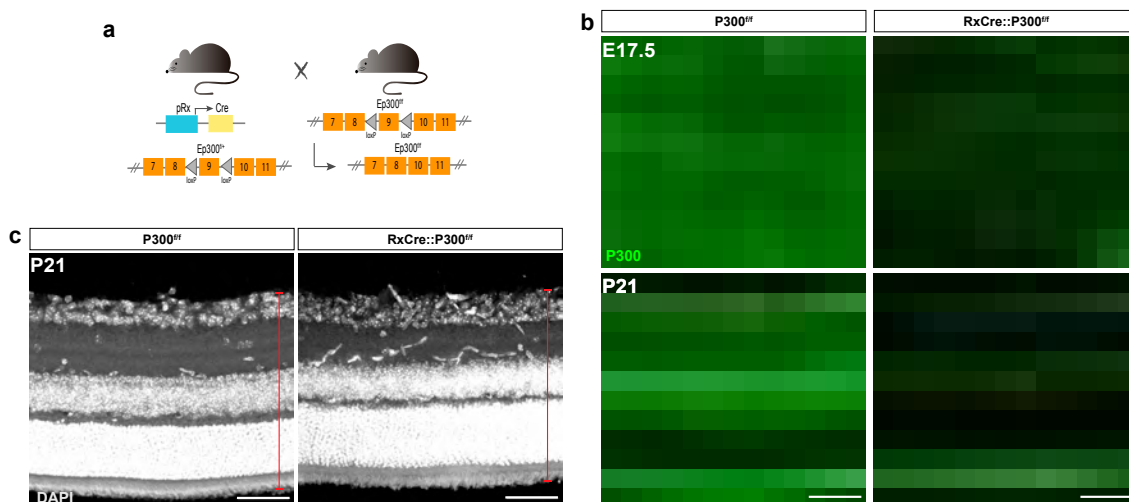


Figure 25. P300 ablation in retinal progenitor cells do not alter retinal formation. (a) Genetic strategy for the production of Rx-Cre::P300^{f/f} mice in which exon 9 of *Ep300* is flanked by loxP sites. (b) Immunostaining for P300 in retinal sections of E17.5 (top) and P21 (bottom) Rx-Cre::P300^{f/f} mice showing a reduction of this marker in the mutant retinas, confirming recombination in the most retinal progenitor cells. (c) Retinal sections of P21 Rx-Cre::P300^{f/f} mice indicates that retinal thickness is not affected after P300 removal in retinal progenitor cells. Scale bars 50µm.

To confirm that the different retinal cell types are not altered after P300 removal from retinal progenitor cells, we crossed these mice with a tdTomato reporter mouse line to label recombined cells (**Fig. 26a**). The analyses of P21 RxCre::P300^{f/f} mice, retinas did not show changes in the thickness or the proportion of photoreceptors (**Fig. 26b**), amacrine and horizontal cells (**Fig. 26c**) or RGCs (**Fig. 26e**). The proportion of cells per layer did not change either (**Fig. 26d, 26f**) compared to control animals (RxCre::tdTomato).

Altogether these results suggest that selective deficiency of P300 in retinal progenitor cells does not cause a defect in retinal development.

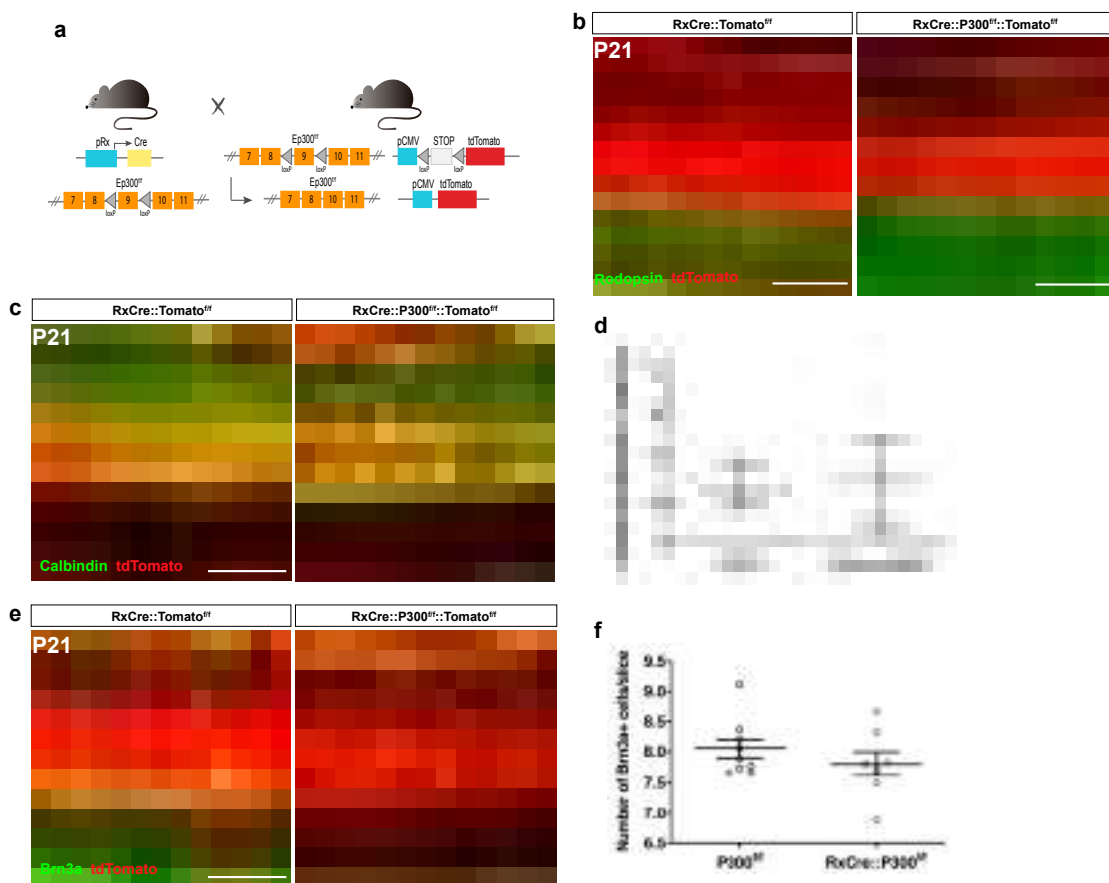


Figure 26. Embryonic ablation of P300 in retinal progenitor cells do not trigger alterations in retinal cell layers. (a) Genetic design for the production of Rx-Cre::P300^{f/f}::tdTomato^{f/f} mice in order to label the recombined cells. (b, c, e) Immunostaining in retinal sections of P21 Rx-Cre::P300^{f/f}::tdTomato^{f/f} mice and controls (Rx-Cre::tdTomato^{f/f}) showing no differences in photoreceptor layer (b), amacrine and horizontal layer (c) or retinal ganglion cell layer (e) after P300 ablation in retinal progenitor cells. (d) Quantitative analysis of calbindin positive cells in control and Rx-P300cKO mice reveals no significant differences in amacrine and horizontal populations. (f) Quantification of Brn3a positive RGCs indicates no statistical differences between groups. Graphs represent mean ± SEM (average of 9 ROIS from a minimum of 3 retinal sections per animal; n=9 animals per genotype). Statistic: t-test. Scale bars 50µm.

5. The absence of CBP in retinal progenitor cells leads to alteration in retinal development

To figure out the function of CBP in retinal progenitor cells we crossed the Rx-Cre mouse line with the CBP floxed mouse line (described in the part I at the results section) (**Fig. 27a**).

We first confirmed that Cre-mediated recombination ablates CBP in the retina, by performing immunohistochemistry for CBP in the retinas of Rx-Cre::CBP^{f/f} mice. In accordance with Sun1-GFP expression, we found that CBP ablation actually occurred in the in most of the retinal cells affecting all retinal cell types, but we observed columns of retinal cells that escaped from recombination and expressed CBP following a random mosaic pattern (**Fig. 27b**). Despite this mosaicism, we noticed that the lack of CBP in the majority of retinal progenitor cells leads to a significant decrease in the thickness of Rx-Cre::CBP^{f/f} mutant retinas as well as the presence of morphological alterations in retinal layering (**Fig. 27c arrows**).

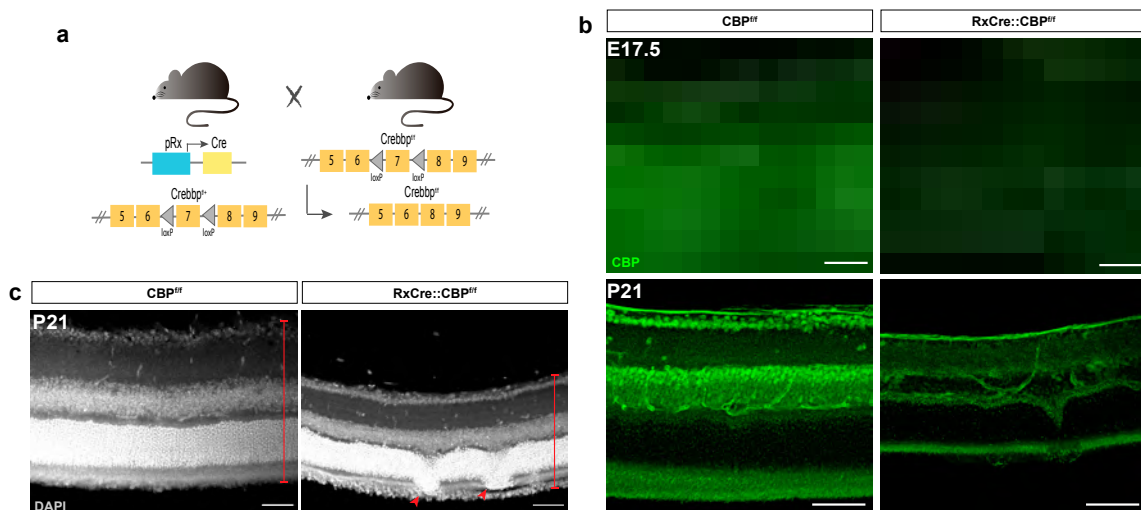


Figure 27. CBP ablation in retinal progenitor cells alters retinal formation. (a) Genetic strategy for the production of Rx-Cre::CBP^{f/f} mice in which exon 7 of *CBP* is flanked by loxP sites. (b) Immunostaining for CBP in retinal sections of P0 (top) and P21 (bottom) Rx-Cre::CBP^{f/f} mice show a reduction of this marker in the mutant retinas, confirming ablation in the most retinal progenitor cells but some cells escaped from recombination and maintained CBP expression. (c) Retinal sections of Rx-Cre::CBP^{f/f} mice counterstained with DAPI show a reduction in the retinal thickness comparing with control animals. Scale bars 50µm. 90

To further investigate this strong reduction in retinal thickness, we crossed the Rx-Cre::CBP^{f/f} mice with tdTomato reporter mice to specifically label the recombined cells (**Fig. 28a**). Immunostaining of retinal sections at P21 showed a reduction in the number of cells expressing the RGCs marker Brn3a (**Fig. 28c,e**) compared with their control littermates. However, the RGC layer was not the only retinal layer affected, since we detected also a reduction in the number of Calbindin positive cells, which are amacrine and horizontal cells (**Fig. 28b,e**).

To better quantify the reduction in the thickness of retinal layers, we dissected, disaggregated the retinas of Rx-Cre::CBP^{f/f} mutant and control mice to then immunostain the cells for different markers and analyzed them by fluorescent activated cell sorting (FACS). Quantitative analysis of retinal populations by FACS revealed that the total number of retinal cells in the Rx-Cre::CBP^{f/f}::tdTomato^{f/f} mutant mice was significantly reduced. Also, the percentage of recombined cells in mutant retinas were reduced (31.68%) compared to the control (54.85%) (**Fig. 28f**). The number of Brn3a+Tomato+ cells was decreased 31% compared to the controls (**Fig. 28f**). The number of Calbindin+Tomato+ cells was also reduced in the absence of CBP (**Fig. 28g**) compared to control retinas.

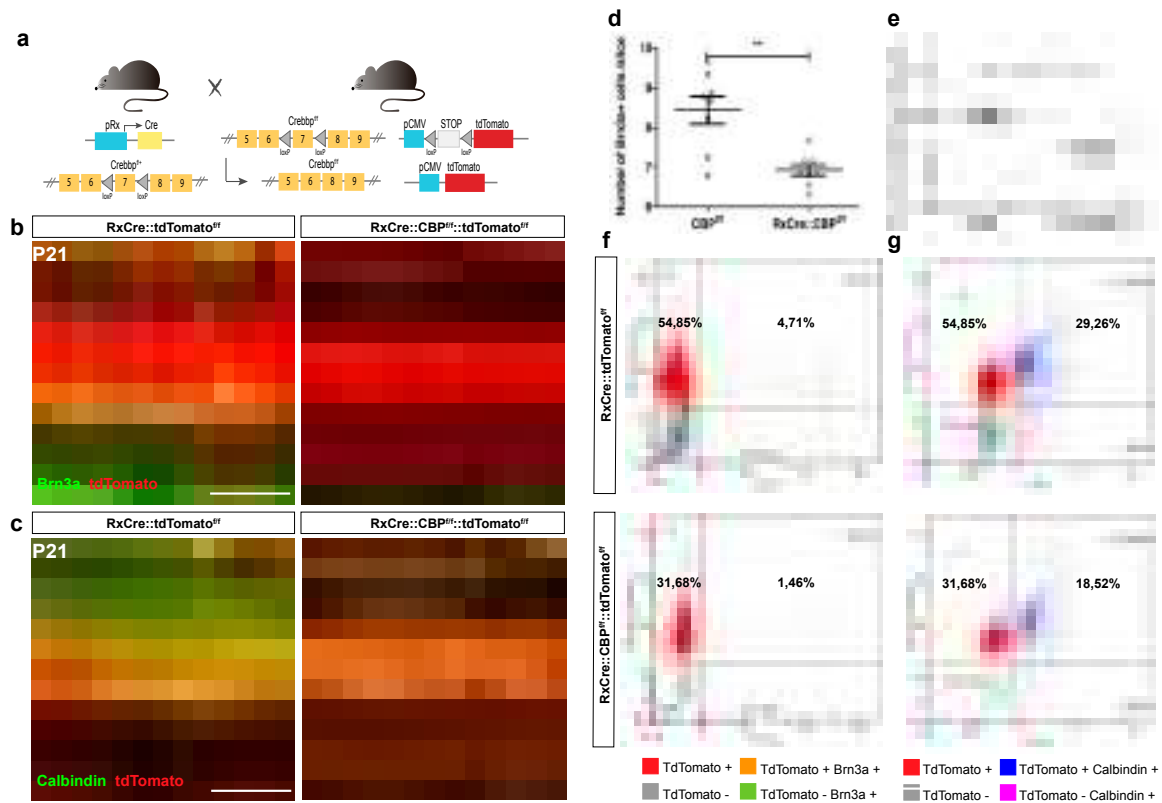


Figure 28. Embryonic ablation of CBP in retinal progenitor cells generate alterations in retinal cell layers. (a) Genetic design for the production of Rx-Cre::CBP^{fl/fl}::tdTomato^{fl/fl} mice in order to label the recombined cells. (b, c) Immunostaining in retinal sections of P21 Rx-Cre::CBP^{fl/fl}::tdTomato^{fl/fl} mice and controls (Rx-Cre::tdTomato^{fl/fl}) reveal a thickness reduction of retinal ganglion cell layer (b) or amacrine and horizontal layer (c) after CBP ablation in retinal progenitor cells. (d,e) Quantitative analysis of Brn3a positive cells and calbindin positive cells in control and Rx-P300cKO mice reveals significant differences in retinal ganglion cells (d) and amacrine and horizontal populations (e) (average of 9 ROIS from a minimum of 3 retinal sections per animal; n=9 animals per genotype). (f, g) Fluorescent-activated sorting plots for immunostained retinal cells from controls and CBP ablated retinal progenitor cell showing counts against forward scatter (FSC) (n=3, each sample contains a pool of retinas from 3 animals).

In addition, we detected aberrant retinal invaginations at different ages in the 100% of Rx-Cre::CBP^{fl/fl} mutant animals although the layering of the different cell types was overall maintained (Fig. 29a). The size of these aberrant retinal structures was variable among individuals likely due to mosaicism of the RxCre mouse line, but it was present in all Rx-Cre::CBP^{fl/fl} mutant animals (n=20). We observed caspase-positive cells in these aberrant retinal structures indicating that some cells undergo apoptosis in the

absence of CBP which may explain the reduction in the number of retinal cells in the Rx-Cre::CBP^{f/f} mutant animals (**Fig. 29b**).

Therefore, these results demonstrate that the lack of CBP in retinal progenitor cells at early embryonic stages produces an alteration in retinal development and hence CBP expression is essential for retinal differentiation.

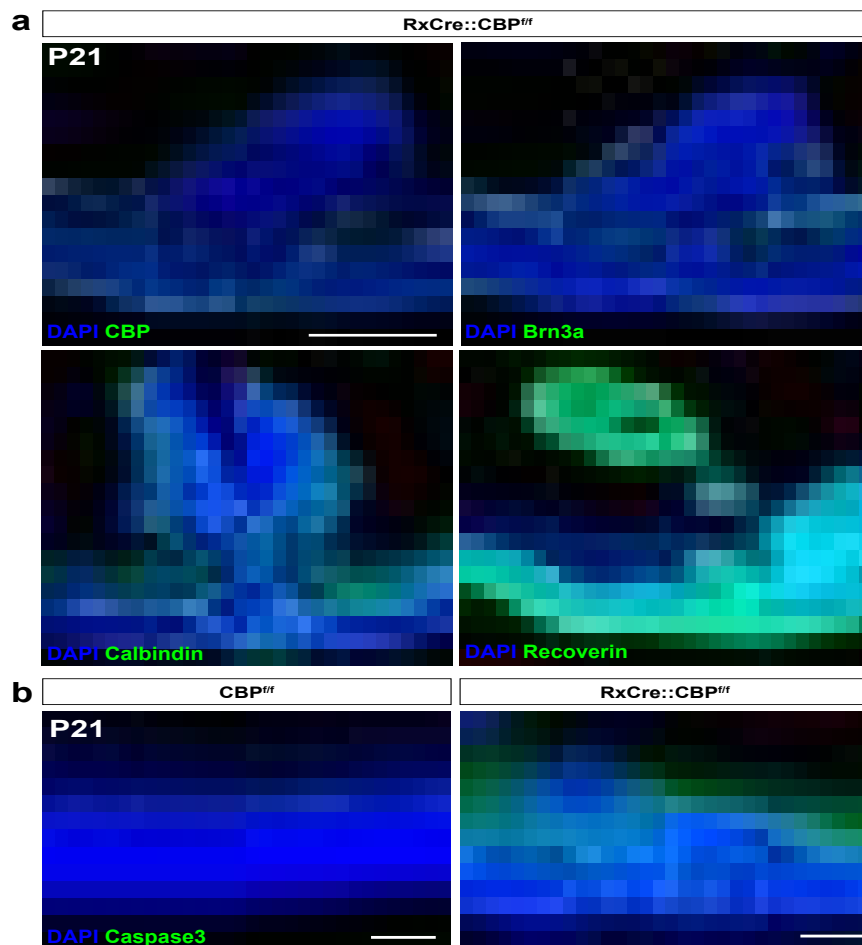


Figure 29. CBP ablation in retinal progenitor cells leads to aberrant retinal structures joined to cell death (a) P21 Rx-Cre::CBP^{f/f} mutant mice reveal retinal invaginations and maintained retinal layering with the differentiated retinal markers Brn3a (RGC marker), Calbindin (Amacrine and Horizontal cell marker) and Recoverin (photoreceptor marker) in green **(b)** Immunostaining for Caspase 3 in retinal sections of P21 Rx-Cre::CBP^{f/f} mutant mice and control mice show an increase in cell death in retinas from Rx-Cre::CBP^{f/f} mutant mice. Scale bars 200µm (a) and 50m (b).

6. Simultaneous elimination of CBP and P300 in Rx progenitor cells leads to a dramatic phenotype and embryonic lethality

To address whether KAT3 proteins play a redundant role in neural progenitor cells *in vivo*, we crossed the RxCre mouse line with the double floxed KAT3 mouse line eliminating both KAT3 proteins in Rx progenitor cells since E7.5 (**Fig. 30a**).

RxCre::CBP^{f/f} and RxCre::P300^{f/f} mice had a normal lifespan. However, simultaneous depletion of CBP and P300 in Rx progenitor cells leads to premature embryonic lethality just before birth, observing live embryos until E17.5.

Embryos at different stages, with simultaneous removal of CBP and P300 in Rx progenitor cells, revealed a severe phenotype. Rx double mutant embryos displayed apparent malformations in the head, with a reduced volume of the telencephalic vesicles and the absence of eyes in some cases (**Fig. 30b**) compared with their control littermates (n=15 litters). Other variable phenotypic alterations in the face were observed, such as flat face or harelips.

In the visual system, some double mutant embryos only present one eye in the proper position, and some others had their eyes in the middle of the brain (**Fig. 30c**), suggesting that transcription factors controlling eye morphogenesis may be seriously altered in these mice. The retinas of these mutant mice exhibit foldings, lens alterations and retinal disorganization that were not present in their control littermates, and the retinal markers of both progenitor and differentiated retinal cells were severely altered (**Fig. 30c**).

The severity of this dramatic phenotype was variable among individuals likely due to mosaicism of the RxCre mouse line, but all double mutant mice exhibit malformations in forebrain and retinas.

Overall, these data demonstrate that the simultaneous loss of CBP and p300 alters normal retinal development among other important areas in the central nervous system, and hence at least one of the KAT3 proteins is required for neural development.

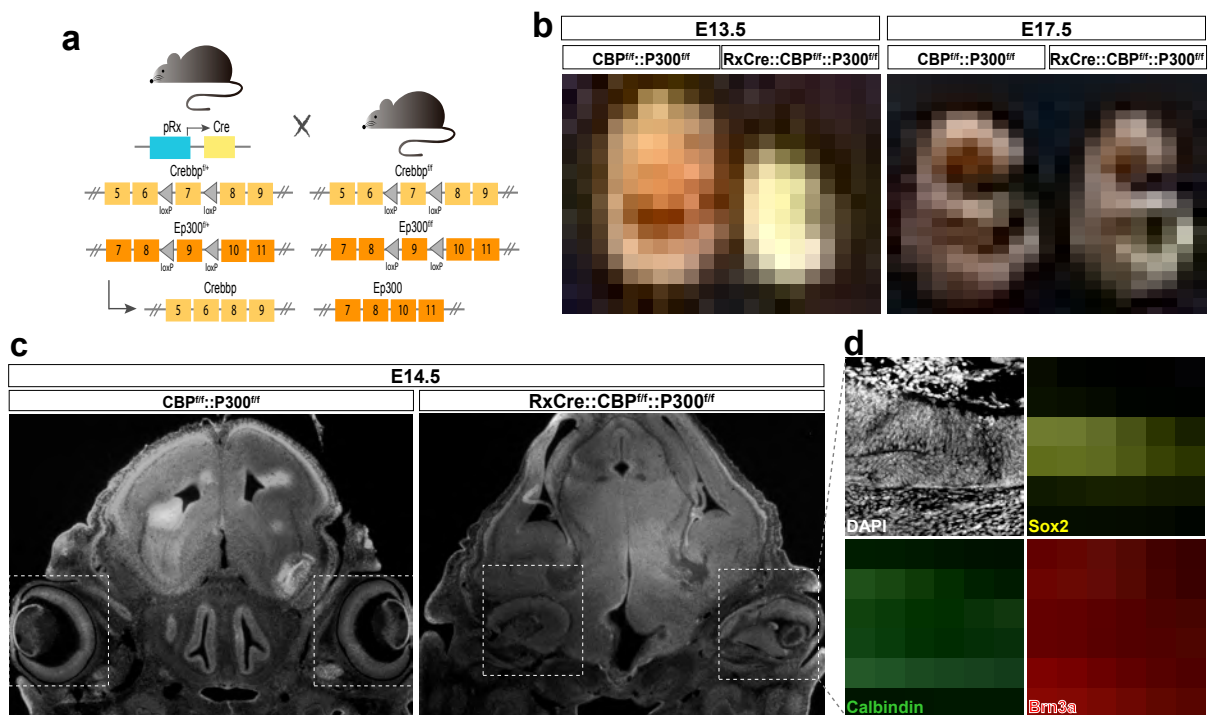


Figure 30. Simultaneous ablation of both KAT3 proteins in retinal progenitor cells leads to a severe phenotype and embryonic lethality. (a) Genetic strategy for the production of Rx-Cre::CBP^{fl/fl}::P300^{fl/fl} to eliminate both KAT3 proteins in neural progenitor cells. (b) Embryos at E13.5 and E17.5 show that simultaneous removal of KAT3 proteins in Rx progenitor cells leads to dramatic phenotypic defects (n=15 litters). (c) Low magnification of coronal sections of E14.5 mice, counterstained with DAPI, show alterations in brain development and eye morphogenesis. (d) Immunostaining in retinal sections of E14.5 double mutant mice show alterations in the progenitor retinal marker Sox2 and in the differentiated retinal markers Brn3a and Calbindin. Scale bars 50µm.

III. The role of KAT3 proteins in neuronal maturation

1. Newborn neurons lacking P300 do not show alterations in dendritic growth

Recent reports from the laboratory of Dr. Barco have demonstrated that CBP is essential to activate the gene programs related to dendritic growth and spine maturation in the last steps of neuronal maturation (Del Blanco *et al.*, 2019). However, the necessity of P300 in this late stage of neural developmental has not been assessed. To address whether P300 is required in the maturation of new neurons, we carried out similar studies to those previously performed for CBP in Del Blanco *et al.*, 2019. We crossed the P300 floxed mouse line with a Nestin-Cre transgenic mouse line to generate mice lacking P300 from Nestin-positive cells (**Fig. 31a**). This Nestin-Cre line has been widely used to direct recombination of neural stem cells (NSCs) and neural progenitor cells (NPC) but it has been reported that recombination is insufficient in early embryonic stages and only occurs at late embryonic and early postnatal periods (Liang *et al.*, 2012) when newborn neurons are generated.

First, we analyzed the survival of the pups, because in the case of the NestinCre::CBP^{f/f} mice, pups die at birth due to respiratory failure as a result of innervation defects at the diaphragm. Contrary to CBP, NestinCre::P300^{f/f} newborn pups survive after birth but the percentage of homozygous mutant mice were reduced compared to Mendelian ratios (n=20 litters) (**Fig. 31b**). These homozygous mutant mice reached adulthood and they developed without obvious phenotypic alterations.

We next investigated whether P300 was required for neuronal maturation performing primary neuronal cultures from hippocampi of E17.5 NestinCre::P300^{f/f} embryos and their control littermates. Primary neuronal cultures were transfected at 9DIV with a plasmid encoding GFP under neuronal-specific synapsin promoter and fixed after 24h to analyze the neuronal morphology (**Fig. 31c**). Immunostaining of

NestinCre::P300^{f/f} and control cultures confirmed the loss of P300 in mutant cultures (**Fig. 31d**). In the absence of P300, we did not observe differences both in the staining against astrocyte marker GFAP (**Fig. 31e**) or in the staining against neuronal marker MAP2, compared to the control cultures (**Fig. 31f**).

To confirm that maturation of newborn neurons was not altered in the NestinCre::P300^{f/f} cultures, we evaluated the morphology of individual neurons transfected with Syn-GFP and we observed that the dendritic tree of neurons lacking P300 did not show differences compared control neurons (**Fig. 31g**).

Overall, these results demonstrate that in contrast to CBP, the lack of P300 does not affect maturation of newborn neurons *in vitro*.

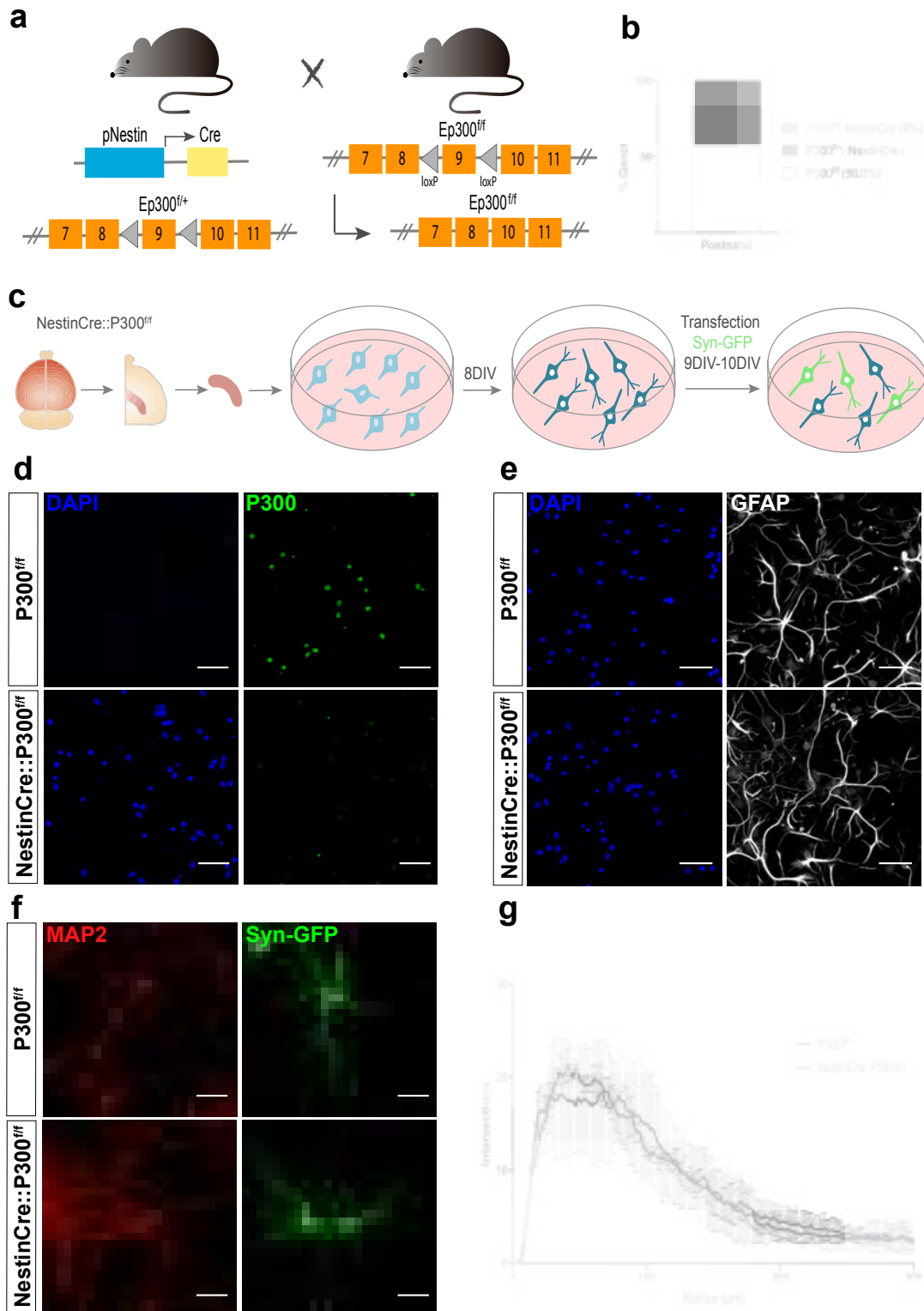


Figure 31. Cultured newborn neurons lacking P300 do not show altered maturation. (a) Genetic strategy used to ablate P300 in neural progenitor cells. (b) Graph represents the proportion of embryos and postnatal animals per genotype in NestinCre::P300^{fl/fl} crosses (n=20 litters). (c) Experimental design of the approach used to study the effect of P300 ablation in hippocampal cultured neurons. (d) Immunofluorescent staining showing P300 loss in NestinCre::P300^{fl/fl} cultured neurons at 10DIV. (e-f) Immunostaining for GFAP (e) and MAP2 (f) in hippocampal neurons transfected with Syn-GFP at 10DIV. Same field is represented in the different stainings. (g) Sholl analysis of hippocampal cultured neurons representing intersections against distance to soma show no differences in the dendritic tree of newborn neurons lacking P300 (n = 4–5 neurons from three independent cultures). Scale bars 50µm.

IV. The role of CBP and P300 in the maintenance of differentiated neurons

1. CBP and P300 are not individually required for the maintenance of RGCs identity

It has been recently reported that combined elimination of KAT3 proteins in forebrain excitatory neurons resulted in a rapidly progressing neurological phenotype associated with dendritic retraction and a rapid loss of neuronal molecular identity (Lipinski *et al.*, 2020). However, the necessity of KAT3 in the maintenance of retinal fate remain unclear.

To approach this question, we used a Brn3b-Cre mouse line, that drives cre recombination specifically in recently differentiated RGCs since embryonic day E13.5. First, we analyzed the effect of individual ablation of CBP or P300 in these differentiated RGCs. Immunostaining confirmed that CBP and P300 were efficiently eliminated from RGCs in Brn3bCre::CBP^{fl/fl} and Brn3bCre::P300^{fl/fl} postnatal mice P21 (**Fig. 32c,d**). The number of Brn3a positive cells found in retinal sections from Brn3bCre::CBP^{fl/fl} and Brn3bCre::P300^{fl/fl} mice was similar to the controls suggesting that removal of CBP or P300 once the cell is differentiated does not revert RGC identity. RGC axons projecting to the brain were labeled by injecting axonal tracers of Cholera toxin-B conjugated with Alexa Fluor™ 594 or Alexa Fluor™ 647 injected in each eye, as we previously described in Escalante *et al.*, 2020; and showed no obvious alterations through the visual pathway (**Fig. 32i**). RGCs specific markers such as Brn3a were normally expressed in Brn3bCre::CBP^{fl/fl} or Brn3bCre::P300^{fl/fl} (**Fig. 32e-h**), indicating that neither CBP or P300 are required for the maintenance of neural identity in differentiated RGCs.

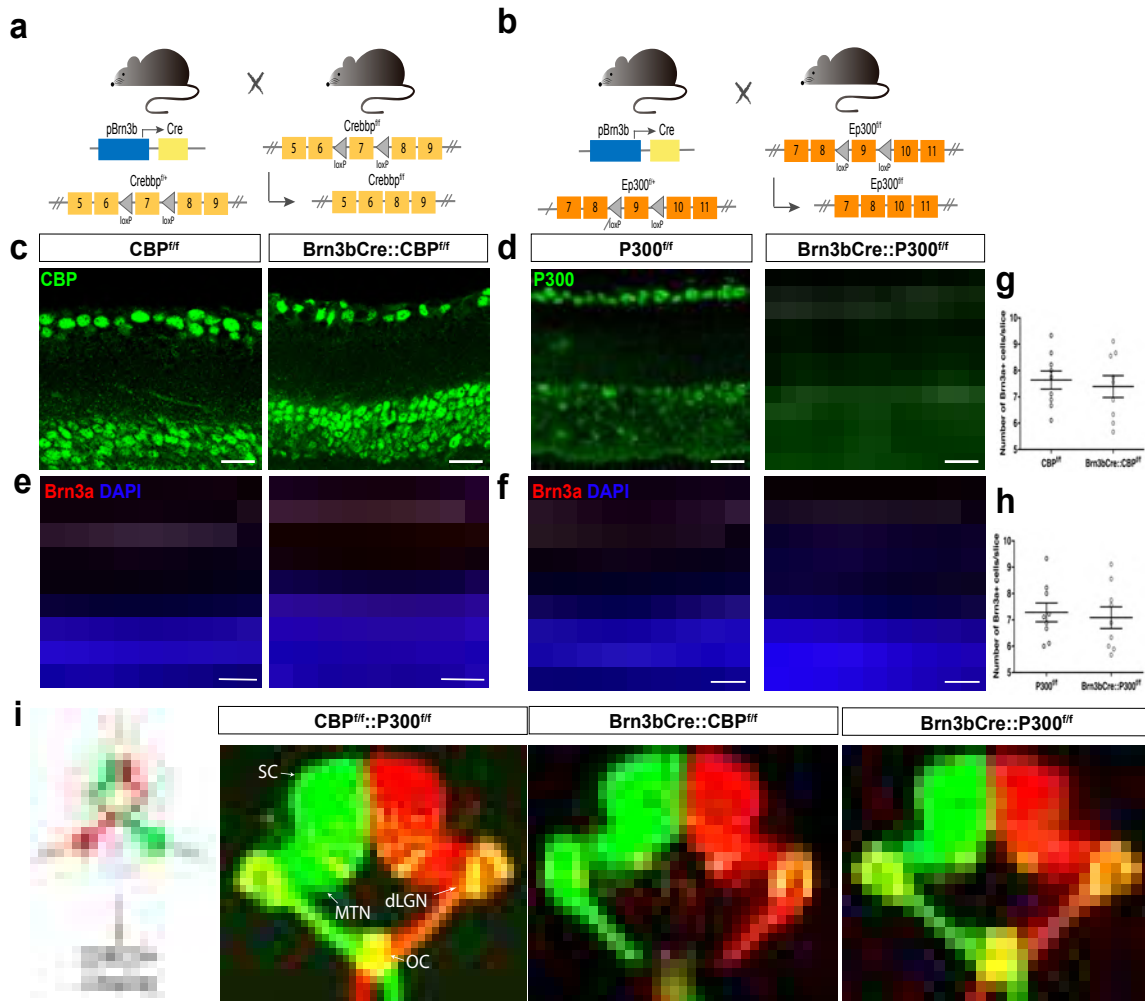


Figure 32. Individual ablation of CBP or P300 in postmitotic RGCs do not alter RGCs specification. (a,b) Genetic strategy for the production of Brn3bCre::CBP^{fl/fl} and Brn3bCre::P300^{fl/fl} to ablate KAT3 proteins in postmitotic RGCs. (c, d) Immunostaining for CBP (c) or P300 (d) in retinal sections of P21 mice reveal a reduction of each protein in the single mutant mice (e,f) Retinal sections of P21 mice, counterstained with DAPI, show similar expression of Brn3a in the Brn3bCre::CBP^{fl/fl} and Brn3bCre::P300^{fl/fl} mice (g,h) Quantitative analysis of Brn3a positive cells in control and Brn3bCre::CBP^{fl/fl} and Brn3bCre::P300^{fl/fl} shows similar number of retinal ganglion cells (average of 9 ROIS from a minimum of 3 retinal sections per animal; n=9 animals per genotype). (i) 3D reconstruction of the visual pathway of control and Brn3bCre::CBP^{fl/fl} and Brn3bCre::P300^{fl/fl} mice at P23, labeled with the axonal tracer Cholera toxin-B conjugated with Alexa Fluor™ 594 or Alexa Fluor™ 647 injected in the eyes, reveals no alteration in the axonal pathway of single mutant mice. SC: superior colliculus; dLGN: lateral geniculate nucleus; OC: optic chiasma; MTN: medial terminal nucleus. Scale bars 50µm.

We next analyzed the retinas of mutant mice in which both KAT3 proteins were removed from postmitotic RGCs (Brn3b-Cre::CBP^{f/f}::P300^{f/f}). Simultaneous ablation of both KAT3 proteins revealed a reduction in the number of RGCs expressing the Brn3a marker (Fig. 33c,d) indicating that at least one of the KAT3 proteins is needed to maintain neuronal identity. Accordingly, the analysis of the visual pathway in these mice, using axonal tracer injection, showed normal axonal trajectories in the double mutant mice (Fig. 33e).

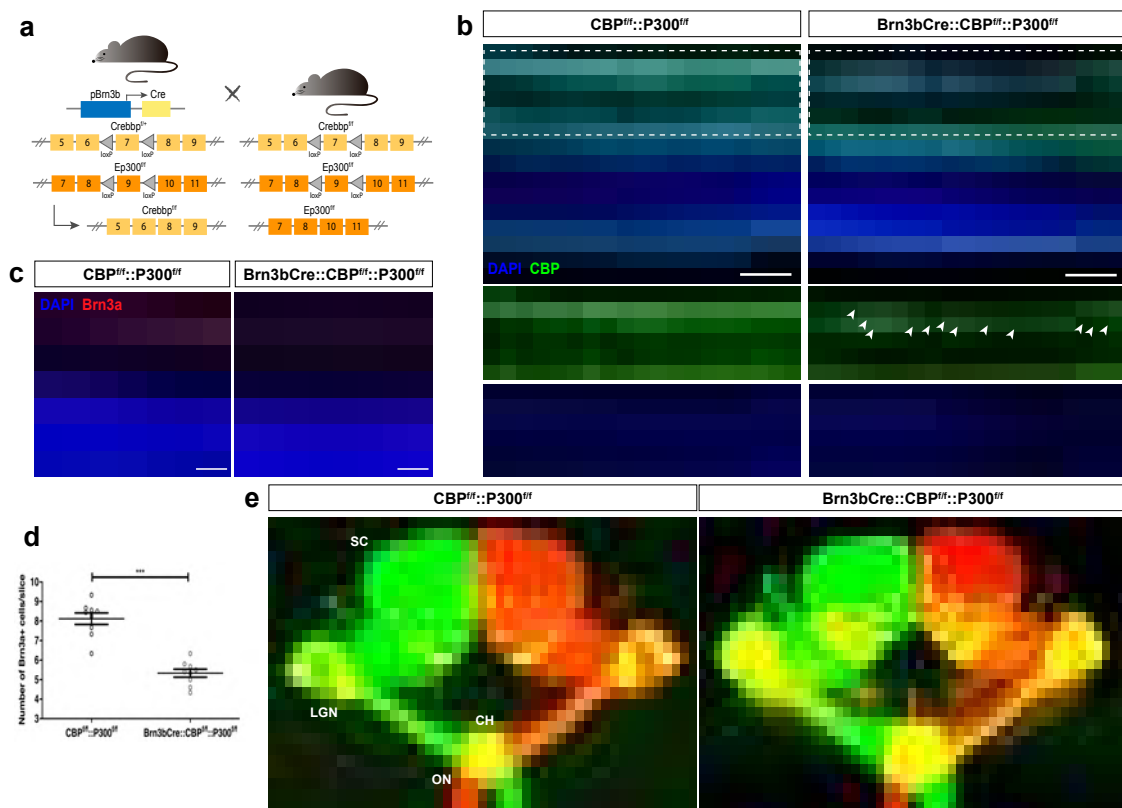


Figure 33. Simultaneous ablation of both KAT3 proteins in postmitotic RGCs reveal a loss of the RGC marker Brn3a without alteration in the visual pathway. (a) Genetic strategy for the production of Brn3b-Cre::CBP^{f/f}::P300^{f/f} to eliminate both KAT3 proteins in postmitotic RGCs. (b) Immunostaining for CBP counterstained with DAPI in retinal sections of P21 mice reveal a reduction of this protein in the double mutant mice without alterations in other retinal layers (c) High magnification of retinal sections of P21 mice, counterstained with DAPI, show a reduction in the expression of Brn3a in the Brn3b-Cre::CBP^{f/f}::P300^{f/f} mice (d) Quantitative analysis of Brn3a positive cells in control and Brn3bCre::CBPcKO-P300cKO mice reveals significant reduction in the number of retinal ganglion cells (average of 9 ROIS from a minimum of 3 retinal sections per animal; n=9 animals per genotype). (e) 3D reconstruction of the visual pathway of control and Brn3b-Cre::CBP^{f/f}::P300^{f/f} mice at P23, labeled with the axonal tracer Cholera toxin-B conjugated with Alexa Fluor™ 594 or Alexa Fluor™ 647 injected in the eyes, reveals no alteration in the axonal pathway of double mutant mice. SC: superior colliculus; LGN: lateral geniculate nucleus; CH: chiasma; ON: optic nerve. Scale bars 50µm (c) and 100µm (e)

DISCUSSION

1. KAT3 proteins play a redundant role in NSC proliferation but they are unable to compensate the lack of the other in the differentiation process.

Conventional knockout mice show embryonic lethality between E9-E12.5 (Yao *et al.*, 1998, Tanaka *et al.*, 2000) due to a failure in neural tube closure and extensive brain hemorrhage, limiting the investigation of the effects of CBP and P300 ablation in the CNS.

First studies suggested that both KAT3 proteins play a similar role in embryonic development because of the almost identical phenotype of conventional knockouts (Yao *et al.*, 1998) and their sequence homology (Breen and Mapp 2018). Most studies over the years have been focused on the role of CBP in different paradigms but more recent studies have shown that in specific tissues, the function of these proteins is not overlapping. For instance, P300 is required for development of lung or heart (Roth *et al.*, 2003; Shikama *et al.*, 2003) whereas CBP have a prominent role in motor neurons differentiation (Lee *et al.*, 2009).

Given these observations we decided to tackle several strategies to ablate either CBP, P300 or both proteins at different developmental stages to determine their functions and potential redundancy. To unravel the function of KAT3 in proliferation and differentiation of NSC we performed neurosphere cultures from the SVZ (Reynolds and Weiss, 1992).

Previously work from Wang and collaborators (Wang *et al.*, 2010) show that, *in vitro*, CBP knockdown has no effect on the percentage of proliferating cortical precursor cells expressing Ki67 or cleaved caspase-3, markers of proliferation and apoptosis,

respectively. Our findings go further and demonstrate that proliferation of neural progenitor cells is not affected not only in the absence of CBP but also in the absence of P300 *in vitro* but is seriously compromised when both proteins are absent.

In addition, neurosphere cultures showed that elimination of either CBP or P300 impeded glial and neuronal differentiation. Few β Tuj positive neurons and S100 β positive mature astrocytes were observed in CBP or P300 lacking cultures, and the morphology of GFAP positive astrocytes was seriously altered in both conditions compared to control differentiated cultures. It has been described that morphological changes of astrocytes can also alter neuronal networks, which can apparently contribute to the development of several diseases such as schizophrenia or Alzheimer, among others (Sofroniew and Vinters, 2010).

Single nuclei RNA Sequencing (snRNA-Seq) analysis were performed to determine more precisely the molecular basis of the dramatic reduction of neurons and mature astrocytes. Bioinformatic analysis of the snRNA-Seq revealed that the astrocyte population completely disappeared after ablation of one of the two KAT3 protein.

snRNA-Seq also showed that a small population of mature neurons was not altered in the absence of CBP or P300. This could be due to neurospheres contain a heterogeneous population of cells in which NSCs coexist with their progeny (more committed progenitors and even differentiated cells). Thus, at the time of ablation, committed progenitors or differentiated neurons could have lost CBP or P300 after acquiring their fate. However, enrichment analysis showed that a large population of immature neurons in CBP or P300 lacking cultures exhibited a downregulation of many DEGs involved in biological processes related to neuronal differentiation such as cell polarity and adhesive functions, axonal projection and guidance or synapse organization

and assembly, including many well-known modulators of these processes such as *Nrxn1*, *Grik2*, *Sema3d*, *Nlgn1* or *Ntm*. Similar results were observed by Calzari *et al.*, 2020 who developed transcriptome analysis of iPSC-derived neurons from Rubinstein-Taybi patients which revealed deficits in neuronal differentiation and an altered neuroprogenitor to neuron transcriptional program.

Regarding astrocytes, cluster population expressing bona fide markers that define astrocytes, such as *Sc11a3* (GLAST), *Sc17a11*, *Gpc5*, or *Rorb*, completely disappeared in CBP or P300 lacking cultures. This disappearance of astrocyte cluster was accompanied by the upregulation of other populations such as Neuron/OPC in the case of P300 lacking cultures. Surprisingly, OPC and oligodendrocyte specific genes were significantly upregulated in the absence of CBP, event that was not possible to visualize in culture due to the small percentage of oligodendrocytes (~4%) (Singec *et al.*, 2006; Chaddah *et al.*, 2012). These results suggested that cells which had to acquired astrocyte fate were not able to develop and acquired a new different fate depending on the absence of each KAT3 protein.

Our work provides significant evidence that support that CBP and P300 lacking NSCs are not able to differentiate properly in all the three neural lineages and also identified the specific transcriptional changes that accompanied these alterations, indicating that in astrocyte and neuron development, KAT3 proteins are not able to compensate the lack of the dose of the other KAT3 protein.

2. Non-redundant roles of KAT3 proteins in retinal progenitor cells.

KAT3 proteins are strongly expressed in murine retinal progenitor cells as we have demonstrated by immunostaining. Based upon its expression, we sought to figure out the role of CBP and P300 in retinal progenitor cells. We designed a genetic strategy to ablate either one or both proteins simultaneously in Rx-positive progenitor cells. The characterization of Rx-mice shows that the system was not totally efficient, resulting in the elimination of KAT3 proteins only in a randomly variable mosaic of the retina, although the elimination of the genes happened in recombined progenitor cells. Surprisingly, the ablation of P300 alone did not cause any alteration in the retina whereas CBP ablation displayed a characteristic phenotype with aberrant invaginations accompanied by a reduction in the thickness of all retinal layers, supporting previous postulations of its important role in brain size regulation (Ateca-Cabarga *et al.*, 2015). This different phenotype between the CBP and P300 conditional mutants could be explained by the different expression levels of KAT3 proteins in distinct tissues since CBP is highly expressed than p300 in the CNS (Lipinski *et al.*, 2019). In fact, we observed a higher expression of CBP in retinal progenitor cells compared to P300 expression, although this differential expression may be due to the quality of the antibodies that we used.

A dramatic phenotype was shown in the simultaneous absence of both proteins. Double mutant mice exhibited exencephaly, retinal malformations such as foldings and disorganizations, lens alterations and embryonic lethality before birth, similar to conventional knockout phenotypes but at later embryonic stages. This could be explained because of the mosaicism generated by the Rx-Cre mice and also, because Rx- expression begins to be expressed at E10, eliminating KAT3 proteins later in development than in

the conventional knockout mice. These results perfectly match with frequently brain malformations observed in RSTS patients, such as microcephaly as well as eye anomalies (Cantani *et al.*, 1998; Hennekam 2006).

Our data provide significant evidence to support that the simultaneous loss of CBP and p300 in early progenitor cells of the retina and forebrain alters normal retinal development among other important areas of the central nervous system, and hence, at least one of the KAT3 proteins are required for neural development. Moreover, our findings demonstrate the non-redundancy of CBP and P300 in the differentiation of retinal progenitor cells. The mechanism behind this process requires further rigorous investigation.

3. The maturation of newborn neurons does not require P300.

KAT3 proteins are known to regulate embryonic development (Yao *et al.*, 1998; Tanaka *et al.*, 2000) and they are also involved in regulate specification of spinal motor neurons, interneurons (Lee *et al.*, 2009; Tsui *et al.*, 2014; Medrano *et al.*, 2019). However, the effects of KAT3 ablation in maturation of neurons have not been thoroughly investigated.

Previous investigations from Del Blanco *et al.*, 2019 described that CBP plays a crucial role activating the gene programs related to dendritic growth and spine maturation in the last steps of differentiation and maturation of newborn neurons. We have conducted similar experiments to investigate the necessity of P300 in this developmental maturation in late embryonic and early postnatal periods, when nestin is expressed (Liang *et al.*, 2012). In contrast to the situation of the CBP conditional Nestin-Cre mice, P300 conditional Nestin-Cre mice do not exhibit embryonic lethality although the ratio of mutant births was reduced. Immunostaining with specific antibodies confirmed the ablation of P300 in newborn neurons of NestinCre::P300^{ff}. However, the lack of P300 did not comprise dendritic growth and spine maturation of newborn neurons.

Overall, these results demonstrate that contrasting to the elimination of CBP, the lack of P300 does not affect maturation of newborn neurons indicating that CBP plays a key role in neuronal maturation process whereas P300 is not required. Contrary to it has been suggested because of the ubiquitously expression and the high sequence homology of KAT3 proteins, this result reveals the non-interchangeable function of CBP and P300 in neuronal maturation. Consequently, the lack of CBP could not be compensate with the normal dose of P300 but it would be interesting to study whether upregulation of specific

domains of P300 could rescue alterations in dendritic growth or spine maturation of newborn neurons, representing an encouraging therapeutic strategy for RSTS.

4. At least one KAT3 protein is required for the maintenance of neuronal identity.

Previous studies have shown that removal of KAT3 proteins leads to deficits in synaptic plasticity and memory storage of differentiated hippocampal neurons (Korzus *et al.*, 2004; Viosca *et al.*, 2010) and are essential for the maintenance of neuronal identity in adult forebrain neurons (Lipinski *et al.*, 2020). However, the role of these proteins in the maintenance of other cell types remain unclear.

Here, we analyzed the necessity of KAT3 in the maintenance of retinal fate. We designed a genetic strategy to remove either one or both proteins using a specific mouse line that drives cre recombination specifically in recently differentiated RGCs. We have demonstrated that individual ablation of CBP or P300, confirmed by immunostaining, did not alter RGCs identity, location or axonal pathways at the visual nuclei.

In contrast, our data have shown that genetic ablation of both KAT3 proteins simultaneously in differentiated RGCs caused a defect in specific RGCs markers. This loss of RGC markers was not accompanied by alterations in the axons of differentiated RGCs once retinal fate was acquired, contrary to hippocampal neurons which retracted axons in the absence of both KAT3 proteins (Lipinski *et al.*, 2020).

Therefore, CBP and p300 alone play an important, although mostly mutually redundant role for the function of maintenance of retinal ganglion cell identity once that is acquired.

5. Future perspectives

The results presented in this Thesis work provide novel insight into the etiology of RSTS and unveiled new aspects of the role of KAT3 proteins in neural development.

The studies reported here contribute to the state-of-the-art with novel findings regarding the non-redundancy roles of CBP and P300 through neural development. We presented here the first sn-RNA-Seq analysis of differentiation of NSCs lacking KAT3 proteins and we provided evidence for the crucial role of KAT3 proteins in the establishment of astrocyte lineage transcriptional program, as well as a potential involvement in the proper differentiation of neurons and oligodendrocytes. Moreover, the studies *in vivo* permitted the dissection of the neurological defects of RSTS patients by unravel the specific functions of KAT3 proteins in progenitor differentiation, maturation and maintenance of a differentiated neurons (**Table 1**).




Cell Stage	Neural Stem Cells	Neural Progenitors	Immature Neurons	Mature Neurons
Process	Proliferation	Differentiation	Outgrowth/ Synaptogenesis	Maintenance
 CBPKO	-	+++	++	-
 P300KO	-	++	-	-
 CBPKO::P300KO	+++	+++	NA	++

Table 1. Summary of the results presented in this Thesis work. Symbols represent NA: not available; + impact in this process; - no impact in this process.

Recent epi-editing techniques based on CRISPR/Cas9 technology have been developed as valuable tools to edit the epigenome (Hilton et al., 2015) and correct epigenetics defects. This progress opens new sights for new therapies that could complement classical pharmacological approaches based on KAT3 activation. Our results could contribute in the knowledge of transcriptional changes that occurs early in development of RSTS to design reversal therapies based on specific epi-editing approaches, and ameliorates RSTS symptoms.

CONCLUSIONS

CONCLUSIONS

1. CBP and P300 are not individually essential for proliferation of NSCs but ablation of both proteins simultaneously seriously compromises proliferation indicating a highly overlapping role of KAT3 proteins in proliferation.
2. Loss of CBP or P300 in NSCs causes significant consequences in neuronal differentiation and transcriptional gene expression of neuronal genes involved in synapse or neuronal projection development.
3. The astrocytic population does not develop in the absence of one of the two KAT3 proteins in NSCs.
4. The oligodendrocyte cell-type-specific genes are upregulated after CBP removal in NSCs.
5. CBP and P300 are expressed in all the retinal cell types from early embryonic development to postnatal stages in all the retinal cell types. However, CBP retinal expression appears to be higher than P300.
6. Loss of CBP in Rx-progenitor cells causes specific alterations of retinal development while individual ablation of P300 does not cause any significant consequences in the retina.
7. Simultaneous removal of KAT3 proteins in Rx-progenitor cells affects dramatically normal development of the telencephalon and the retina as well as animal survival.
8. While CBP is necessary for dendritic growth and spine maturation of newborn neurons while loss of P300 as far as we explored, does not appear to affect neuronal maturation.
9. CBP and P300 play redundant roles in the maintenance of differentiated retinal ganglion cells.

10. Removal of both KAT3 proteins in differentiated RGCs eliminates the expression of RGCs markers but does not affect axonal projections once the ganglion cell fate is acquired.

CONCLUSIONES

1. CBP y P300 no son individualmente necesarias para la proliferación de NSCs pero la eliminación de ambas proteínas simultáneamente compromete seriamente la proliferación, indicando un amplio solapamiento del papel de estas proteínas en proliferación.
2. La pérdida de CBP o P300 en NSCs causa consecuencias significativas en la diferenciación neuronal así como en la expresión transcripcional de genes implicados en sinapsis o desarrollo de proyecciones neuronales.
3. La población de astrocitos no es capaz de desarrollarse en ausencia en NSCs de una de las dos proteínas KAT3.
4. Los genes específicos del tipo celular de oligodendrocitos se encuentran regulados positivamente tras la eliminación de CBP en NSCs.
5. CBP y P300 son expresados en todos los tipos celulares de la retina desde el desarrollo embrionario temprano hasta etapas postnatales. Sin embargo, la expresión de CBP en la retina parece ser mayor que P300.
6. La pérdida de CBP en progenitores RX causa alteraciones específicas en el desarrollo de la retina, mientras que la eliminación de P300 no causa ninguna consecuencia significativa.
7. La eliminación simultánea de las proteínas KAT3 en progenitores RX afecta de forma dramática al desarrollo normal del telencéfalo y la retina, así como a la supervivencia.
8. Mientras que CBP es necesaria para el crecimiento dendrítico y maduración de espinas de neuronas mientras que la pérdida de P300 no afecta a la maduración neuronal.

9. CBP y P300 tienen papeles redundantes en el mantenimiento de células ganglionares de la retina diferenciadas.
10. La eliminación de ambas proteínas KAT3 en RGCs diferenciadas elimina la expresión de marcadores de RGCs pero no afecta a las proyecciones axonales una vez que el destino de célula ganglionar ha sido adquirido.

BIBLIOGRAPHY

- Abdolmaleky HM, Cheng KH, Russo A, Smith CL, Faraone SV, Wilcox M, Shafa R, Glatt SJ, Nguyen G, Ponte JF, Thiagalingam S, Tsuang MT. Hypermethylation of the reelin (RELN) promoter in the brain of schizophrenic patients: a preliminary report. *Am J Med Genet B Neuropsychiatr Genet.* 2005 Apr 5;134B(1):60-6.
- Alari V, Russo S, Terragni B, Ajmone PF, Sironi A, Catusi I, Calzari L, Concolino D, Marotta R, Milani D, Giardino D, Mantegazza M, Gervasini C, Finelli P, Larizza L. iPSC-derived neurons of CREBBP- and EP300-mutated Rubinstein-Taybi syndrome patients show morphological alterations and hypoexcitability. *Stem Cell Res.* 2018 Jul;30:130-140.
- Allfrey, V. G., Faulkner, R. and Mirsky, A. E. (1964). Acetylation and methylation of histones and their possible role in the regulation of RNA synthesis. *Proc Natl Acad Sci U S A* 51: 786-794.
- Arany Z, Sellers WR, Livingston DM, Eckner R. E1A-associated p300 and CREB-associated CBP belong to a conserved family of coactivators. *Cell* 1994;77:799–800.
- Armstrong JA, Emerson BM. Transcription of chromatin: these are complex times. *Curr Opin Genet Dev.* 1998 Apr;8(2):165-72.
- Ateca-Cabarga JC, Cosa A, Pallarés V, López-Atalaya JP, Barco Á, Canals S, Moratal D (2015) Brain size regulations by cbp haploinsufficiency evaluated by in-vivo MRI based volumetry. *Sci Rep* 5:16256
- Baden, T.; Berens, P.; Franke, K.; Roman Roson, M.; Bethge, M.; Euler, T. The functional diversity of retinal ganglion cells in the mouse. *Nature* 2016, 529, 345–350.
- Bannister AJ, Kouzarides T. The CBP co-activator is a histone acetyltransferase. *Nature.* 1996 Dec 19-26;384(6610):641-3.

- Bartsch O, Kress W, Kempf O, Lechno S, Haaf T, Zechner U. Inheritance and variable expression in Rubinstein-Taybi syndrome. *Am J Med Genet A*. 2010 Sep;152A(9):2254-61.
- Baye LM, Link BA. Interkinetic nuclear migration and the selection of neurogenic cell divisions during vertebrate retinogenesis. *J Neurosci*. 2007 Sep 19;27(38):10143-52.
- Bedford DC, Kasper LH, Fukuyama T, Brindle PK. Target gene context influences the transcriptional requirement for the KAT3 family of CBP and p300 histone acetyltransferases. *Epigenetics*. 2010;5:9–15.
- Belenguer G, Domingo-Muelas A, Ferrón SR, Morante-Redolat JM, Fariñas I. Isolation, culture and analysis of adult subependymal neural stem cells. *Differentiation*. 2016 Apr-Jun;91(4-5):28-41.
- Benito E, Valor LM, Jimenez-Minchan M, Huber W, Barco A. cAMP response element-binding protein is a primary hub of activity-driven neuronal gene expression. *J Neurosci*. 2011;31:18237–50.
- Boot, M.V.; van Belzen, M.J.; Overbeek, L.I.; Hijmering, N.; Mendeville, M.; Waisfisz, Q.; Wesseling, P.; Hennekam, R.C.; de Jong, D. Benign and Malignant Tumors in Rubinstein-Taybi Syndrome. *Am. J. Med. Genet. A* 2018, 176, 597–608.
- Breen, M.E.; Mapp, A.K. Modulating the Masters: Chemical Tools to Dissect CBP and P300 Function. *Curr. Opin. Chem. Biol.* 2018, 45, 195–203.
- Brei, T.J.; Burke, M.J.; Rubinstein, J.H. Glaucoma and Findings Simulating Glaucoma in the Rubinstein-Taybi Syndrome. *J. Pediatr. Ophthalmol. Strabismus* 1995, 32, 248–252.
- Brittis PA, Canning DR, Silver J. Chondroitin sulfate as a regulator of neuronal patterning in the retina. *Science*. 1992 Feb 7;255(5045):733-6.

- Buenaventura, D.F.; Ghinia-Tegla, M.G.; Emerson, M.M. Fate-restricted retinal progenitor cells adopt a molecular profile and spatial position distinct from multipotent progenitor cells. *Dev. Biol.* 2018, 443, 35–49.
- Butler A. Hoffman P. Smibert P. Papalexi E. Satija R. Integrating single-cell transcriptomic data across different conditions, technologies, and species. *Nat. Biotechnol.* 2018; 36: 411-420.
- Calzari L, Barcella M, Alari V, Braga D, Muñoz-Viana R, Barlassina C, Finelli P, Gervasini C, Barco A, Russo S, Larizza L. Transcriptome Analysis of iPSC-Derived Neurons from Rubinstein-Taybi Patients Reveals Deficits in Neuronal Differentiation. *Mol Neurobiol.* 2020 Sep;57(9):3685-3701.
- Cantani A, Gagliesi D. Rubinstein-Taybi syndrome. Review of 732 cases and analysis of the typical traits. *Eur Rev Med Pharmacol Sci.* 1998;2:81–7.
- Chaddah R, Arntfield M, Runciman S, Clarke L, van der Kooy D. Clonal neural stem cells from human embryonic stem cell colonies. *J Neurosci.* 2012 Jun 6;32(23):7771-81.
- Chan HM, La Thangue NB. p300/CBP proteins: HATs for transcriptional bridges and scaffolds. *J Cell Sci.* 2001 Jul;114(Pt 13):2363-73.
- Cid E, Marquez-Galera A, Valero M, Gal B, Medeiros DC, Navarron CM, Ballesteros-Esteban L, Reig-Viader R, Morales AV, Fernandez-Lamo I, Gomez-Dominguez D, Sato M, Hayashi Y, Bayés À, Barco A, Lopez-Atalaya JP, de la Prida LM. Sublayer- and cell-type-specific neurodegenerative transcriptional trajectories in hippocampal sclerosis.
- Cross, E.; Duncan-Flavell, P.J.; Howarth, R.J.; Hobbs, J.I.; Thomas, N.S.; Bunyan, D.J. Screening of a Large Rubinstein-Taybi Cohort Identified Many Novel Variants

- and Emphasizes the Importance of the CREBBP Histone Acetyltransferase Domain. *Am. J. Med. Genet. A* 2020, 182, 2508–2520.
- Dancy BM, Cole PA. Protein lysine acetylation by p300/CBP. *Chem Rev.* 2015 Mar 25;115(6):2419-52.
 - Deiner MS, Kennedy TE, Fazeli A, Serafini T, Tessier-Lavigne M, Sretavan DW. Netrin-1 and DCC mediate axon guidance locally at the optic disc: loss of function leads to optic nerve hypoplasia. *Neuron.* 1997 Sep;19(3):575-89.
 - Del Blanco B, Guiretti D, Tomasoni R, Lopez-Cascales MT, Muñoz-Viana R, Lipinski M, Scandaglia M, Coca Y, Olivares R, Valor LM, Herrera E, Barco A. CBP and SRF co-regulate dendritic growth and synaptic maturation. *Cell Death Differ.* 2019 Nov;26(11):2208-2222.
 - Drager, U.C. Birth dates of retinal ganglion cells giving rise to the crossed and uncrossed optic projections in the mouse. *Proc. R. Soc. Lond. B Biol. Sci.* 1985, 224, 57–77.
 - Escalante A, González-Martínez R, Herrera E. New techniques for studying neurodevelopment. *Fac Rev.* 2020 Nov 25;9:17.
 - Erskine L, Herrera E. Connecting the retina to the brain. *ASN Neuro.* 2014 Dec 12;6(6):1759091414562107.
 - Erskine L, Reijntjes S, Pratt T, Denti L, Schwarz Q, Vieira JM, Alakakone B, Shewan D, Ruhrberg C. VEGF signaling through neuropilin 1 guides commissural axon crossing at the optic chiasm. *Neuron.* 2011 Jun 9;70(5):951-65.
 - Fauquier L, Azzag K, Parra MAM, Quillien A, Boulet M, Diouf S, Carnac G, Waltzer L, Gronemeyer H, Vandel L. CBP and P300 regulate distinct gene networks required for human primary myoblast differentiation and muscle integrity. *Sci Rep.* 2018 Aug 22;8(1):12629.

- Fekete DM, Perez-Miguelsanz J, Ryder EF, Cepko CL. Clonal analysis in the chicken retina reveals tangential dispersion of clonally related cells. *Dev Biol.* 1994 Dec;166(2):666-82.
- Fergelot, P.; van Belzen, M.; van Gils, J.; Afenjar, A.; Armour, C.M.; Arveiler, B.; Beets, L.; Burglen, L.; Busa, T.; Collet, M.; et al. Phenotype and Genotype in 52 Patients with Rubinstein–Taybi Syndrome Caused by EP300 Mutations. *Am. J. Med. Genet. A* 2016, 170, 3069–3082.
- Ferron SR, Andreu-Agullo C, Mira H, Sanchez P, Marques-Torrejon MA, Farinas I. A combined ex/in vivo assay to detect effects of exogenously added factors in neural stem cells. *Nat Protoc.* 2007;2(4):849-859.
- García-Frigola C, Carreres MA, Vegar C, Mason CA and Herrera E* (2008). *Zic2* promotes axonal divergence at the optic chiasm midline by EphB1-dependent and – independent mechanisms. *Development* 135(10):1833-41
- Gaub P, Joshi Y, Wuttke A, Naumann U, Schnichels S, Heiduschka P, Di Giovanni S. The histone acetyltransferase p300 promotes intrinsic axonal regeneration. *Brain.* 2011 Jul;134(Pt 7):2134-48.
- Gräff J, Tsai LH. Histone acetylation: molecular mnemonics on the chromatin. *Nat Rev Neurosci.* 2013 Feb;14(2):97-111.
- Graw J. Eye development. *Curr Top Dev Biol.* 2010;90:343-86.
- Godement P, Salaün J, Imbert M. Prenatal and postnatal development of retinogeniculate and retinocollicular projections in the mouse. *J Comp Neurol.* 1984 Dec 20;230(4):552-75.
- Guibert S, Forne T, Weber M. Dynamic regulation of DNA methylation during mammalian development. *Epigenomics* 1: 81-98.

- Heavner W, Pevny L. Eye development and retinogenesis. *Cold Spring Harb Perspect Biol.* 012;4(12). Epub 2012/10/17.
- Hennekam RC. Rubinstein-Taybi syndrome. *Eur J Hum Genet.* 2006 Sep;14(9):981-5.
- Hennekam, R.C.; Lommen, E.J.; Strengers, J.L.; van Spijker, H.G.; Jansen-Kokx, T.M. Rubinstein-Taybi Syndrome in a Mother and Son. *Eur. J. Pediatr.* 1989, 148, 439–441.
- Henry RA, Kuo YM, Bhattacharjee V, Yen TJ, Andrews AJ. Changing the selectivity of p300 by acetyl-CoA modulation of histone acetylation. *ACS Chem Biol.* 2015 Jan 16;10(1):146-56.
- Herrera E, Brown L, Aruga J, Rachel R, Dolen G, Mikoshiba K, Brown S, Mason CA (2003). The transcription factor *Zic2* designates the uncrossed retinal ganglion cell axon projection. *Cell.* 114, 545-557.
- Herrera E, Erskine L, Morenilla-Palao C. Guidance of retinal axons in mammals. *Semin Cell Dev Biol.* 2019 Jan;85:48-59.
- Huang da W, Sherman BT, Lempicki RA. Systematic and integrative analysis of large gene lists using DAVID bioinformatics resources. *Nat Protoc.* 2009;4(1):44-57.
- Huberman AD, Niell CM. What can mice tell us about how vision works? *Trends Neurosci.* 2011 Sep;34(9):464-73.
- Hufnagel, R.B.; Le, T.T.; Riesenber, A.L.; Brown, N.L. *Neurog2* controls the leading edge of neurogenesis in the mammalian retina. *Dev. Biol.* 2010, 340, 490–503.
- Impey S, Fong AL, Wang Y, et al. Phosphorylation of CBP mediates transcriptional activation by neural activity and CaM kinase IV. *Neuron* 2002; 34: 235-44.

- Jaubert-Miazza L, Green E, Lo FS, Bui K, Mills J, Guido W. Structural and functional composition of the developing retinogeniculate pathway in the mouse. *Vis Neurosci.* 2005 Sep-Oct;22(5):661-76.
- Jeffery G, Erskine L. Variations in the architecture and development of the vertebrate optic chiasm. *Prog Retin Eye Res.* 2005 Nov;24(6):721-53.
- Kalkhoven E. CBP and p300: HATs for different occasions. *Biochem Pharmacol.* 2004 Sep 15;68(6):1145-55.
- Kandel ER. The molecular biology of memory storage: a dialogue between genes and synapses. *Science.* 2001 Nov 2;294(5544):1030-8.
- Kasper LH, Fukuyama T, Biesen MA, et al. Conditional knockout mice reveal distinct functions for the global transcriptional coactivators CBP and p300 in T-cell development. *Mol Cell Biol.* 2006;26:789–809.
- Kleefstra T, Schenck A, Kramer JM, van Bokhoven H. The genetics of cognitive epigenetics. *Neuropharmacology.* 2014 May;80:83-94.
- Kohwi M, Doe CQ. Temporal fate specification and neural progenitor competence during development. *Nat Rev Neurosci.* 2013 Dec;14(12):823-38.
- Kolpak A, Zhang J, Bao ZZ. Sonic hedgehog has a dual effect on the growth of retinal ganglion axons depending on its concentration. *J Neurosci.* 2005 Mar 30;25(13):3432-41.
- Kouzarides T. Chromatin modifications and their function. *Cell.* 2007 Feb 23;128(4):693-705.
- Kumar JP, Jamal T, Doetsch A, Turner FR, Duffy JB. CREB binding protein functions during successive stages of eye development in *Drosophila*. *Genetics.* 2004;168: 877–893.

- Kung AL, Rebel VI, Bronson RT, Ch'ng LE, Sieff CA, Livingston DM, Yao TP. Gene dose-dependent control of hematopoiesis and hematologic tumor suppression by CBP. *Genes Dev.* 2000 Feb 1;14(3):272-7.
- Kuwajima T, Yoshida Y, Takegahara N, Petros TJ, Kumanogoh A, Jessell TM, Sakurai T, Mason C. Optic chiasm presentation of Semaphorin6D in the context of Plexin-A1 and Nr-CAM promotes retinal axon midline crossing. *Neuron.* 2012 May 24;74(4):676-90.
- Laboissonniere LA, Goetz JJ, Martin GM, Bi R, Lund TJS, Ellson L, Lynch MR, Mooney B, Wickham H, Liu P, Schwartz GW, Trimarchi JM. Molecular signatures of retinal ganglion cells revealed through single cell profiling. *Sci Rep.* 2019 Oct 31;9(1):15778.
- Lee S, Lee B, Lee JW, Lee SK. Retinoid signaling and neurogenin2 function are coupled for the specification of spinal motor neurons through a chromatin modifier CBP. *Neuron.* 2009 Jun 11;62(5):641-54.
- Lipinski M, Del Blanco B, Barco A. CBP/p300 in brain development and plasticity: disentangling the KAT's cradle. *Curr Opin Neurobiol.* 2019 Dec;59:1-8.
- Lipinski M, Muñoz-Viana R, Del Blanco B, Marquez-Galera A, Medrano-Relinque J, Caramés JM, Szczepankiewicz AA, Fernandez-Albert J, Navarrón CM, Olivares R, Wilczyński GM, Canals S, Lopez-Atalaya JP, Barco A. KAT3-dependent acetylation of cell type-specific genes maintains neuronal identity in the adult mouse brain. *Nat Commun.* 2020 May 22;11(1):2588.
- Lois C, Hong EJ, Pease S, Brown EJ, Baltimore D. Germline transmission and tissue-specific expression of transgenes delivered by lentiviral vectors. *Science.* 2002 Feb 1;295(5556):868-72.

- Lopez-Atalaya JP, Barco A. Can changes in histone acetylation contribute to memory formation? *Trends Genet.* 2014 Dec;30(12):529-39
- Lopez-Atalaya, J.P.; Valor, L.M.; Barco, A. Chapter—Epigenetic Factors in Intellectual Disability: The Rubinstein–Taybi Syndrome as a Paradigm of Neurodevelopmental Disorder with Epigenetic Origin. In *Progress in Molecular Biology and Translational Science; Epigenetics and Neuroplasticity—Evidence and Debate*; Lubin, F., Akbarian, S., Eds.; Academic Press: Cambridge, MA, USA, 2014; Volume 128, pp. 139–176.
- López, M.; García-Oguiza, A.; Armstrong, J.; García-Cobaleda, I.; García-Miñaur, S.; Santos-Simarro, F.; Seidel, V.; Domínguez-Garrido, E. Rubinstein-Taybi 2 Associated to Novel EP300 Mutations: Deepening the Clinical and Genetic Spectrum. *BMC Med. Genet.* 2018, 19, 36.
- López M, Seidel V, Santibáñez P, Cervera-Acedo C, Castro-de Castro P, Domínguez-Garrido E. First case report of inherited Rubinstein-Taybi syndrome associated with a novel EP300 variant. *BMC Med Genet.* 2016 Dec 13;17(1):97.
- Maddox SA, Watts CS, Schafe GE. p300/CBP histone acetyltransferase activity is required for newly acquired and reactivated fear memories in the lateral amygdala. *Learn Mem.* 2013 Jan 17;20(2):109-19.
- Madisen L, Zwingman TA, Sunkin SM, Oh SW, Zariwala HA, Gu H, Ng LL, Palmiter RD, Hawrylycz MJ, Jones AR, Lein ES, Zeng H. A robust and high-throughput Cre reporting and characterization system for the whole mouse brain. *Nat Neurosci.* 2010 Jan;13(1):133-40.
- Marquardt T, Ashery-Padan R, Andrejewski N, Scardigli R, Guillemot F, Gruss P. Pax6 is required for the multipotent state of retinal progenitor cells. *Cell.* 2001 Apr 6;105(1):43-55.

- Matsushima D, Heavner W, Pevny LH. Combinatorial regulation of optic cup progenitor cell fate by SOX2 and PAX6. *Development*. 2011 Feb;138(3):443-54.
- McInnes L., Healy J., Melville J. UMAP: Uniform Manifold Approximation and Projection for Dimension Reduction. *arXiv*. 2018; (arXiv:1802.03426).
- Medrano-Fernández A, Delgado-Garcia JM, Del Blanco B, Llinares M, Sánchez-Campusano R, Olivares R, Gruart A, Barco A. The Epigenetic Factor CBP Is Required for the Differentiation and Function of Medial Ganglionic Eminence-Derived Interneurons. *Mol Neurobiol*. 2019 Jun;56(6):4440-4454.
- Milani, D.; Manzoni, F.; Pezzani, L.; Ajmone, P.; Gervasini, C.; Menni, F.; Esposito, S. Rubinstein-Taybi Syndrome: Clinical Features, Genetic Basis, Diagnosis, and Management. *Ital. J. Pediatr*. 2015, 41, 4.
- Mo A, Mukamel EA, Davis FP, Luo C, Henry GL, Picard S, Urich MA, Nery JR, Sejnowski TJ, Lister R, Eddy SR, Ecker JR, Nathans J. Epigenomic Signatures of Neuronal Diversity in the Mammalian Brain. *Neuron*. 2015 Jun 17;86(6):1369-84.
- Morenilla-Palao C , López-Cascales MT, López-Atalaya JP, Baeza D, Calvo L, Barco A, Herrera E (2020) A *Zic2*-regulated switch in a non-canonical Wnt/ β -catenin pathway is essential for the formation of bilateral circuits. *Science Advances*. 6(46): eaaz8797.
- Morin, L.P.; Studholme, K.M. Retinofugal projections in the mouse. *J. Comp. Neurol*. 2014, 522, 3733–3753.
- Moore LD, Le T, Fan G. DNA methylation and its basic function. *Neuropsychopharmacology*. 2013 Jan;38(1):23-38.
- Negri G, Magini P, Milani D, Colapietro P, Rusconi D, Scarano E, Bonati MT, Priolo M, Crippa M, Mazzanti L, Wischmeijer A, Tamburrino F, Pippucci T, Finelli P, Larizza L, Gervasini C. From Whole Gene Deletion to Point Mutations of EP300-

Positive Rubinstein-Taybi Patients: New Insights into the Mutational Spectrum and Peculiar Clinical Hallmarks. *Hum Mutat.* 2016 Feb;37(2):175-83.

- Nemeč, S., Kilian, K.A. Materials control of the epigenetics underlying cell plasticity. *Nat Rev Mater* 6, 69–83 (2021).
- Ogryzko VV, Schiltz RL, Russanova V, Howard BH, Nakatani Y. The transcriptional coactivators p300 and CBP are histone acetyltransferases. *Cell.* 1996 Nov 29;87(5):953-9.
- Opravil S, Mechtler K, Ponting CP, Allis CD, Jenuwein T. Regulation of chromatin structure by site-specific histone H3 methyltransferases. *Nature* 2000, 406:593-599.
- Oron-Karni V, Farhy C, Elgart M, Marquardt T, Remizova L, Yaron O, Xie Q, Cvekl A, Ashery-Padan R. Dual requirement for Pax6 in retinal progenitor cells. *Development.* 2008 Dec;135(24):4037-4047.
- Oster SF, Bodeker MO, He F, Sretavan DW. Invariant Sema5A inhibition serves an ensheathing function during optic nerve development. *Development.* 2003 Feb;130(4):775-84.
- Pérez-Grijalba, V.; García-Oguiza, A.; López, M.; Armstrong, J.; García-Miñaur, S.; Mesa-Latorre, J.M.; O'Callaghan, M.; Pineda Marfa, M.; Ramos-Arroyo, M.A.; Santos-Simarro, F.; et al. New Insights into Genetic Variant Spectrum and Genotype-Phenotype Correlations of Rubinstein-Taybi Syndrome in 39 CREBBP-Positive Patients. *Mol. Genet. Genomic Med.* 2019, 7, e972.
- Pevny LH, Nicolis SK. Sox2 roles in neural stem cells. *Int J Biochem Cell Biol.* 2010 Mar;42(3):421-4.
- Plump AS, Erskine L, Sabatier C, Brose K, Epstein CJ, Goodman CS, Mason CA, Tessier-Lavigne M. Slit1 and Slit2 cooperate to prevent premature midline crossing of retinal axons in the mouse visual system. *Neuron.* 2002 Jan 17;33(2):219-32.

- Poleskaya A, Harel-Bellan A. Acetylation of MyoD by p300 requires more than its histone acetyltransferase domain. *J Biol Chem.* 2001 Nov 30;276(48):44502-3.
- Rando OJ. Combinatorial complexity in chromatin structure and function: revisiting the histone code. *Curr Opin Genet Dev.* 2012 Apr;22(2):148-55.
- Renier N, Adams EL, Kirst C, Wu Z, Azevedo R, Kohl J, Autry AE, Kadiri L, Umadevi Venkataraju K, Zhou Y, Wang VX, Tang CY, Olsen O, Dulac C, Osten P, Tessier-Lavigne M. Mapping of Brain Activity by Automated Volume Analysis of Immediate Early Genes. *Cell.* 2016 Jun 16;165(7):1789-1802.
- Reynolds BA, Weiss S. Generation of neurons and astrocytes from isolated cells of the adult mammalian central nervous system. *Science.* 1992 Mar 27;255(5052):1707-10.
- Rheume, B.A.; Jereen, A.; Bolisetty, M.; Sajid, M.S.; Yang, Y.; Renna, K.; Sun, L.; Robson, P.; Trakhtenberg, E.F. Single cell transcriptome profiling of retinal ganglion cells identifies cellular subtypes. *Nat. Commun.* 2018, 9, 3203.
- Roelfsema JH, Peters DJ. Rubinstein-Taybi syndrome: clinical and molecular overview. *Expert Rev Mol Med.* 2007 Aug 20;9(23):1-16.
- Roelfsema, J.H.; White, S.J.; Ariyürek, Y.; Bartholdi, D.; Niedrist, D.; Papadia, F.; Bacino, C.A.; den Dunnen, J.T.; van Ommen G.-J.B.; Breuning, M.H.; et al. Genetic Heterogeneity in Rubinstein-Taybi Syndrome: Mutations in Both the CBP and EP300 Genes Cause Disease. *Am. J. Hum. Genet.* 2005, 76, 572–580.
- Roth S.Y Denu J.M. Allis C.D. Histone acetyltransferases. *Annu. Rev. Biochem.* 2001; 70: 81-120.
- Roth JF, Shikama N, Henzen C, et al. Differential role of p300 and CBP acetyltransferase during myogenesis: p300 acts upstream of MyoD and Myf5. *EMBO J.* 2003;22:5186–5196.

- Rubinstein, J. H. and Taybi, H. Broad thumbs and toes and facial abnormalities. A possible mental retardation syndrome. *Am J Dis Child*. 1963 Jun;105:588-608.
- Rundlett S.E. Carmen A.A. Suka N. Turner B.M. Grunstein M. Transcriptional repression by UME6 involves deacetylation of lysine 5 of histone H4 by RPD3. *Nature*. 1998; 392: 831-835.
- Sanes, J.R.; Masland, R.H. The types of retinal ganglion cells: Current status and implications for neuronal classification. *Annu. Rev. Neurosci*. 2015, 38, 221–246.
- Seaberg RM, Smukler SR, Kieffer TJ, Enikolopov G, Asghar Z, Wheeler MB, Korbitt G, van der Kooy D. Clonal identification of multipotent precursors from adult mouse pancreas that generate neural and pancreatic lineages. *Nat Biotechnol*. 2004 Sep;22(9):1115-24.
- Shahbazian MD, Grunstein M. Functions of site-specific histone acetylation and deacetylation. *Annu Rev Biochem*. 2007;76:75-100.
- Shikama N, Lutz W, Kretzschmar R, et al. Essential function of p300 acetyltransferase activity in heart, lung and small intestine formation. *EMBO J*. 2003;22:5175–5185.
- Simmons AB, Bloomsburg SJ, Billingslea SA, Merrill MM, Li S, Thomas MW, Fuerst PG. Pou4f2 knock-in Cre mouse: A multifaceted genetic tool for vision researchers. *Mol Vis*. 2016 Jun 23;22:705-17.
- Singec I, Knoth R, Meyer RP, Maciaczyk J, Volk B, Nikkhah G, Frotscher M, Snyder EY. Defining the actual sensitivity and specificity of the neurosphere assay in stem cell biology. *Nat Methods*. 2006 Oct;3(10):801-6.
- Sofroniew MV, Vinters HV. Astrocytes: biology and pathology. *Acta Neuropathol*. 2010 Jan;119(1):7-35.
- Spena S, Milani D, Rusconi D, Negri G, Colapietro P, Elcioglu N, Bedeschi F, Pilotta A, Spaccini L, Ficcadenti A, Magnani C, Scarano G, Selicorni A, Larizza L, Gervasini

- C. Insights into genotype-phenotype correlations from CREBBP point mutation screening in a cohort of 46 Rubinstein-Taybi syndrome patients. *Clin Genet*. 2015 Nov;88(5):431-40.
- Stevens CA. Rubinstein-Taybi Syndrome. 2002 Aug 30 [updated 2019 Aug 22]. In: Adam MP, Ardinger HH, Pagon RA, Wallace SE, Bean LJH, Mirzaa G, Amemiya A, editors. *GeneReviews*® [Internet]. Seattle (WA): University of Washington, Seattle; 1993–2021.
 - Stuart T, Butler A, Hoffman P, Hafemeister C, Papalexi E, Mauck 3rd, W.M, Hao Y, Stoeckius M, Smibert P, Satija R. Comprehensive Integration of Single-Cell Data. *Cell*. 2019; 177: 1888-1902.e21.
 - Sweatt JD. The emerging field of neuroepigenetics. *Neuron*. 2013 Oct 30;80(3):624-32.
 - Swindell EC, Bailey TJ, Loosli F, Liu C, Amaya-Manzanares F, Mahon KA, Wittbrodt J, Jamrich M. Rx-Cre, a tool for inactivation of gene expression in the developing retina. *Genesis*. 2006 Aug;44(8):361-3.
 - Tanaka Y, Naruse I, Hongo T, Xu M, Nakahata T, Maekawa T, Ishii S. Extensive brain hemorrhage and embryonic lethality in a mouse null mutant of CREB-binding protein. *Mech Dev*. 2000 Jul;95(1-2):133-45.
 - Tanaka Y, Naruse I, Maekawa T, Masuya H, Shiroishi T, Ishii S. Abnormal skeletal patterning in embryos lacking a single Cbp allele: a partial similarity with Rubinstein-Taybi syndrome. *Proc Natl Acad Sci U S A*. 1997 Sep 16;94(19):10215-20.
 - Tapias A, Wang ZQ. Lysine Acetylation and Deacetylation in Brain Development and Neuropathies. *Genomics Proteomics Bioinformatics*. 2017 Feb;15(1):19-36.

- Taranova OV, Magness ST, Fagan BM, Wu Y, Surzenko N, Hutton SR, Pevny LH. SOX2 is a dose-dependent regulator of retinal neural progenitor competence. *Genes Dev.* 2006 May 1;20(9):1187-202.
- Thompson H, Camand O, Barker D, Erskine L. Slit proteins regulate distinct aspects of retinal ganglion cell axon guidance within dorsal and ventral retina. *J Neurosci.* 2006 Aug 2;26(31):8082-91.
- Tran NM, Shekhar K, Whitney IE, Jacobi A, Benhar I, Hong G, Yan W, Adiconis X, Arnold ME, Lee JM, Levin JZ, Lin D, Wang C, Lieber CM, Regev A, He Z, Sanes JR. Single-Cell Profiles of Retinal Ganglion Cells Differing in Resilience to Injury Reveal Neuroprotective Genes. *Neuron.* 2019 Dec 18;104(6):1039-1055.e12.
- Tronche F, Kellendonk C, Kretz O, Gass P, Anlag K, Orban PC, Bock R, Klein R, Schütz G. Disruption of the glucocorticoid receptor gene in the nervous system results in reduced anxiety. *Nat Genet.* 1999 Sep;23(1):99-103.
- Tropepe V, Sibilian M, Ciruna BG, Rossant J, Wagner EF, van der Kooy D. Distinct neural stem cells proliferate in response to EGF and FGF in the developing mouse telencephalon. *Dev Biol.* 1999 Apr 1;208(1):166-88.
- Tsui D, Voronova A, Gallagher D, Kaplan DR, Miller FD, Wang J. CBP regulates the differentiation of interneurons from ventral forebrain neural precursors during murine development. *Dev Biol.* 2014 Jan 15;385(2):230-41.
- Turner DL, Cepko CL. A common progenitor for neurons and glia persists in rat retina late in development. *Nature.* 1987 Jul 9-15;328(6126):131-6.
- Turner DL, Snyder EY, Cepko CL. Lineage-independent determination of cell type in the embryonic mouse retina. *Neuron.* 1990 Jun;4(6):833-45.

- Valor LM, Viosca J, Lopez-Atalaya JP, Barco A. Lysine acetyltransferases CBP and p300 as therapeutic targets in cognitive and neurodegenerative disorders. *Curr Pharm Des.* 2013;19(28):5051-64.
- Van der Maaten L., Hinton G. Visualizing Data using t-SNE. *J. Mach. Learn. Res.* 2009; 9: 2579-2605
- Van Genderen, M.M.; Kinds, G.; Riemsdag, F.; Hennekam, R. Ocular Features in Rubinstein–Taybi Syndrome: Investigation of 24 Patients and Review of the Literature. *Br. J. Ophthalmol.* 2000, 84, 1177–1184.
- Van Gils, J, Magdinier, F, Fergelot, P, Lacombe, D. Rubinstein-Taybi Syndrome: A Model of Epigenetic Disorder. *Genes* 2021, 12, 968.
- Vanzan, L., Sklias, A., Herceg, Z. and Murr, R. Mechanisms of Histone Modifications. *Handbook of Epigenetics: 25-46* (2007).
- Vernerey, J., Magalon, K. and Durbec, P. (2013). Primary Culture of SVZ-derived Progenitors Grown as Neurospheres. *Bio-protocol* 3(16): e868.
- Viosca, J.; Lopez-Atalaya, J.P.; Olivares, R.; Eckner, R.; Barco, A. Syndromic Features and Mild Cognitive Impairment in Mice with Genetic Reduction on P300 Activity: Differential Contribution of P300 and CBP to Rubinstein–Taybi Syndrome Etiology. *Neurobiol. Dis.* 2010, 37, 186–194.
- Wang F, Marshall CB, Ikura M. Transcriptional/epigenetic regulator CBP/p300 in tumorigenesis: structural and functional versatility in target recognition. *Cell Mol Life Sci.* 2013 Nov;70(21):3989-4008.
- Wang J, Weaver IC, Gauthier-Fisher A, Wang H, He L, Yeomans J, Wondisford F, Kaplan DR, Miller FD. CBP histone acetyltransferase activity regulates embryonic neural differentiation in the normal and Rubinstein-Taybi syndrome brain. *Dev Cell.* 2010 Jan 19;18(1):114-25.

- Wang Z, Zang C, Cui K, et al. Genome-wide mapping of HATs and HDACs reveals distinct functions in active and inactive genes. *Cell* 2009; 138: 1019-31.
- Webster KA, Muscat GE, Kedes L. Adenovirus E1A products suppress myogenic differentiation and inhibit transcription from muscle-specific promoters. *Nature*. 1988 Apr 7;332(6164):553-7.
- Wetts R, Fraser SE. Multipotent precursors can give rise to all major cell types of the frog retina. *Science*. 1988 Mar 4;239(4844):1142-5.
- Wiley S, Swayne S, Rubinstein JH, Lanphear NE, Stevens CA. Rubinstein–Taybi syndrome medical guidelines. *Am J Med Genet A*. 2003;119:101–110.
- Williams SE, Mann F, Erskine L, Sakurai T, Wei S, Rossi DJ, Gale NW, Holt CE, Mason CA, Henkemeyer M. Ephrin-B2 and EphB1 mediate retinal axon divergence at the optic chiasm. *Neuron*. 2003 Sep 11;39(6):919-35.
- Xiong F, Gao H, Zhen Y, Chen X, Lin W, Shen J, Yan Y, Wang X, Liu M, Gao Y. Optimal time for passaging neurospheres based on primary neural stem cell cultures. *Cytotechnology*. 2011 Dec;63(6):621-31.
- Yao TP, Oh SP, Fuchs M, Zhou ND, Ch'ng LE, Newsome D, Bronson RT, Li E, Livingston DM, Eckner R. Gene dosage-dependent embryonic development and proliferation defects in mice lacking the transcriptional integrator p300. *Cell*. 1998 May 1;93(3):361-72.
- Young RW. Cell differentiation in the retina of the mouse. *Anat Rec*. 1985 Jun;212(2):199-205.
- Yuan LW, Giordano A. Acetyltransferase machinery conserved in p300/CBP-family proteins. *Oncogene* 2002;21:2253–60.

- Yuan ZM, Huang Y, Ishiko T, Nakada S, Utsugisawa T, Shioya H, et al. Function for p300 and not CBP in the apoptotic response to DNA damage. *Oncogene* 1999;18:5714–7.
- Zhang Z, Hofmann C, Casanova E, Schutz G, Lutz B. Generation of a conditional allele of the CBP gene in mouse. *Genesis*. 2004;40:82–89.
- Zocchi L, Sassone-Corsi P. Joining the dots: from chromatin remodeling to neuronal plasticity. *Curr Opin Neurobiol*. 2010 Aug;20(4):432-40.

ANNEX 1. Indications of quality of the thesis

This thesis includes the following publication, of which I am the second author, as an indication of quality.

- **New techniques for studying neurodevelopment.**

Escalante A, **González-Martínez R**, Herrera E.

Faculty Rev. 2020;9:17. Published 2020 Nov 25. Doi:10.12703/r/9-17.

New techniques for studying neurodevelopment

Augusto Escalante ^{1*} Rocío González-Martínez ¹ Eloísa Herrera ¹

¹Instituto de Neurociencias (Consejo Superior de Investigaciones Científicas-Universidad Miguel Hernández, CSIC-UMH), Campus San Juan, Av. Ramón y Cajal s/n, Alicante 03550, Spain

Abstract

The extraordinary diversity, variability, and complexity of cell types in the vertebrate brain is overwhelming and far exceeds that of any other organ. This complexity is the result of multiple cell divisions and intricate gene regulation and cell movements that take place during embryonic development. Understanding the cellular and molecular mechanisms underlying these complicated developmental processes requires the ability to obtain a complete registry of interconnected events often taking place far apart from each other. To assist with this challenging task, developmental neuroscientists take advantage of a broad set of methods and technologies, often adopted from other fields of research. Here, we review some of the methods developed in recent years whose use has rapidly spread for application in the field of developmental neuroscience. We also provide several considerations regarding the promise that these techniques hold for the near future and share some ideas on how existing methods from other research fields could help with the analysis of how neural circuits emerge.

Keywords

Neural development tools, Light sheet microscopy, Clearing, scRNAseq, Machine learning

Peer Review

The peer reviewers who approve this article are:

1. **Nicolas Renier**, Sorbonne Université, Paris Brain Institute, Inserm, CNRS, Paris, France

Competing interests: No competing interests were disclosed.

2. **Carol Mason**, Departments of Pathology and Cell Biology, Neuroscience, and Ophthalmology, Zuckerman Institute, Columbia University, College of Physicians and Surgeons, New York, USA

Competing interests: No competing interests were disclosed.

***Corresponding author:** Augusto Escalante (aescalante@umh.es)

Competing interests: The authors declare that they have no competing interests.

Grant information: The laboratory of EH is funded by the following grants: PID2019-110535GB-I00 from the National Grant Research Program, PROMETEO Program (2020/007) from Generalitat Valenciana, and RAF-20191956 from the Ramón Areces Foundation. AE is funded by LaCaixa Foundation through the Postdoctoral Junior Leader Fellowship Programme (LCF/BQ/PI18/11630005).

The funders had no role in study design, data collection and analysis, decision to publish, or preparation of the manuscript.

Copyright: © 2020 Escalante A et al. This is an open access article distributed under the terms of the [Creative Commons Attribution License](#), which permits unrestricted use, distribution, and reproduction in any medium, provided the original work is properly cited.

How to cite this article: Escalante A, González-Martínez R and Herrera E. **New techniques for studying neurodevelopment.** Faculty Reviews 2020 9:(17) <https://doi.org/10.12703/r/9-17>

Published: 25 Nov 2020, Faculty Reviews 9:(17) <https://doi.org/10.12703/r/9-17>

Moving forward

Long gone are the times when budding neuroscientists would picture themselves working like Don Santiago Ramón y Cajal using only a simple microscope and a shelf full of chemical reagents¹. Today, neuroscientists of all stripes, including those working on the development of the nervous system, are taking advantage of the breadth of new methods and technologies that Don Santiago could have only dreamt about. These methods accelerate our capacity to collect and analyse biological information in large and complex specimens. For instance, we can now reconstruct in three dimensions (3D) the complete peripheral nervous system of a cleared lizard embryo² or obtain a transcriptomic map of gene expression at the single cell (or nucleus) resolution from almost any tissue and species, including humans. Science and technology have been interconnected always, and advances in one historically translate into important progress in the other. Today, the number of available advanced techniques can be overwhelming. In this review, we discuss some recently developed techniques that are currently becoming common in laboratories studying neural development.

Shining light through the 3D embryonic nervous system

Our capacity to document the 3D organisation of the embryonic brain to understand the basic mechanisms underlying circuit formation has been limited until very recently. Studies on the development of the nervous system of most vertebrates have traditionally relied on histological sectioning methods or open book preparations that enable the visualisation of two-dimensional organisation of the axon tracts in the samples under epifluorescence or confocal microscopes. These approaches, which are based on the observation of selected slices or planes of observation (a process that can inherently introduce biases), provide only partial information about the sample. Even though 3D imaging of small embryos had been performed for many years using wide-field and confocal microscopy³, these techniques were very slow and do not scale well to larger embryos or postnatal tissues. This situation began to change with the appearance of light sheet fluorescence microscopy (LSFM). The main advantage of LSFM is the high speed of acquisition and the ability to image large sample sizes that were unpractical to image with conventional microscopes. LSFM was initially used in the field of colloidal chemistry⁴, and about 30 years ago it was adapted to biology to visualise guinea-pig cochleas in 3D⁵. LSFM combines the speed of wide-field imaging with optical sectioning and low photobleaching. In conventional fluorescence microscopy, the entire thickness of the sample is illuminated in the same direction as the detection optics, and, as such, the regions outside the detection focal plane of the objective are potentially damaged by extraneous out-of-focus light that increases the photobleaching. In contrast, in LSFM, the sample is illuminated from the side, perpendicular to the direction of observation, thereby placing the excitation light only where it is required. Therefore, this technique enables the visualisation of tissue samples by shining a sheet of light through the specimen, generating a series of images that can then be digitally reconstructed thanks to the development of sophisticated algorithms and huge improvement in the

capacity of computers to store and analyse data⁶. In developmental biology, LSFM was used for the first time to visualise the transparent tissues of zebrafish and *Drosophila* embryos in 3D *in vivo*. About 8 years ago, Tomer and colleagues were able to visualise the development of the *Drosophila* ventral nerve cord for the first time⁷, and Ahrens and co-authors measured the activity of single neurons in the brain of larval zebrafish embryos⁸ using *in vivo* light sheet microscopy.

However, what eventually enabled LSFM to be used for the analysis of the nervous system was the remarkable improvement in brain clearing techniques. The rapid optimisation of clearing protocols has expanded the application of LSFM in the field of developmental neuroscience in the last 4 to 5 years. Since then, a myriad of different approaches to perform tissue clearing have been developed; these approaches vary based on the type of chemical reagents used and depend on the size of the samples. Although exhaustive reviews about the diversity of clearing protocols have been published^{9–11}, it is worth mentioning the variants of the CUBIC and DISCO series because their excellent results and easy performance ultimately exalted them as the most widespread methods for brain clearing (see <https://idisco.info> and <http://cubic.riken.jp>).

Now that we have methods to make the mammalian brain transparent and visualise it in 3D, a new world has opened up. The combination of tissue clearing and LSFM in neurodevelopmental research is rapidly contributing to important findings in the areas of cell migration and axon pathfinding. One representative example of such advances is the discovery of a small population of neurons in human embryos that secrete gonadotropin-releasing hormones and follow two different pathways of migration beyond the hypothalamus¹². In axon guidance studies, this combination approach is proving to be extremely useful for visualising neuronal axons growing across the whole embryo and for detecting pathfinding defects in mutants of different members of the main families of axon guidance molecules¹³. It has been possible to visualise for the first time the development of the peripheral nervous system and the innervation patterns of human embryos¹⁴. Now, the power of combining these approaches with axonal tracings¹⁵ or antibody staining after functional manipulations (transgenesis¹⁶, *in utero* electroporation, or viral transduction¹⁷) holds the promise of interesting times ahead (Figure 1). The possibility of applying these techniques with large samples is attractive, and many labs worldwide use them for their studies in many different species^{18–23}. Understanding how developmental processes take place in 3D will certainly extend our comprehension of how the brain develops in both healthy and diseased states.

Deconstructing development one cell at a time

The complexity and diversity of cell types is one of the most remarkable characteristics of the mature nervous system. Corticospinal neurons that connect the brain with the spinal cord, sensory neurons that detect and conduct touch information from the skin surrounding our bodies to the central nervous system, or glial cells that modulate neural activity are different

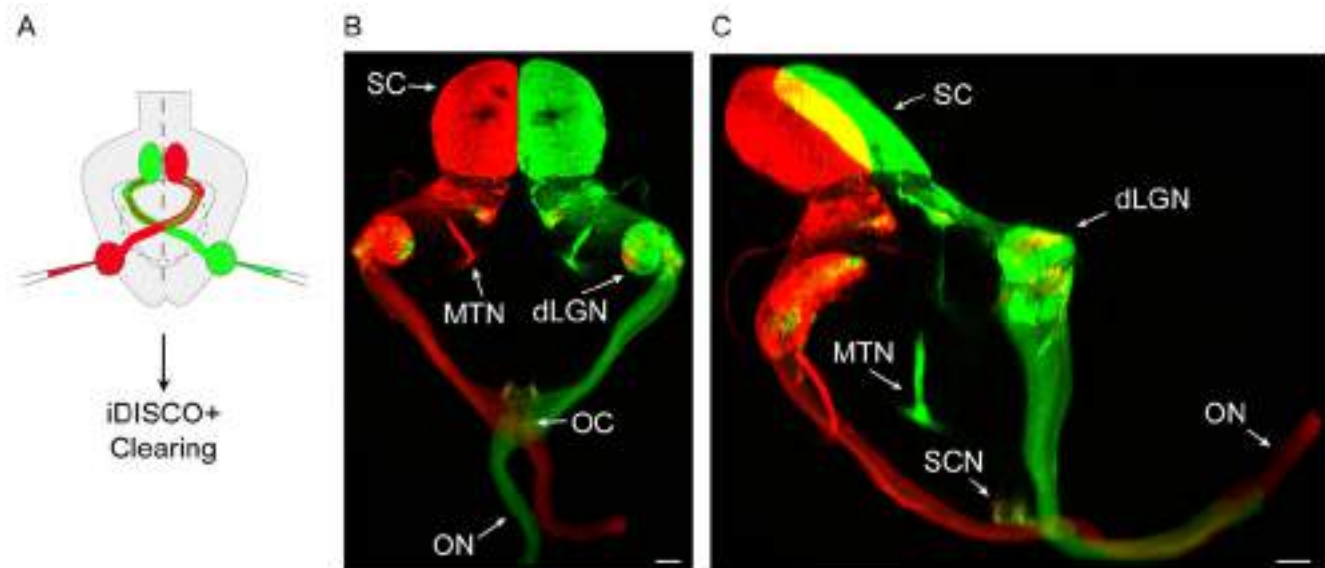


Figure 1. Three-dimensional (3D) view of retinal axons projecting to the visual nuclei within the mouse brain. A. Scheme of the experimental approach. A postnatal mouse is injected with fluorescent tracers of different colours in each eye and then processed through the iDISCO+ clearing protocol²⁴. **B.** Dorsal view of a light sheet fluorescence microscope (LSFM)-acquired 3D image stack from the whole brain of a mouse injected with different colour tracers into each eye. dLGN, dorsal lateral geniculate nucleus; OC, optic chiasm; ON, optic nerve; MTN, medial terminal nucleus; SC, superior colliculus. Scale bar: 300 μm . **C.** Mediolateral view of an LSFM-acquired 3D image stack from the whole brain of a mouse injected with different colour tracers into each eye. dLGN, dorsal lateral geniculate nucleus; MTN, medial terminal nucleus; ON, optic nerve; SC, superior colliculus; SCN, suprachiasmatic nucleus. Scale bar: 300 μm .

examples of the richness and huge variability in cell types that make up the nervous system. Cell specification occurs during development and, until recently, researchers had very limited ways to quantify cell diversity. For many years, the quantification of diversity was constrained by the use of pooling approaches and techniques that require either harvesting cells from the same tissue or combining cells from different individuals to obtain enough material for downstream analysis. For example, in bulk RNA sequencing (RNAseq) approaches, the transcriptomic expression level of a particular gene is not measured from an individual cell but rather as the average level of expression of that gene over many cells present within the same sample. The revolution in the molecular analysis of individual neural progenitors started when the ability to sequence DNA or RNA at the single-cell level became possible. In 2013, the journal *Nature Methods* highlighted the ability to sequence DNA and RNA in single cells as the “Method of the Year”²⁵, and since then single cell approaches have been continuously developed to measure and characterise different aspects of cell identity (chromatin accessibility, the genome, transcriptome, and proteome). In fact, combinations of transcriptomics plus epigenomics or transcriptomics plus proteomics in single cell analyses are rapidly emerging^{26,27}. Here, we focus our attention on one of the most frequently used modalities in neural development, the transcriptomic characterisation of single cells.

The first protocol to perform single cell RNAseq (scRNAseq) was published in 2009²⁸, and the myriad of protocols that have been developed since then have quickly transformed several research fields and the way developmental studies are performed. The key step in scRNAseq protocols consists of tagging all transcripts inside each cell in such a way that RNA molecules coming from the same cell are easily identifiable and quantifiable²⁹. scRNAseq enables transcriptomic cell types in the sampled tissue to be defined through the analysis of differentially expressed genes in each cell.

Nowadays, commercialisation of droplet-based sequencing, for example the 10x Genomic Chromium platform, has enabled the widespread use of scRNAseq. In the field of developmental neuroscience, scRNAseq has been used to profile the entire developing mouse brain and spinal cord³⁰ as well as the prefrontal cortex of human embryos³¹ or the temporal changes in the transcriptional landscape of apical progenitors and their successive cohorts of daughter neurons in the cortex³². In general, developing tissues are characterised by the presence of a mix of cells in different stages of differentiation (progenitors, neuroblasts, early postmitotic neurons, and mature neurons). These stages are captured at the time of scRNAseq processing, thus resulting in a continuous representation of cellular states transitioning from one to another. These transitional stages may be

modelled computationally by recapitulating the probable trajectory of the cells through a representation called pseudotime³³, which defines the order of the cells through development. This representation therefore enables mapping of particular cell types to different states of the developmental trajectory³⁴.

Unfortunately, this now-widespread technique has an important weakness: the loss of spatial information. Tissues, especially during development, are highly structured and dynamic, a fact that underpins the biological relevance of spatial information. The preparation of single cell suspensions needed to perform scRNAseq analyses requires the homogenisation of tissues and,

as such, results in a loss of such spatial information. To overcome this limitation, several labs have now developed a series of methods commonly referred to as spatial transcriptomics. These methods vary in the way in which they maintain spatial information in the tissue sample as well as in their sensitivity, the number of transcripts that can be probed, and the spatial resolution attainable³⁵⁻³⁹, with the latest iteration of the high-definition spatial transcriptomics (HDST) method⁴⁰ reaching a spatial resolution of 2 μm (Figure 2).

It is also worth mentioning that scRNAseq approaches can be similarly applied to single nuclei. The advantages become

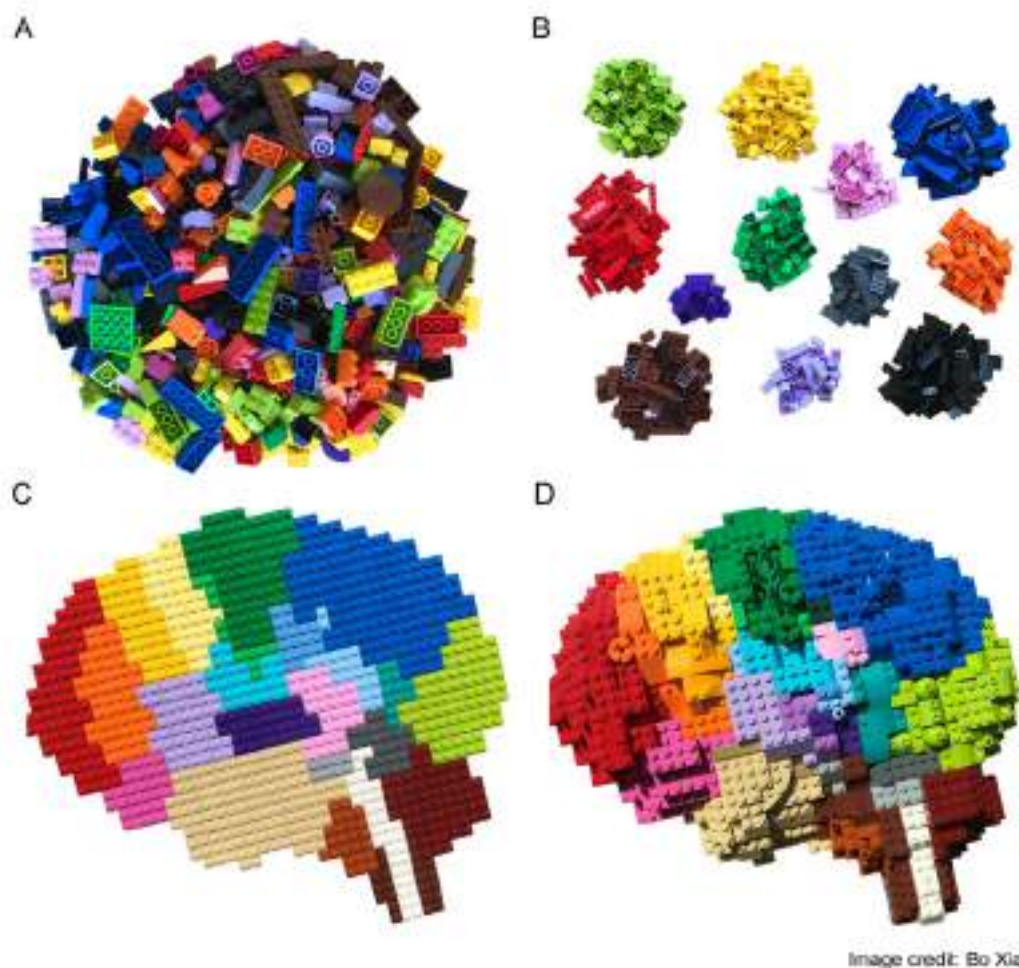


Figure 2. Building-block representation of single cell transcriptome modalities. **A.** Bulk RNA sequencing (RNAseq) experiments use a large number of cells as starting material, which results in a high depth and resolution at the transcriptomic level. However, because the measurements obtained represent an average of gene expression across all of the cells present in the sample, any differences between cells become occluded. **B.** Single cell RNAseq (scRNAseq) methods are capable of maintaining cell individuality during isolation of mRNA molecules. mRNAs are tagged and reconstructed informatically so that they can be assigned to a particular cell. This enables the identification of cell clusters according to their transcriptomic signatures, but spatial information is still lost. **C.** The spatial location of each cell is maintained in spatial transcriptomics approaches. By fluorescently tagging each mRNA species or recording the position *in situ* with barcodes, spatial information may be assigned to each cell together with their transcriptomic profile. Currently, the best attainable resolution is within the tens of microns range, which is still far from ideal and sensitivity remains low. As this is a novel method, the availability of the protocol is scarce and its adoption outside originator labs is therefore difficult. **D.** Researchers are now advancing towards an integrated (genetic, transcriptomic, and proteomic) representation of the brain in time and space. This figure has been reused with permission from the creator Bo Xia.

obvious when we consider that nuclei extraction is a routine method performed in molecular biology labs, that nucleic acids are stable in fixed and frozen samples, and that clinical human tissue banks from where nuclei can be easily obtained are abundant. Moreover, enzymatic dissociation during sample preparation is not required for single nuclei RNAseq (snRNAseq), thereby yielding cell types that are more representative of the original tissue and less affected by transcriptional artefacts. A potential disadvantage of using nuclei is that lower quantities of messenger RNA are obtained from the nuclei than from whole cells, and consequently fewer genes are typically detected. Nonetheless, recent studies have shown that single nuclei and single cell approaches identify similar cell types^{41,42}.

Exploiting artificial intelligence to understand neural development

The heading of this section might sound as if it were taken from a sci-fi movie. However, combining the computational power of modern processors and graphics processing units (GPUs) is exactly what high-throughput methodologies such as those described above require. These techniques generate huge quantities of data that need to be analysed. The simple generation of sequencing results or imaging data by itself does not provide new insights that can advance our understanding of how the nervous system develops. Intense developments in the field of machine learning have generated algorithms that may now be used to deconstruct the complexity of such data.

The imaging of a mouse brain by high-resolution LSFM generates between 20 gigabytes and up to several terabytes of data depending on the resolution⁹. Navigating your way through such an enormous amount of information to draw conclusions quickly becomes a dead-end, both in time and in computing requirements. Working with such vast quantities of bytes imposes a heavy processing burden on a lab's computing capability but also makes analysing such datasets a time-consuming task. To solve this problem, the development of software capable of handling huge quantities of data becomes an urgent requirement; it becomes just as important as the need for the hardware that generates the dataset itself.

Paradoxically, even though a researcher spends just a few minutes to image a whole mouse embryo in 3D using LSFM, the quantification of such datasets often relies on tools and systems that require manual and time-consuming annotations. Fortunately, in the last few years, an unparalleled development of informatics tools has begun to help researchers quickly and accurately analyse big datasets in a short period of time. Some examples of these programs are *Cell Profiler* from the Broad Institute, which can easily segment nuclei in dense tissue images, and its more powerful sibling, *Cell Profiler Analyst*, which makes use of machine learning algorithms to recognise defined cell types from large imaging datasets^{43,44}. *Cell Profiler* has been used, for example, to quantify the differences in neuronal numbers between the sulci and gyri of the cortex of Flrt3 mutant mouse embryos⁴⁵ and to help elucidate the role of PTPRD in

neurogenesis⁴⁶. More recently, the Pachitariu lab⁴⁷ released a complementary approach for cell segmentation called *Cellpose*. This is a generalist algorithm for cellular segmentation and is based on the use of a neural network that is trained on thousands of images from different microscope modalities (fluorescent, bright field, etc.) combined with non-biological images of similar structure. The system creates a platform capable of recognising cells from a wide array of image types. It also enables the generation of researcher-defined custom models by training the algorithm on specific types of images.

The use of machine learning, particularly neural networks trained to recognise structures of interest such as nuclei, cells, blood vessels, noise, etc. in images, has exploded in the last few years, and it is quickly becoming the go-to solution for many biomedical research problems⁴⁸⁻⁵⁷. Beyond solving imaging tasks, machine learning approaches may be used in many other applications within the field of neurodevelopment. The quantity of data generated during sequencing experiments such as scRNAseq face the same challenges as those derived from large imaging experiments. Newer and more refined technologies yielding an ever-increasing number of sequenced cells quickly translate not only into larger datasets but also into a higher number of dimensions that need to be non-linearly reduced to define particular cell types. Several packages that allow the processing of sequencing data and perform efficient dimensionality reduction or help to identify defined cell types of interest within the datasets have been released^{58,59}. While processing of image and sequencing data are both examples from the blooming field of computational biology that are useful for studying neural development, many more developments and applications are predicted to emerge⁶⁰.

What lies ahead?

Although transformational technological revolutions are constantly occurring in science, the advances that have been made in the last few years have been spectacular. Here we have highlighted what, in our opinion, are very relevant and novel approaches for investigating the developmental processes that control the formation of neural circuits. It is our belief that we will experience amazing changes in the years to come that will dwarf what we know today. We envision that tissue clearing technologies will evolve into fully applicable methods that will no longer be limited by antibody compatibility. The recent publication of CUBIC-HistoVision points in that direction, as it describes a systematic interrogation of the properties and conditions that preserve antigens and facilitate antibody penetration into fixed animal tissues⁶¹. Community crowd-sharing of resources such as those mentioned, antibody-related optimisations, and tested protocol modifications and reagents will form the basis for advancing current and future protocols, likely to the point that many antibodies will work for 3D immunostaining applications. Concurrently with advancements in staining methods, parallel development of LSFM will likely enhance the imaging resolution of transparent samples while also reducing the time required for acquisition^{62,63}.

The most important missing piece for single cell approaches is the development of high-throughput proteomics to individually measure protein content in each cell with enough depth to cover the whole proteome. Beyond basic estimation per cell, single cell DNA or RNA technologies are incapable of measuring the abundance and activity of proteins, which are regulated by both post-translational modifications and degradation. Although single cell proteomic approaches are already available, most of them currently rely on antibodies to detect the proteins of interest; this imposes an important throughput limitation. Methods to quantify thousands of proteins in hundreds of cells through the use of mass spectrometry (MS) are emerging, and improvements in MS are expected to increase the sensitivity of single cell proteomics⁶⁴. The development of effective and high-throughput approaches in single cell proteomics will aid the quest to fully characterize cells, their functional and developmental states, and the mechanisms involved in transitioning from one state to another. Matched single cell genetic, transcriptomic, and proteomic data will help to elucidate the mechanisms behind the formation of a fully developed nervous system.

The application of machine learning in the field of developmental neuroscience is still in its infancy but will likely explode in the near future. Examples stemming from cancer research⁶⁵, such as those using neural networks trained to identify different types of tumours based on their location and composition in cleared whole mouse bodies⁶⁶, highlight the possibilities of gathering current computing power so that it can be applied to other fields such as neural development. Similar applications of machine learning algorithms could aid in the recognition of changing mRNA/protein expression patterns in brain development. Labour-intensive tasks commonly used to study the developing nervous system could also greatly benefit from the implementation of tools developed in other neuroscience-related areas. For example, the automated identification and tracking of migrating neurons should be easily adopted following the lead










of algorithms like DeepLabCut that behavioural neuroscience labs are using to track the position of different parts of the mouse body without the use of markers⁶⁷. ClearMap is another algorithm that maps cells automatically in the mouse brain of LSFM datasets, which could be applied to neonate brains²⁴. Another very promising avenue is the algorithm Trailmap, which was recently developed in the Luo lab to automatically identify and extract axonal projections in 3D image volumes⁶⁸ and may be easily implemented to improve the quantification of axon guidance studies. Adoption of such neural networks will probably require re-training and optimisation to the specific use-case scenario and dataset, which highlights the need for fast-training computational strategies in order to facilitate the broader use of these techniques.

Therefore, despite the impressive amount of state-of-the-art technologies developed in the last few years, there is still room for improvement of some of the latest methods available to study the developing nervous system. We could envision a not-so-distant day when 3D embryonic brain imaging will be combined with single-cell technologies to elucidate the chromatin, mRNA, and protein signatures of each cell *in situ* at the same time. Such datasets would contain information about what are considered the main determinants of cell identity while maintaining the intact structure, shape, and form of the tissue. This “fantasy technical improvement” could be pictured even one step further by introducing the fourth dimension into account and analyse datasets of embryos at different stages of development to provide the most detailed description of development progression to date. However, writing a “what will the future look like” piece is bound to fail. History has demonstrated that both the imagination and the driving force of scientists are many orders of magnitude beyond what can be anticipated. As such, while this review will likely become obsolete shortly, it will be a good sign that developmental neuroscience maintains its exponential progression in advancing our understanding of the assembly of neural circuits.

References

1. The Cajal Legacy: Consejo Superior de Investigaciones Científicas - CSIC - csic.es.
[Reference Source](#)
2. Alain Chédotal en Twitter: 'It was a risky experiment but thanks to Ripley we did it: this is our contribution to #AlienDay enjoy <https://t.co/QyZHFtIkYy>' / Twitter. <https://twitter.com/alainchedotal/status/1254456825514254337>.
3. Dent JA, Polson AG, Klymkowsky MW: **A whole-mount immunocytochemical analysis of the expression of the intermediate filament protein vimentin in *Xenopus***. *Development*. 1989; **105**(1): 61–74.
[PubMed Abstract](#)
4. Keller PJ, Dodt HU: **Light sheet microscopy of living or cleared specimens**. *Curr Opin Neurobiol*. 2012; **22**(1): 138–43.
[PubMed Abstract](#) | [Publisher Full Text](#)
5. Voie AH, Burns DH, Spelman FA: **Orthogonal-plane fluorescence optical sectioning: Three-dimensional imaging of macroscopic biological specimens**. *J Microsc*. 1993; **170**(Pt 3): 229–36.
[PubMed Abstract](#) | [Publisher Full Text](#)
6. Amat F, Höckendorf B, Wan Y, *et al.*: **Efficient processing and analysis of large-scale light-sheet microscopy data**. *Nat Protoc*. 2015; **10**(11): 1679–96.
[PubMed Abstract](#) | [Publisher Full Text](#)
7. Tomer R, Khairy K, Amat F, *et al.*: **Quantitative high-speed imaging of entire developing embryos with simultaneous multiview light-sheet microscopy**. *Nat Methods*. 2012; **9**(7): 755–63.
[PubMed Abstract](#) | [Publisher Full Text](#)
8. Ahrens MB, Orger MB, Robson DN, *et al.*: **Whole-brain functional imaging at**

- cellular resolution using light-sheet microscopy. *Nat Methods*. 2013; 10(5): 413–20.
[PubMed Abstract](#) | [Publisher Full Text](#)
9.  Ueda HR, Ertürk A, Chung K, *et al.*: Tissue clearing and its applications in neuroscience. *Nat Rev Neurosci*. 2020; 21(2): 61–79.
[PubMed Abstract](#) | [Publisher Full Text](#) | [Faculty Opinions Recommendation](#)
 10. Vigouroux RJ, Belle M, Chédotal A: Neuroscience in the third dimension: Shedding new light on the brain with tissue clearing. *Mol Brain*. 2017; 10(1): 33.
[PubMed Abstract](#) | [Publisher Full Text](#) | [Free Full Text](#)
 11.  Porter DDL, Morton PD: Clearing techniques for visualizing the nervous system in development, injury, and disease. *J Neurosci Methods*. 2020; 334: 108594.
[PubMed Abstract](#) | [Publisher Full Text](#) | [Faculty Opinions Recommendation](#)
 12. Casoni F, Malone SA, Belle M, *et al.*: Development of the neurons controlling fertility in humans: New insights from 3D imaging and transparent fetal brains. *Development*. 2016; 143(21): 3969–81.
[PubMed Abstract](#) | [Publisher Full Text](#)
 13. Belle M, Godefroy D, Dominici C, *et al.*: A simple method for 3D analysis of immunolabeled axonal tracts in a transparent nervous system. *Cell Rep*. 2014; 9(4): 1191–201.
[PubMed Abstract](#) | [Publisher Full Text](#)
 14.  Belle M, Godefroy D, Couly G, *et al.*: Tridimensional Visualization and Analysis of Early Human Development. *Cell*. 2017; 169(1): 161–173.e12.
[PubMed Abstract](#) | [Publisher Full Text](#) | [Faculty Opinions Recommendation](#)
 15.  Vigouroux RJ, Cesar Q, Chédotal A, *et al.*: Revisiting the role of Dcc in visual system development with a novel eye clearing method. *eLife*. 2020; 9: e51275.
[PubMed Abstract](#) | [Publisher Full Text](#) | [Free Full Text](#) | [Faculty Opinions Recommendation](#)
 16.  Moreno-Bravo JA, Puiggrós SR, Blockus H, *et al.*: Commissural neurons transgress the CNS/PNS boundary in absence of ventricular zone-derived netrin 1. *Development*. 2018; 145(2): dev159400.
[PubMed Abstract](#) | [Publisher Full Text](#) | [Faculty Opinions Recommendation](#)
 17.  Yu T, Zhu J, Li Y, *et al.*: RTF: A rapid and versatile tissue optical clearing method. *Sci Rep*. 2018; 8(1): 1964.
[PubMed Abstract](#) | [Publisher Full Text](#) | [Free Full Text](#) | [Faculty Opinions Recommendation](#)
 18.  Pende M, Becker K, Wanis M, *et al.*: High-resolution ultramicroscopy of the developing and adult nervous system in optically cleared *Drosophila melanogaster*. *Nat Commun*. 2018; 9(1): 4731.
[PubMed Abstract](#) | [Publisher Full Text](#) | [Free Full Text](#) | [Faculty Opinions Recommendation](#)
 19.  Wan Y, Wei Z, Looger LL, *et al.*: Single-Cell Reconstruction of Emerging Population Activity in an Entire Developing Circuit. *Cell*. 2019; 179(2): 355–372.e23.
[PubMed Abstract](#) | [Publisher Full Text](#) | [Free Full Text](#) | [Faculty Opinions Recommendation](#)
 20.  McDole K, Guignard L, Amat F, *et al.*: In Toto Imaging and Reconstruction of Post-Implantation Mouse Development at the Single-Cell Level. *Cell*. 2018; 175(3): 859–876.e33.
[PubMed Abstract](#) | [Publisher Full Text](#) | [Faculty Opinions Recommendation](#)
 21. Whitman MC, Nguyen EH, Bell JL, *et al.*: Loss of CXCR4/CXCL12 Signaling Causes Oculomotor Nerve Misrouting and Development of Motor Trigeminal to Oculomotor Synkinesis. *Invest Ophthalmol Vis Sci*. 2018; 59(12): 5201–9.
[PubMed Abstract](#) | [Publisher Full Text](#) | [Free Full Text](#)
 22.  Wu Z, Makihara S, Yam PT, *et al.*: Long-Range Guidance of Spinal Commissural Axons by Netrin1 and Sonic Hedgehog from Midline Floor Plate Cells. *Neuron*. 2019; 101(4): 635–647.e4.
[PubMed Abstract](#) | [Publisher Full Text](#) | [Faculty Opinions Recommendation](#)
 23.  Hertz NT, Adams EL, Weber RA, *et al.*: Neuronally Enriched RUFY3 Is Required for Caspase-Mediated Axon Degeneration. *Neuron*. 2019; 103(3): 412–422.e4.
[PubMed Abstract](#) | [Publisher Full Text](#) | [Faculty Opinions Recommendation](#)
 24.  Renier N, Adams EL, Kirst C, *et al.*: Mapping of Brain Activity by Automated Volume Analysis of Immediate Early Genes. *Cell*. 2016; 165(7): 1789–802.
[PubMed Abstract](#) | [Publisher Full Text](#) | [Free Full Text](#) | [Faculty Opinions Recommendation](#)
 25. **Method of the year 2013.** *Nat Methods*. 2014; 11(1): 1.
[PubMed Abstract](#) | [Publisher Full Text](#)
 26.  Lake BB, Chen S, Sos BC, *et al.*: Integrative single-cell analysis of transcriptional and epigenetic states in the human adult brain. *Nat Biotechnol*. 2018; 36(1): 70–80.
[PubMed Abstract](#) | [Publisher Full Text](#) | [Free Full Text](#) | [Faculty Opinions Recommendation](#)
 27.  Schenk S, Bannister SC, Sedlazeck FJ, *et al.*: Combined transcriptome and proteome profiling reveals specific molecular brain signatures for sex, maturation and circalunar clock phase. *eLife*. 2019; 8: e41556.
[PubMed Abstract](#) | [Publisher Full Text](#) | [Free Full Text](#) | [Faculty Opinions Recommendation](#)
 28.  Tang F, Barbacioru C, Wang Y, *et al.*: mRNA-Seq whole-transcriptome analysis of a single cell. *Nat Methods*. 2009; 6(5): 377–82.
[PubMed Abstract](#) | [Publisher Full Text](#) | [Faculty Opinions Recommendation](#)
 29. Chen G, Ning B, Shi T: Single-Cell RNA-Seq Technologies and Related Computational Data Analysis. *Front Genet*. 2019; 10: 317.
[PubMed Abstract](#) | [Publisher Full Text](#) | [Free Full Text](#)
 30.  Rosenberg AB, Roco CM, Muscat RA, *et al.*: Single-cell profiling of the developing mouse brain and spinal cord with split-pool barcoding. *Science*. 2018; 360(6385): 176–82.
[PubMed Abstract](#) | [Publisher Full Text](#) | [Free Full Text](#) | [Faculty Opinions Recommendation](#)
 31.  Zhong S, Zhang S, Fan X, *et al.*: A single-cell RNA-seq survey of the developmental landscape of the human prefrontal cortex. *Nature*. 2018; 555(7697): 524–8.
[PubMed Abstract](#) | [Publisher Full Text](#) | [Faculty Opinions Recommendation](#)
 32.  Telley L, Agirman G, Prados J, *et al.*: Temporal patterning of apical progenitors and their daughter neurons in the developing neocortex. *Science*. 2019; 364(6440): eaav2522.
[PubMed Abstract](#) | [Publisher Full Text](#) | [Faculty Opinions Recommendation](#)
 33. Trapnell C, Cacchiarelli D, Grimsby J, *et al.*: The dynamics and regulators of cell fate decisions are revealed by pseudotemporal ordering of single cells. *Nat Biotechnol*. 2014; 32(4): 381–6.
[PubMed Abstract](#) | [Publisher Full Text](#) | [Free Full Text](#)
 34. Griffiths JA, Scialdone A, Marioni JC: Using single-cell genomics to understand developmental processes and cell fate decisions. *Mol Syst Biol*. 2018; 14(4): e8046.
[PubMed Abstract](#) | [Publisher Full Text](#) | [Free Full Text](#)
 35. Codeluppi S, Borm LE, Zeisel A, *et al.*: Spatial organization of the somatosensory cortex revealed by osmFISH. *Nat Methods*. 2018; 15(11): 932–5.
[PubMed Abstract](#) | [Publisher Full Text](#)
 36.  Eng CHL, Lawson M, Zhu Q, *et al.*: Transcriptome-scale super-resolved imaging in tissues by RNA seqFISH. *Nature*. 2019; 568(7751): 235–9.
[PubMed Abstract](#) | [Publisher Full Text](#) | [Free Full Text](#) | [Faculty Opinions Recommendation](#)
 37. Salmén F, Ståhl PL, Mollbrink A, *et al.*: Barcoded solid-phase RNA capture for Spatial Transcriptomics profiling in mammalian tissue sections. *Nat Protoc*. 2018; 13(11): 2501–34.
[PubMed Abstract](#) | [Publisher Full Text](#)
 38.  Wang X, Allen WE, Wright MA, *et al.*: Three-dimensional intact-tissue sequencing of single-cell transcriptional states. *Science*. 2018; 361(6400): eaat5691.
[PubMed Abstract](#) | [Publisher Full Text](#) | [Free Full Text](#) | [Faculty Opinions Recommendation](#)
 39.  Rodrigues SG, Stickels RR, Goeva A, *et al.*: Slide-seq: A scalable technology for measuring genome-wide expression at high spatial resolution. *Science*. 2019; 363(6434): 1463–7.
[PubMed Abstract](#) | [Publisher Full Text](#) | [Free Full Text](#) | [Faculty Opinions Recommendation](#)
 40.  Vickovic S, Eraslan G, Salmén F, *et al.*: High-definition spatial transcriptomics for in situ tissue profiling. *Nat Methods*. 2019; 16(10): 987–90.
[PubMed Abstract](#) | [Publisher Full Text](#) | [Free Full Text](#) | [Faculty Opinions Recommendation](#)
 41. Habib N, Avraham-Davidi I, Basu A, *et al.*: Massively parallel single-nucleus RNA-seq with DroNc-seq. *Nat Methods*. 2017; 14(10): 955–8.
[PubMed Abstract](#) | [Publisher Full Text](#) | [Free Full Text](#)
 42.  Bakken TE, Hodge RD, Miller JA, *et al.*: Single-nucleus and single-cell transcriptomes compared in matched cortical cell types. *PLoS One*. 2018; 13(12): e0209648.
[PubMed Abstract](#) | [Publisher Full Text](#) | [Free Full Text](#) | [Faculty Opinions Recommendation](#)
 43. Carpenter AE, Jones TR, Lamprecht MR, *et al.*: CellProfiler: Image analysis software for identifying and quantifying cell phenotypes. *Genome Biol*. 2006; 7(10): R100.
[PubMed Abstract](#) | [Publisher Full Text](#) | [Free Full Text](#)
 44. Jones TR, Carpenter AE, Lamprecht MR, *et al.*: Scoring diverse cellular morphologies in image-based screens with iterative feedback and machine learning. *Proc Natl Acad Sci U S A*. 2009; 106(6): 1826–31.
[PubMed Abstract](#) | [Publisher Full Text](#) | [Free Full Text](#)
 45.  Del Toro D, Ruff T, Cederfjäll E, *et al.*: Regulation of Cerebral Cortex Folding by Controlling Neuronal Migration via FLRT Adhesion Molecules. *Cell*. 2017; 169(4): 621–635.e16.
[PubMed Abstract](#) | [Publisher Full Text](#) | [Faculty Opinions Recommendation](#)

46.  Tomita H, Cornejo F, Aranda-Pino B, *et al.*: **The Protein Tyrosine Phosphatase Receptor Delta Regulates Developmental Neurogenesis.** *Cell Rep.* 2020; **30**(7): 215–228.e5.
[PubMed Abstract](#) | [Publisher Full Text](#) | [Faculty Opinions Recommendation](#)
47. Stringer C, Wang T, Michaelos M, *et al.*: **Cellpose: a generalist algorithm for cellular segmentation.** 2020.
[Publisher Full Text](#)
48. Caicedo JC, Cooper S, Heigwer F, *et al.*: **Data-analysis strategies for image-based cell profiling.** *Nat Methods.* 2017; **14**(9): 849–63.
[PubMed Abstract](#) | [Publisher Full Text](#) | [Free Full Text](#)
49. Tetteh G, Efremov V, Forkert ND, *et al.*: **DeepVesselNet: Vessel Segmentation, Centerline Prediction, and Bifurcation Detection in 3-D Angiographic Volumes.** 13.
[Reference Source](#)
50. Weigert M, Schmidt U, Boothe T, *et al.*: **Content-aware image restoration: Pushing the limits of fluorescence microscopy.** *Nat Methods.* 2018; **15**(12): 1090–7.
[PubMed Abstract](#) | [Publisher Full Text](#)
51.  Wang H, Rivenson Y, Jin Y, *et al.*: **Deep learning enables cross-modality super-resolution in fluorescence microscopy.** *Nat Methods.* 2019; **16**(1): 103–10.
[PubMed Abstract](#) | [Publisher Full Text](#) | [Free Full Text](#) | [Faculty Opinions Recommendation](#)
52.  Falk T, Mai D, Bensch R, *et al.*: **U-Net: deep learning for cell counting, detection, and morphometry.** *Nat Methods.* 2019; **16**(1): 67–70.
[PubMed Abstract](#) | [Publisher Full Text](#) | [Faculty Opinions Recommendation](#)
53. Dorkenwald S, Schubert PJ, Killinger MF, *et al.*: **Automated synaptic connectivity inference for volume electron microscopy.** *Nat Methods.* 2017; **14**(4): 435–42.
[PubMed Abstract](#) | [Publisher Full Text](#)
54.  Livne M, Rieger J, Aydin OU, *et al.*: **A U-Net Deep Learning Framework for High Performance Vessel Segmentation in Patients With Cerebrovascular Disease.** *Front Neurosci.* 2019; **13**: 97.
[PubMed Abstract](#) | [Publisher Full Text](#) | [Free Full Text](#) | [Faculty Opinions Recommendation](#)
55.  Todorov MI, Paetzold JC, Schoppe O, *et al.*: **Machine learning analysis of whole mouse brain vasculature.** *Nat Methods.* 2020; **17**(4): 442–9.
[PubMed Abstract](#) | [Publisher Full Text](#) | [Free Full Text](#) | [Faculty Opinions Recommendation](#)
56.  Kirst C, Skriabine S, Vieites-Prado A, *et al.*: **Mapping the Fine-Scale Organization and Plasticity of the Brain Vasculature.** *Cell.* 2020; **180**(4): 780–795.e25.
[PubMed Abstract](#) | [Publisher Full Text](#) | [Faculty Opinions Recommendation](#)
57. Di Giovanna AP, Tibo A, Silvestri L, *et al.*: **Whole-Brain Vasculature Reconstruction at the Single Capillary Level.** *Sci Rep.* 2018; **8**(1): 12573.
[PubMed Abstract](#) | [Publisher Full Text](#) | [Free Full Text](#)
58. Ding J, Condon A, Shah SP: **Interpretable dimensionality reduction of single cell transcriptome data with deep generative models.** *Nat Commun.* 2018; **9**(1): 2002.
[PubMed Abstract](#) | [Publisher Full Text](#) | [Free Full Text](#)
59.  Torroja C, Sanchez-Cabo F: **DigitalDropper: Deep-Learning on scRNA-Seq to Deconvolute Gene Expression Data.** *Front Genet.* 2019; **10**: 978.
[PubMed Abstract](#) | [Publisher Full Text](#) | [Free Full Text](#) | [Faculty Opinions Recommendation](#)
60. Zheng J, Wang K: **Emerging deep learning methods for single-cell RNA-seq data analysis.** *Quant Biol.* 2019; **7**: 247–54.
[Publisher Full Text](#)
61.  Susaki EA, Shimizu C, Kuno A, *et al.*: **Versatile whole-organ/body staining and imaging based on electrolyte-gel properties of biological tissues.** *Nat Commun.* 2020; **11**: 1982.
[Publisher Full Text](#) | [Faculty Opinions Recommendation](#)
62. Saghafi S, Haghi-Danaloo N, Becker K, *et al.*: **Reshaping a multimode laser beam into a constructed Gaussian beam for generating a thin light sheet.** *J Biophotonics.* 2018; **11**(6): e201700213.
[PubMed Abstract](#) | [Publisher Full Text](#)
63.  Voigt FF, Kirschenbaum D, Platonova E, *et al.*: **The mesoSPIM initiative: open-source light-sheet microscopes for imaging cleared tissue.** *Nat Methods.* 2019; **16**(11): 1105–8.
[PubMed Abstract](#) | [Publisher Full Text](#) | [Free Full Text](#) | [Faculty Opinions Recommendation](#)
64. Slavov N: **Unpicking the proteome in single cells.** *Science.* 2020; **367**(6477): 512–3.
[PubMed Abstract](#) | [Publisher Full Text](#) | [Free Full Text](#)
65. Levine AB, Schlosser C, Grewal J, *et al.*: **Rise of the Machines: Advances in Deep Learning for Cancer Diagnosis.** *Trends Cancer.* 2019; **5**(3): 157–69.
[PubMed Abstract](#) | [Publisher Full Text](#)
66.  Pan C, Schoppe O, Parra-Damas A, *et al.*: **Deep Learning Reveals Cancer Metastasis and Therapeutic Antibody Targeting in the Entire Body.** *Cell.* 2019; **179**(7): 1661–1676.e19.
[PubMed Abstract](#) | [Publisher Full Text](#) | [Free Full Text](#) | [Faculty Opinions Recommendation](#)
67. Mathis A, Mamidanna P, Abe T, *et al.*: **Markerless tracking of user-defined features with deep learning.** *ArXiv180403142 Cs Q-Bio Stat.* 2018.
[Reference Source](#)
68.  Friedmann D, Pun A, Adams EL, *et al.*: **Mapping mesoscale axonal projections in the mouse brain using a 3D convolutional network.** *Proc Natl Acad Sci U S A.* 2020; **117**(20): 11068–75.
[PubMed Abstract](#) | [Publisher Full Text](#) | [Free Full Text](#) | [Faculty Opinions Recommendation](#)

AGRADECIMIENTOS

A los seres que me llenan...

Parecía que este momento nunca iba a llegar y... aquí estoy, escribiendo el capítulo de la tesis con los resultados más estadísticamente significativos de una de las etapas más importantes de mi vida.

En primer lugar, quiero darle las gracias a mi directora de tesis, Eloísa. Gracias Elo por confiar en mí y por darme la oportunidad de ser parte de tu laboratorio. He aprendido muchísimo de ti a lo largo de estos 6 años, y no solo científicamente hablando. Gracias por apoyarme en los momentos de frustración, por motivarme a seguir avanzando y por comprenderme en los momentos más duros. De verdad, gracias.

Y nada hubiera sido lo mismo de no ser por el resto del laboratorio, que desde el primer momento me acogió como una más, por todos los momentos que hemos vivido (tensiones, risas, conversaciones locas de viernes, comidas improvisadas...) y por hacer que las horas en el laboratorio pasaran volando...

Gracias a Vero. Fuiste de las primeras personas que conocí al llegar al laboratorio y desde el principio te convertiste en un gran pilar para mí. Me has enseñado prácticamente todo lo que se de laboratorio, me has ayudado siempre que lo he necesitado, has soportado mis frustraciones y nunca me has dejado tirar la toalla.

Gracias a Marta, por enseñarme tantas cosas y ayudarme en todo lo que he necesitado. Sin vosotras chicas, mi estancia en el laboratorio no hubiera sido lo mismo. Nunca os olvidaré.

Gracias a Maca, por tu gran ayuda durante esta tesis, no sólo técnica, sino personal. Por ser tan graciosa como tú eres y transmitir esa paz y tranquilidad que ayuda a ver los problemas desde otra perspectiva. Muchísimas gracias por todo, eres un solete.

Gracias a Yaiza y Diana, todo hubiera sido muy difícil sin vuestra ayuda. A Bea, a pesar de que ahora estamos más distanciadas, hemos pasado muy buenos momentos. A Cruz, por su conocimiento y por las ideas locas que tiene que te alegran la tarde (todavía está por ahí la muestra de "eau de lab"). A Augusto, por transmitir ese positivismo con acento andaluz que suaviza siempre los peores problemas. Gracias a Carlos por tus buenas ideas. Y gracias al resto: Mayte, Iván, Luis, Santi, mi querida Irene... por haber formado parte de esta pequeña familia.

No puedo olvidarme de alguien muy importante, Beatriz del Blanco. Has sido mi guía durante esta etapa y gracias a tus consejos y sinceridad, esta tesis es lo que es. Gracias por todo lo que has hecho por mi.

Gracias también a Angel Barco, Jose López-Atalaya y Victor Borrell por todos sus comentarios, consejos y ayuda a lo largo de estos años. He aprendido mucho de vosotros.

Gracias a mis miércoles tontos, Aida y Marta. Formamos un buen equipo donde los problemas del INA siempre se han quedado a un lado, donde somos libres de hablar de cualquier cosa y siempre encontramos algo por lo que sonreír.

A toda esa gente del INA que ha formado parte de esta etapa (seguro que me olvido de muchos): Ana, Maribel, Sandra, Alex, Rafa, Angel Marquez, Noe, Adri, Ana, Cris, Quique, Deli, Sergio Velasco, Khalil, Trini, Mercedes, Aroa... Gracias a toda la gente del laboratorio de Angel Barco, en especial a Román, Michal, Marylin, Sergio y Juan Paraíso, por ser nuestros hermanos científicos. Gracias a Javi y Antonio Caler, por todas nuestras conversaciones de cualquier cosa, vuestro consejo y vuestro apoyo en uno de los peores momentos de la tesis en los que estaba hundida. Voy a echar mucho de menos los viernes de citómetro y musicote en Radio3 a la vez que planeábamos festivales.

A Sergio, mi querido Sergio. ¿Qué hubiera sido de mí sin ti? Te conocí justo en el momento que más lo necesitaba y ahora eres indispensable. Hemos compartido grandes momentos y creo que nuestra amistad no tiene fecha de caducidad. Gracias por todo tu apoyo, más que científico, personal. Te quiero amigo.

A mis amigos alicantinos, mi batiburrillo de gente que ha estado conmigo desde mi llegada y me han hecho la vida un poco más fácil. Gracias a Andrea, Alberto, Citri. Subi, Guille, Bárbara, Celia, Alex, Isabela, Alvarito...

A Paula, mi sevillana favorita y sin duda mi gran apoyo durante estos años, no me imagino esta etapa sin ti. Gracias a todas las casualidades que me llevaron a conocerte. Hemos compartido todo durante estos años: piso, buenos amigos, corazones rotos, risas, un chino guarrete, agobios de tesis, confidencias, pero sobre todo buenísimos momentos. Y no somos nosotras muy “exaltadoras de la amistad” pero no nos hace falta decir que nos queremos “una jartá”.

A Tony, otro de los protagonistas importantes de mi paso por Alicante. Gracias por ser como eres, aunque a veces te hagas el “sueco”. Gracias por estar siempre ahí, por tus ánimos y por soportar no una, sino dos científicas, e intentar entender el mundillo en el que vivimos aunque a veces no entendieras ni papa (aun recuerdo el día de los eppendorf y los griffindor).

A Laura, el soplo de aire fresco que necesitaba en mi vida. Gracias por vivir conmigo un año maravilloso y loco, y por seguir ahí a pesar de la distancia. Tengo pendiente una visita a Galicia, lo prometo titi.

No puedo olvidarme de mi familia científica valenciana “diga bananaa”: Javi, Noe, Carmen, Piotr, Isa, Andrej, Josep... Recuerdo cuando os conocí, yo aun era un pollito terminando la carrera cuando vosotros erais casi posdoc, y me sentí como una más. Sois una mezcla fantástica de biólogos de bata, bota y vino. Gracias por todos los momentos: almuerzos, fallas, cenas, fiestas, amigos investibles, catas de vino (había que aprovechar que las microbiólogas se llevaban los “deberes” a casa jaja).

A Javi. Gracias por confiar en mí, por hacerme ver que tenía potencial, por destacar siempre mis virtudes (sigo siendo muy resolutiva) y enseñarme a mejorar en mis defectos. Gracias por darme la oportunidad de ser tu alumna, por enseñarme tantísimo y darme el empujón que necesitaba para empezar esta etapa. Sin ti esta tesis no existiría.

A mi Té verde, mis mejores amigas: Petos, Pili, María, Vane, Isa y Eva. Esas amigas que llevan conmigo prácticamente toda la vida, desde los 4 años algunas, y que a pesar de la distancia, de no vernos en mucho tiempo, o de no tener ni tiempo para llamarnos, nos reencontramos y es como si el nada no hubiera pasado. Gracias por las risas y locuras, por los desahogos y por vuestro cariño y apoyo, porque siempre habéis estado y estáis ahí, en las buenas, y en las no tan buenas. Os adoro.

A mi 8 imperdible. Apareciste en el momento más inesperado de mi vida y espero que nunca desaparezcas. Gracias por tus consejos, tu enorme paciencia en mis momentos de estrés, tu apoyo y tu amor. Gracias por conocerme tanto, por saber reconocer en un segundo mi estado de ánimo y por darme las fuerzas necesarias para no tirar la toalla en los momentos más difíciles. Te quiero Lorenzo.

Y por ultimo a lo más importante, gracias a mi familia,

A mis abuelos, los mejores abuelos del mundo. Ellos, que todas las semanas me preguntan si he descubierto algo nuevo y, aunque no entiendan nada de lo que les cuento, siempre me miran con orgullo y una gran sonrisa. A mi abuela Isabel, porque aunque ya no esté presente, siempre me ha acompañado y me acompañará.

A mis padres, que han luchado siempre para que no nos faltara nada y fuésemos libres de ser lo que quisiéramos ser (no habéis tenido suficiente con una bióloga que os han salido dos). Gracias por creer en mi, vuestro cariño, amor y apoyo incondicional.

A mi pequeña gran revolución, mi hermana Irene. Eres la mejor persona que conozco. Porque me encantas, por nuestras conversaciones cabezonas, debates científicos, riñas, robos de calcetines y risas infinitas. Vas a llegar muy lejos y serás una grande en el mundo de la ciencia, de eso no me cabe duda (papá ya lo veía de pequeña, cuando eras una “ingenierilla”). Os quiero.

Y a todos los que, a lo largo de estos 6 años, han pasado por mi vida, porque estoy segura que sin los momentos vividos nunca hubiera llegado a ser lo que soy.

GRACIAS

